Methylmercury Production in Riverbank Sediments of the South River, Virginia (USA) and Assessment of Biochar as a Mercury Treatment Option

by

Krista Paulson

A thesis
presented to the University of Waterloo
in fulfillment of the
thesis requirement for the degree of
Master of Science
in
Earth Sciences

Waterloo, Ontario, Canada, 2014

Author's Declaration

I hereby declare that I am the sole author of this thesis.

This is a true copy of the thesis, including any required final revisions, as accepted by my examiners.

I understand that my thesis may be made electronically available to the public.

Abstract

Mercury (Hg) is a toxic element which bioaccumulates in the food chain when methylated and poses a health risk to the human population mainly through fish consumption. It is released into the environment through both natural and anthropogenic processes. Remediation of river systems contaminated with Hg presents challenges due to complexities associated with dynamic transport and deposition processes and cyclic methylation. The South River watershed in Virginia, USA contains elevated concentrations of Hg within sediment and floodplain soils as a result of historical releases from a textile manufacturing plant from 1929-1950.

Methylation of Hg is a bacterially mediated process which is controlled by the availability of electron donors, electron acceptors and Hg, amongst other factors. To evaluate the factors controlling Hg methylation at the South River site, four column experiments were conducted that involved saturating site sediments with South River water, followed by subjecting the columns to influent solution containing differing organic carbon and sulfate amendments. These amendments included acetate, lactate, and lactate combined with excess SO_4^{2-} and the production of MeHg relative to a control was monitored both spatially and temporally. Production of MeHg was observed in all four columns, with the lowest mass found in the effluent generated by the control column (8.7 ng L^{-1}), and a slightly higher mass in the acetate and lactate amended column effluents (53.7 ng L^{-1} and 30.1 ng L^{-1} reached respectively). The aqueous MeHg in the column amended with lactate and SO_4^{2-} reached a maximum of 4910 ng L^{-1} near the output of the column. The results from these column experiments suggest that excess SO_4^{2-} did not inhibit methylation under saturated flow conditions in the South River sediments. The bacterial species *Desulfovibrio putealis*, *Geobacter spp*., *Desulfobacterium* and *Desulfosporosinus* were identified in the column sediments and are potential contributors to the observed Hg methylation.

Experiments were conducted to evaluate the potential removal of Hg and MeHg from sediment pore water. The experiments consisted of two columns connected in series. The first column contained Hg-

bearing sediment with South River water as an influent solution to provide a source of Hg for the treatment column. The effluent from the first column was then connected to a treatment column which contained 1:1 volume ratio of biochar and silica sand. This treatment column was loaded with Hg for 182 pore volumes, disconnected, and then subjected to new influent solutions consisting of first background river water and then simulated acid rain water. The purpose was to determine the potential of the biochar material to retain Hg under saturated flow conditions. No significant release of Hg was observed in the column effluent with the South River water. After the influent was switched to simulated acid rain water (pH ~ 4.6), there was an increase in Hg concentrations in the column effluent for one sampling period, but then the unfiltered and 0.45 μm filtered Hg concentrations returned to < 8.5 ng L^{-1}. Total Hg extractions on the biochar column material at four locations suggested that the majority of the Hg in the column resided in the first 5 cm of material even after influent perturbations, with a maximum of 0.26 μg g^{-1} dry weight in the 2 cm closest to the influent. Mercury sequential extraction results on the biochar material at the termination of the column revealed the majority (67%) of the Hg on the biochar material was removed with 12 M HNO_3 (F4 fraction), followed by 0.1 M KOH (F3 fraction) at 31%. Less than 1.2% of the THg was removed after subjecting the biochar material to deionized water (F1 fraction) and 0.01M HCl + 0.1M CH_3COOH (F2 fraction). A solid-phase analysis of MeHg on the same biochar material resulted in a concentration of 0.20 ng g^{-1} dry weight, or <0.08% of total solid-phase Hg. These results suggest that application of biochar may represent an effective approach for treating Hg in passive flow through systems.

Acknowledgements

I would like to extend thanks and appreciation to my thesis advisor Dr. Carol Ptacek. The patience and guidance I received from her over the past few years were invaluable, and I am very grateful to have had the opportunity to study under her supervision. I would also like to acknowledge and thank Dr. David Blowes and Dr. Doug Gould, for their feedback and interest in this research.

I would like to thank Richard Landis, James Dyer, Erin Mack and Nancy Grosso for their interest and support in this research project, and for their encouragement along the way. I would like to thank the past and current members of the GGR group who contributed to this research, especially Alana (Ou) Wang, Jing Ma, Krista Desrochers, Matthew Lindsay, Blair Gibson, Peng Liu, Steve Holland, James Tordiff, Laura Groza, and Joy Hu, as well as the coop students over the years who provided a great help. I am thankful for the friendship and support provided along the way by Jessica Leung, Erin Liljestrand, Alyssa Gross, Sana Louie, Helen Powley and my family.

Table of Contents

List of Figures

List of Tables

List of Abbreviations

ACS	American Chemical Society
ARW	Acid rain water
CVAFS	Cold vapour atomic fluorescence spectrometry
EPA	Environmental Protection Agency
HDPE	High-density polyethylene
ICP-MS	Inductively coupled plasma mass spectrometry
ICP-OES	Inductively coupled plasma optical emission spectrometry
IR	Infrared
IRB	Iron reducing bacteria
MeHg	Methyl mercury
MPN	Most probable number
PCR	Polymerase chain reaction
PFTE	Polytetrafluoroethylene
RRM	Relative river mile
SR	South River
SRB	Sulfate reducing bacteria
SRD	South River sediment, location D
SRW	South River water
THg	Total mercury
THg-0.45	0.45 μm filtered total mercury

Chapter 1: *Introduction*

1.1 Mercury Background

Mercury (Hg) is found naturally as elemental Hg and as the very insoluble mineral cinnabar (HgS). Different Hg forms (metallic, inorganic and organic Hg compounds) are connected to neurodegenerative diseases in humans. The detrimental effects of Hg exposure to humans (especially the highly toxic methylated form) have been well-documented, with public awareness increased through the Minimata Bay tragedy in Japan (Langford & Ferner, 1999).

Mercury contamination is a global problem resulting from both natural and anthropogenic sources. The main source of anthropogenic release of Hg at present is coal combustion resulting in large areas contaminated through atmospheric deposition (Zhang, Wang et al., 2012). Mining and industrial activities are also important anthropogenic sources of Hg which have impacted lakes and rivers (Wang et al., 2012). There are many locations across the world impacted by Hg from mining and industrial activities coupled with biogeochemical cycling including the historical Idrija mine in Slovenia (Hines et al., 2000; Horvat et al., 2003), the Carson River, Nevada, USA (Oremland, 1995) and the Madeira River Basin in Brazil (Lechler et al., 2000). Sources of Hg in lakes and river systems can originate from the use of Hg to remove gold and silver from ores (Stamenkovic et al., 2003). In lakes and river systems secondary sources of Hg are formed through the remobilisation and deposition of soil and sediment containing elevated Hg concentrations adding to the persistent nature of Hg contamination.

1.2 Site Background

The South River is a 4th order, high gradient stream located in the Shenandoah Valley downstream from the city of Waynesboro, Virginia, USA (Flanders et al., 2010; Eggleston, 2009). The South River combines with the North and Middle Rivers to form the South Fork Shenandoah River, which then combines with the North Fork Shenandoah River to form the Shenandoah River. The South River

watershed covers an estimated 608 km^2, comprising an elevation range of 316 m at the mouth of the river to a maximum of 1173 m at the Blue Ridge Mountains (Eggleston, 2009).

Mercury sulfate was used as a catalyst in a fabric manufacturing process at a textile plant in Waynesboro, VA, USA. Though most of this catalyst was collected and re-used, there was a loss to the river resulting in secondary sources of Hg. Other sources for the Hg contamination in the South River system were examined (such as atmospheric deposition and agricultural fungicides) and determined insignificant in comparison to that of the plant (Eggleston, 2009). Spanning the years 1929 to 1950, the textile plant at Waynesboro discharged Hg waste into the South River which has since then been transported through erosion and deposition along the length of the river to as far downstream as the South Fork Shenandoah and Shenandoah rivers (Eggleston, 2009). The impact of bank erosion was heightened with the removal of mill dams along the rivers during the 1950s- 1970s, becoming an important aspect affecting Hg release at this site (Pizzuto and O'Neal, 2009). Approximately 40 km of the South River now contains elevated concentrations of Hg as a result of the historical release (Eggleston, 2009).

1.3 Rivers and Mercury

River environments undergo erosional and depositional processes which influence the Hg in contaminated sediments providing new sources and sinks of Hg. Within these environments the transport of Hg is connected to the specific pore water chemistry of the site which influences the release of colloidal Hg particles (Lowry et al., 2004). Dissolved organic matter (DOM) in rivers has a major role in controlling the toxicity of Hg as it is known to prevent the aggregation of particulate HgS (Ravichandran et al. 1999; Slowey, 2010; Aiken et al., 2011). Recent studies by Zhang et al. (2012) have elucidated the role DOM plays in controlling the bioavailability of Hg and methylation to include nanoparticulate HgS. Elemental Hg (Hg^0) also has been included among Hg forms considered available for methylation, adding further complexities to understanding methylation processes (Hu et al., 2013). After Hg enters ecosystems, a

complex biogeochemical cycle begins resulting in bioaccumulation of methyl mercury (MeHg) up the food chain (Marvin-Dipasquale et al., 2009) posing risk to the human population.

1.4 Bacterial Methylation

The interactions between bacteria and Hg are complex and greatly influence the toxicity of Hg through methylation. Different hypotheses exist as to the purpose behind bacterial Hg methylation, including reducing Hg toxicity to the bacteria (Ehrlich & Newman, 2009) and that Hg methylation is a metabolic mistake (Gilmour et al., 2011). Sulfate-reducing bacteria (SRB) in particular have long been known to dominate MeHg production in the environment, but recent developments suggest MeHg formation to be more complex. *Geobacter*, a genus of Fe(III)-reducing bacteria (IRB) contains known methylators of Hg (Fleming et al., 2006; Kerin et al., 2006). With the recent discovery of the genetic basis for Hg methylation (Parks et al., 2013) it is now possible to confirm the likely species responsible for Hg methylation in a particular environment and highlights the role of methylating species which are outside the anaerobic branch of SO_4^{2-}-reducing Deltaproteobacteria. As the main MeHg production process has so far been limited to anaerobic conditions, this would suggest implications for subsequent treatment designs.

1.5 Mercury Treatment

Options for treatment of Hg in aquatic systems must take into account possibilities for Hg methylation, suppression of Hg mobilization and the subsequent longevity of the treatment. There are a variety of different techniques for removal and/or treatment of Hg, including soil washing, thermal desorption, phytoextraction and soil stabilization/solidification (Wang et al., 2012). At the South River site elevated concentrations of Hg are dispersed over a wide area, making economic consideration and practical limitations very important.

One of the treatment options being considered as part of an integrated solution for the South River banks is application of Cowboy Charcoal (biochar) as a reactive mat laid against the banks providing both protection against bank erosion and also a site for Hg adsorption (Desrochers, 2013). An important aspect of this scenario is to determine how stable the Hg is on the treatment material under long-term leaching, saturated flow-through conditions.

1.6 Research Objectives

The main purpose of this thesis is to understand MeHg production in the riverbank sediments of the South River, VA and the impact that different organic amendments have on MeHg production under saturated flow conditions. Another important aspect of this thesis is to characterize the suitability of biochar as a treatment material for application under saturated flow conditions, and assessment of how the reactive material responds to perturbations.

The specific objectives of this thesis are to:

- Further understand the Hg methylation production under saturated flow conditions at the South River site,
- Evaluate the possibility of MeHg inhibition under saturated flow in the presence of high concentrations of H_2S,
- Determine the resilience of Cowboy Charcoal as a treatment material for Hg

1.7 Thesis Organization

This thesis is comprised of two research papers that address the objectives. Chapter 2 describes four anaerobic saturated column experiments with differing organic carbon amendments and a comparison of their pore water chemistry and the solid phase analyses on the column sediments following the termination of the experiments. Chapter 3 is a continuation of investigations of biochar as a treatment

material in a saturated flow scenario, with a focus on changes in the pore water chemistry induced by perturbations, and the solid-phase analyses of the column sediments.

Chapter 2: *Methylmercury Production in the Riverbank Sediments of the South River, VA (USA)*

2.1 Executive Summary

Mercury (Hg) transport and methyl mercury (MeHg) production in riverbank sediments are complex processes that are influenced by site conditions. These processes are important when assessing methods for remediation. The South River watershed in VA, USA contains elevated concentrations of Hg in riverbank and floodplain sediments, which has the potential to methylate. The role of specific organic carbon sources in promoting methylation reactions in natural sediments is not well understood under saturated flow conditions. Four column experiments were conducted, including a control column which received South river water as an influent solution, and three treatment columns. The treatment column influent water was South River water amended with: acetate (5.8 mM), lactate (5.7 mM), and lactate (5.7 mM) combined with SO_4^{2-} (10.1 mM). Aqueous-phase concentrations of MeHg and other parameters were monitored in the column influent and effluent solutions and periodically along the length of the columns. Concentrations of Hg in the control column reached a maximum of 7.1 μg L^{-1} (in 0.45 μm filtered samples) at early times, before declining to 1.6 μg L^{-1}; concentrations of MeHg reached maximum values at the end of the experiment. Effluent from the column receiving acetate had higher concentrations of Hg compared to the control. Concentrations of Hg initially increased and then stabilized to approximately 10 μg L^{-1} and concentrations of MeHg increased after the addition of acetate to a maximum of 54 ng L^{-1} in the effluent. Effluent from the column receiving lactate showed an increase in MeHg similar to the acetate column, with similar masses of total Hg leached as the control. The column receiving lactate and SO_4^{2-} had the highest MeHg concentrations of 1.8 μg L^{-1} in the effluent and 4.9 μg L^{-1} in the column pore water near the effluent and also the highest total mass of total Hg released in the effluent. Elevated concentrations of H_2S present in the lactate-sulfate column did not appear to suppress Hg methylation. At the termination of the column experiments, the lactate-sulfate column sediments contained the greatest populations of SRB and the acetate column sediments had the greatest IRB

populations as determined through enumerations. Sequential extraction analyses designed to target specific Hg-bearing phases showed a loss of the sulfide/residual F5 Hg fraction and a conversion to the elemental/strongly complexed F4 fraction in the column sediments in comparison to the original sediment with the exception of the lactate and lactate-sulfate columns. The greatest solid-phase MeHg was observed on the lactate-sulfate column sediments with 530 ng g^{-1} dry wt. ±100 on the sediment interval closest to the influent. *Desulfovibrio putealis* and *Geobacter spp.* were identified in the column sediments and may be species that promoted MeHg formation.

2.2 Introduction

2.2.1 Mercury and methylation

Mercury (Hg) is a toxic element which is converted through microbial processes to form methylmercury (MeHg), and can bioaccumulate up the food chain (Boening, 2000; Hsu-Kim et al., 2013) posing risks to aquatic and terrestrial life. The ability of the organic forms of Hg to pass the blood-brain barrier and its lipophilic nature result in its level of toxicity, because it can accumulate in sensitive organs such as the liver and brain. Elevated concentrations of Hg are a persistant issue in many riverine ecosystems, including Steamboat Creek and Truckee River (Stamenkovic et al., 2003) and the Carson River in Nevada (Miller et al., 1999). The forms of Hg which are considered bioavailable include inorganic Hg(II), elemental (Hg^0), and finely disseminated HgS (Hu et al., 2013; Zhang et al., 2012), which under anaerobic conditions can be methylated.

Understanding of the types of bacteria which methylate Hg has developed from a focus on the sulfur-reducing bacteria (SRB) of the Deltaproteobacteria to include species of Fe(III)-reducing bacteria (IRB) (Kerin et al., 2006; Fleming et al., 2006). With the discovery of the genes associated with methylation in bacteria (Parks et al., 2013) specific bacteria are being confirmed and identified as Hg methylators.

The addition of organic amendments and presence of terminal electron acceptors can promote the growth of different types of bacteria and influence MeHg production. Acetate has been added at different field sites to stimulate the IRB species *Geobacter* in concentrations of 5-30 mM (Williams et al., 2011) and 3 mM (Anderson et al., 2003) to promote remediation of U(VI) through dissimilatory Fe(III)-reduction. The growth of IRB is not necessarily impacted by the growth of SRB when in the presence of excess acetate (Bartlett et al., 2012). Lactate as a substrate can be degraded through an oxidative or fermentative metabolic pathway. If there is sufficient SO_4^{2-} present as a terminal electron acceptor then lactate can be completely oxidized by SRB (Oyekola et al., 2009). Acetate promoted greater methylation than lactate amended slurries in batch experiments by King et al. (2000). The relationship between Fe(III)-reduction

and SO_4^{2-} reduction is important for MeHg production. The role of IRB on Hg methylation in sediments from the South River, VA has been explored recently through inhibition of SRB metabolism and additions of Fe(III) (Yu et al., 2012).

Conflicting ideas exist concerning H_2S formation regulating MeHg production. It has been suggested that dissolved SO_4^{2-} and H_2S concentrations inhibit Hg methylation rates (Gilmour et al., 1991; Gilmour et al., 1992), and a study which involved the addition of 50 μm of H_2S to an existing H_2S pore water concentration of 200 μm inhibited methylation (Gilmour et al., 1998). Batch studies by King et al. (2000) observed no impact of dissolved H_2S concentrations on MeHg production. Determining how pore water H_2S concentrations impact MeHg formation is key to understanding bioavailability of Hg in sediments.

The South River, VA, USA is a high gradient stream located in the Shenandoah Valley downstream from the city of Waynesboro, VA. From 1929 to the 1950s Hg was used at a textile plant as a catalyst. A portion of this Hg was released to the South River through an incomplete recovery process. Bank sediments and floodplain soils contain elevated Hg concentrations along 39.6 km stretch of the river (Eggleston, 2009). The microbial communities present in the riverbank sediments are of great importance when considering remedial options as they play a key role in MeHg formation.

2.2.2 Purpose of experiments

Four saturated column experiments were conducted under controlled flow conditions to stimulate the growth of different bacterial species through the addition of different organic carbon amendments and SO_4^{2-}. The experiments were designed to observe net MeHg production in differing (bio)geochemical environments, and under transport conditions representative of the South River site. The interpretation of bacterial enumerations and PCR data of the column sediments may indicate the relative importance of IRB, in particular, for Hg methylation at the South River site, as well as the possibility of inhibiting Hg methylation under reducing conditions. High H_2S and SO_4^{2-} concentrations have been cited as possible inhibitors of MeHg production. These hypotheses were explored in greater detail in this study through a

column experiment which was amended with high SO_4^{2-}. How the Hg is distributed between fractions in the South River sediment under saturated flow experiments will be addressed, along with formation of solid-phase MeHg.

2.3 Methodology

2.3.1 Collection of sediment and water samples

Sediment was collected in a 5 L bucket in October 2010 from the surface water-bank sediment interface at ~5.6 km (relative river mile 3.5, location D, Fig.2.1) downstream from the point of historical mercury release, shipped to the University of Waterloo and stored at 4°C. The sediment was later homogenized by mechanical mixing, separated into 1 L Nalgene wide-mouth bottles, wrapped in aluminum foil and stored at 4°C. The South River water (SRW) used in the column experiments was collected on an approximately bimonthly basis upstream from the point of historical release and shipped on ice to the University of Waterloo, Waterloo, ON where it was stored at 4°C and kept under dark conditions.

2.3.2 Mineral and total carbon /sulfur analysis of sediment

The composition of the sediment was analyzed for total elemental concentrations through digestion in aqua regia followed by analysis on ICP-MS following EPA method 3050b (U.S. EPA, 1996). Total carbon and total sulfur analyses were conducted using an Eltra CS 2000 CS Determinator. Total inorganic and organic carbon was analyzed at SGS Lakefield Laboratories in Lakefield, ON, Canada; 0.5 g of sediment was digested with 40 mL of 10% H_2SO_4, shaken vigorously and then allowed to stand for 30 minutes. The extract was filtered through a glass fibre filter, the filtered solids were air-dried, then analyzed for total carbon using an induction furnace with an IR detection system. The filtrate was analyzed by a segmented flow analyzer from which the value for total organic carbon was derived. The total inorganic carbon is assumed to be the difference between the total carbon and organic carbon values.

2.3.3 Column design/experimental set-up

Four custom-machined acrylic columns 14.6 cm in length with a 3.81 cm inner diameter and two threaded 0.64 cm diameter ports installed along their length were packed with 1 cm of silica sand on the bottom followed by South River sediment then another 1 cm of silica sand at the top. The silica sand on the top and bottom were bounded by coarse-and fine-mesh NITEX screens. Before packing the columns had a water volume of 178.9 cm^3 ± 5.0 cm^3.

The columns were packed in a fume hood until the top silica sand layer, which was completed in a 5% H_2/balance N_2 vinyl anaerobic chamber (COY, Mandel Scientific Company, Guelph CA) and then sealed. The column experiments were conducted in the anaerobic chamber. Teflon tubing connected the column influent to 0.89 mm pump tubing (PharMed® BPT, Cole-Parmer, Montreal CA) (Fig. 2.2). Controlled flow through the columns was achieved using a multi-channel peristaltic pump (Ismatec Precision, Cole-Parmer, Montreal CA). The flow direction was against gravity, from the bottom to the top of the column. The average pore volume per week for the control, acetate, lactate and lactate-sulfate columns were 2.97 (±0.09), 3.15 (±0.06), 2.80 (±0.03) and 2.92 (±0.06), respectively. The influent solutions for all four columns consisted initially of South River water (SRW) with the influent composition subsequently changed for three of the columns (acetate, lactate and lactate-sulfate) at 2.7 (±0.08) pore volumes of flow (Table 2.2). The influent solutions were stored in 1.5 L amber narrow-mouth bottles throughout the duration of the experiments.

2.3.4 Aqueous phase sample collection

Column effluent was collected in a 200 mL sealed narrow-mouth amber bottle. Effluent samples were collected from this amber bottle using polypropylene/polyethylene 20 mL sterile luer-lock syringes (Norm-Ject, Thermo Fisher Scientific, Burlington CA) with the exception of samples for S^{2-} analyses and port sampling where acid-washed re-useable 20 mL and 50 mL glass syringes (BD Multi-fit, VWR, Mississauga, CA) were used.

2.3.5 Port sampling

The column ports were sampled a total of four times; at approximately 1.5, 6, 12 (±0.4) and 21 (±1.0) pore volumes of flow. Port sampling involved the use of glass syringes that exploited the flow rate to collect samples. Six pore volumes represented the sampling time immediately after the influents were switched for the three columns.

2.3.6 General aqueous sampling

Determinations of pH were made on unfiltered samples shortly after collection using a gel-filled combination electrode with a $Ag/AgCl_2$ reference electrode (Orion 9107B, Thermo Fisher Scientific, Burlington CA). The pH probe was calibrated before each analysis with pH 7, 4 and 10 buffers (Orion, Thermo Fisher Scientific, Burlington CA). Redox potential (Eh) was determined with a platinum redox combination electrode with a $Ag/AgCl_2$ reference electrode (Orion 9678 BNWP, Thermo Fisher Scientific, Burlington CA) checked against Zobell's and Light's solutions.

Samples that were filtered at the time of collection were passed through 32 mm diameter 0.45 μm Supor® membrane filters (Acrodisc®, VWR, Burlington CA). Alkalinity concentrations in the effluent were analysed on 0.45 μm filtered samples at the time of sample collection with a digital titrator using standardized 0.16 N H_2SO_4 (HACH, VWR, Mississauga CA). Phenolphthalein was used as an indicator above pH 8.27 for determination of carbonate and hydroxide alkalinity where applicable, and bromocresol-green methyl red below pH 8.27 as an indicator of bicarbonate alkalinity (reported as mg L^{-1} $CaCO_3$).

Samples for H_2S analysis were collected with glass syringes (BD multi-fit) and passed through a 0.45 μm filter immediately before being analyzed using the methylene blue method (Standard Method 4500-S^{2-} D for wastewater) with a spectrophotometer (HACH DR 2800, Mississauga, CA).

Vacuum and ionized 15 mL amber borosilicate bottles (Qorpak, VWR, Burlington CA) with PFTE-lined screw-caps were used for THg, and MeHg collection while anion and cation samples were collected in 15 mL HDPE narrow mouth Nalgene bottles. Samples for anion, cation and THg analyses were stored at 4°C and samples for MeHg were frozen immediately after collection at -20°C.

Anion samples were 0.45 μm filtered and left un-acidified, stored at 4°C and analyzed within two weeks of collection using ion chromatography (Dionex DX 600, Thermo Scientific) with the use of a hydroxide eluent for organic acids (lactate, acetate, propionate and formate) and a carbonate eluent for major ions. Samples for cation analysis were 0.45 μm filtered and acidified to a pH <2 with ACS grade 69-70% HNO_3 (JT Baker, VWR, Burlington CA) and stored at 4°C until analysis. Cation analysis for trace metal concentrations was completed using inductively coupled plasma mass spectroscopy (ICP-MS, X-Series 2, Thermo Scientific) and major cation analysis was completed using inductively coupled plasma optical emission spectrometry (ICP-OES, iCAP 6000, Thermo Scientific).

Samples for THg and MeHg were filtered at every sample collection time through 0.45 μm filters, with unfiltered samples collected in addition to filtered samples at every other sampling time. The unfiltered and 0.45 μm filtered samples for THg were acidified with 69-70% HNO_3 (JT Baker, VWR, Burlington, CA) and analyzed using the cold vapour atomic fluorescence spectroscopy technique (CVAFS, Tekran® 2600 Sample Analysis System) applying the EPA 1631 Revision E method (U.S. EPA, 2002). Samples for MeHg were acidified with ACS grade 36.5-38% HCl (JT Baker, VWR, Burlington CA). Methyl mercury was analyzed through distillation, aqueous ethylation and purge and trap with the CVAFS technique (Tekran® 2750 methylmercury distillation system and a Tekran® 2700 automated methyl mercury analyzer) following EPA method 1630 (U.S. EPA, 2001).

Samples for phosphate and ammonia analysis were passed through 0.45 μm membranes and acidified to a pH <2 with OmniTrace Ultra High Purity H_2SO_4 (EMD, VWR, Burlington CA). Reactive phosphorus PO_4-P (orthophosphate) was determined through the ascorbic acid spectrophotometric method (based off

of method 4500-P from the Standard Methods for Examination of Water and Waste Water) and analyzed with a spectrophotometer (HACH DR 2800). Ammonia-nitrogen (NH_3-N) was analysed using the salicylate method with a spectrophotometer (HACH DR 2800, Method 8155 from the DR 2800 manual).

2.3.7 Solid-phase sample collection

After 23.1 (±1.06) pore volumes of flow (55.68 days ±0.03) the experiments were terminated and the columns were sectioned at 2 cm intervals with autoclaved and 70% ethanol-washed tools with samples from the 4-6, 8-10 and 12-14 cm locations in the column relative to the influent. Samples were immediately separated for DNA extraction and microbial enumerations. The remaining column sediments were sealed in 40 mL glass EPA vials under anaerobic conditions and frozen immediately at -20°C.

2.3.8 Microbial enumerations

Growth medium for SRB was prepared following a modified Postgate medium C recipe (Postgate, 1984) after Lindsay et al. (2011) and Benner et al. (1999) with chemicals dissolved in deionized water in the following ratios (g L^{-1}): 0.5 KH_2PO_4, 1.0 NH_4Cl, 4.5 Na_2SO_4, 0.04 $CaCl_2.H_2O$, 0.06 $MgSO_4.7H_2O$, 0.004 $FeSO_4.7H_2O$, 2.92 60% Na-Lactate, 1.28 Na-acetate, 1.0 Yeast extract, 0.3 Na-citrate dihydrate. The medium was mixed using a magnetic stir bar and buffered to a pH of 7.5 with NaOH. Finally 2.0 mL L^{-1} of 0.1% resazurin was added as an oxygen indicator. The medium was boiled and purged with Ar(g) to remove remaining dissolved oxygen.

The SRB medium was transferred immediately after preparation to an anaerobic chamber where it was dispensed in 9 mL aliquots into 20 mL glass serum bottles containing an ethanol washed Fe nail. Serum bottles were then sealed with butyl rubber septa and aluminum crimp caps and autoclaved at 121°C for 20 minutes before being returned to the anaerobic chamber to cool.

Growth medium for IRB was prepared by dissolved chemicals in deionized water in the following ratios from Lindsay et al. (2011) and Gould et al. (2003) (g L^{-1}): 2.5 $NaHCO_3$, 1.5 NH_4Cl, 0.6 $NaH_2PO_4.H_2O$, 0.1 $CaCl_2.2H_2O$, 0.1 KCl, 0.1 $MgCl_2.6H_2O$, 0.005 $MnCl_2.4H_2O$, 0.001 $Na_2MoO_4.2H_2O$, 1.84 Fe(III) EDTA, 1.5 protease peptone. The medium was mixed using a magnetic stir bar and buffered to a final pH of 7 with HCl. The medium was boiled and purged with Ar(g) to remove dissolved oxygen. Once purged for a sufficient amount of time, the media was transferred to an anaerobic chamber and then dispensed with an auto pipette into 20 mL glass serum bottles. Bottles were subsequently sealed with butyl rubber septa and an aluminum crimp cap, autoclaved at 121°C for 20 minutes and cooled in an anaerobic chamber.

After the bottles were sufficiently cooled, 1.0 g (± 0.05) of column sediment was added to 5 replicate serum bottles in the anaerobic chamber, and then serially diluted to the 10^{th} dilution level outside the anaerobic chamber using argon purged needles and 1 mL sterile syringes. After the dilutions were completed, the inoculated serum bottles were covered in aluminum foil to block natural light and transferred back into an anaerobic chamber for a 4 week incubation period. Positive results for SRB are indicated by the presence of a black FeS precipitate, while positive results for IRB are indicated by a purple colour after injection of 0.2 mL of 0.15% ferrozine reagent to detect the presence of reduced Fe. Finally an MPN table from Cochran et al. (1950) was used to determine the estimated bacterial cells g^{-1} for each column level.

2.3.9 Polymerase chain reaction

DNA purification for PCR analysis was completed on the column sediment immediately after column sectioning following the manufacturer's protocol given in the UltraClean® Soil DNA Isolation Kit (Mo Bio Laboratories) and use of a Clean-Ceil™ Fan Filter Module (Microzone). Purified DNA was then shipped frozen for PCR analysis (MR DNA, Shallowater, Texas,). A single-step 30 cycle PCR analysis using a HotStarTaq Plus Master Mix Kit (Qiagen, Valencia, CA) was done using the universal 16s primer

pair 27f/519r. This process involved denaturation at 94°C for 3 minutes, 28 cycles at 94°C of 30 second denaturation, 53°C for 40 seconds, 72°C for 1 minute followed by a final elongation step at 72°C for 5 minutes to complete amplification. Agencourt Ampure beads (Agencourt Bioscience Corporation, MA, USA) were used to purify all the amplicon products from the PCR analysis that had been mixed in equal concentrations. A Roche 454 FLX titanium instrument with reagents following the manufacturer's protocol was used for 16S rRNA pyrosequencing.

A proprietary analysis pipeline (www.mrdnalab.com) was used to process the Q25 sequence data. Sequences were first depleted of barcodes and primers with sequences of <200 base pairs, ambiguous base calls and homopolymer runs exceeding 6bp were removed and then denoised and chimeras were removed. Operational taxonomic units (OTUs) were defined as those sequences clustering at 3% divergence (Dowd, Callaway et al., 2008; Dowd, Sun et al., 2008; Edgar, 2010). Sequences identified using BLASTn were subsequently compared to the GreenGenes database and used for taxonomic classification (DeSantis et al., 2006).

2.3.10 Total Hg, MeHg and Hg sequential extractions

Sediment samples from the columns underwent digestion for three days using aqua regia to extract the THg present in the material. The digestate was analyzed using the CVAFS technique described previously for aqueous Hg samples. Solid-phase Hg sequential extractions were completed on frozen samples with the following reagants: deionized water (F1 fraction), 0.1 M CH_3COOH and 0.01 M HCl at pH 2 (F2 fraction), 0.1 M KOH (F3 fraction), 12M HNO_3 (F4 fraction), and aqua regia (F5 fraction) following the method by Bloom et al. (2003). The subsequent Hg digestate was analyzed using CVAFS with a Tekran 2600 instrument and the EPA 1631 Revision E method (U.S. EPA, 2002). Solid samples for MeHg were prepared with 20 % KCl, 8 M H_2SO_4 and $CuSO_4$ for distillation to improve recovery before undergoing aqueous ethylation and CVAFS as described previously for aqueous MeHg samples.

2.3.11 Modelling

Saturation indices and charge balance errors were calculated with the MINTEQA2 geochemical speciation program (Allison et al., 1990). Alkalinity values used for modelling of the organic-amended columns were adjusted to remove interferences from propionate, acetate and lactate.

2.4 Results

2.4.1 Control column aqueous concentrations

The 0.45 μm filtered THg (THg-0.45) concentrations in the control column effluent increased initially to 7.1 μg L^{-1} and then declined to 1.6 μg L^{-1} over the duration of the column experiment (Fig. 2.3). The 0.45 μm filtered MeHg concentrations increased from 0.67 ng L^{-1} to 8.76 ng L^{-1}. The pH of the effluent rose from 7.36 to 7.79 and the redox potential declined from 350 mV to -7.7 mV. Alkalinity concentrations fluctuated between 148 and 193 mg L^{-1} as $CaCO_3$. Effluent Mn rose from 0.01 mg L^{-1} to 2.08 mg L^{-1}, and Fe increased rapidly around 20 pore volumes to reach a maximum of 3.36 mg L^{-1} from an initial value of 0.13 mg L^{-1}. Sulfate concentrations declined from an influent of 11.6 mg L^{-1} to 0.91 mg L^{-1}, whereas H_2S concentrations were consistently observed at or below the detection limit of 5 μg L^{-1}. Ammonia-N concentrations plateaued at 1.7 mg L^{-1} and then declined to 0.5 mg L^{-1}, while NO_3^- declined from an initial release of 310.9 mg L^{-1} to <0.03 mg L^{-1} by 5 pore volumes of flow. Concentrations of PO_4-P increased from an initial 0.03 mg L^{-1} to a final concentration of 0.68 mg L^{-1}. The concentrations of all organic acids measured in the effluent and influent remained at <0.03 mg L^{-1}.

The highest THg-0.45 value of 9.2 μg L^{-1} (Fig. 2.4) was observed in pore water collected from the top port of the control column. The highest value of aqueous MeHg was observed in the top port of the column with 11.1 ng L^{-1} measured at the last sampling of the top port. The Eh varied the greatest over time in the bottom port where the lowest value of 40.4 mV was attained at 21 pore volumes.

Concentrations of both aqueous Fe and Mn increased along the length of the column while H_2S remained at <5 μg L^{-1}.

2.4.2 Acetate column aqueous concentrations

After the addition of acetate to the SRW influent solution, the THg-0.45 concentrations in the acetate column effluent increased from 1.1 μg L^{-1} to the eventual plateau of 9.3-10.2 μg L^{-1} at 12 pore volumes (Fig. 2.5). Concentrations of MeHg increased from an initial 0.73 ng L^{-1} to 53.7 ng L^{-1} at 16.4 pore volumes in the column effluent and decreased to 23.0 ng L^{-1} at the time of column sectioning. The pH rose from 7.42 to 7.90 while the Eh declined from 287.7 mV to -98.0 mV over the duration of the column experiment. Concentrations of alkalinity peaked at 563 mg L^{-1} as $CaCO_3$ after the influent switch, and then declined to the influent level around 380 mg L^{-1}. Aqueous Mn reached 4.2 mg L^{-1} and stabilized around 1.9 mg L^{-1}, while the Fe concentrations peaked at 5.6 mg L^{-1} and remained within the range of 4.6-5.8 mg L^{-1}. Effluent SO_4^{2-} concentrations declined to <0.03 mg L^{-1} within 9 pore volumes, while H_2S was observed around the detection limit of 5 μg L^{-1}. Ammonia-N concentrations in the effluent increased over the duration of the column experiment to a maximum of 2.5 mg L^{-1}, while NO_3^- declined to <0.03 mg L^{-1} and PO_4-P concentrations reached a maximum of 1.8 mg L^{-1}. After the influent switch, acetate concentrations remained similar to the influent concentration levels of >300 mg L^{-1} though near the end of the column the concentrations in the effluent had declined to 248 mg L^{-1}. There was no observable (>0.03 mg L^{-1}) lactate or propionate in the effluent over the duration of the column experiment.

The greatest THg-0.45 value of 15.8 μg L^{-1} was observed in the top port of column at 6 pore volumes of flow (Fig. 2.6). Concentrations of MeHg increased in the ports immediately after the influent switch to the high acetate influent solution with the highest measurement of 159.6 ng L^{-1} found in the top port at the last port sampling at 22 PV. The highest observed aqueous Mn concentration within the column port sampling times was measured in the top port at 6 pore volumes of flow with a value of 2.6 mg L^{-1}. The Fe concentrations increased along the column length and also over time within the column ports. Sulfate

concentrations declined to <0.03 mg L^{-1} by the first port after the influent solution switch, with no H_2S >5 μg L^{-1} observed.

2.4.3 Lactate column aqueous concentrations

After the addition of lactate to the SRW influent, the THg-0.45 concentrations reached 7.3 μg L^{-1} in the lactate column effluent and then declined to a range of 4.0 – 4.6 μg L^{-1} over 21.8 pore volumes (Fig. 2.7). The concentrations of MeHg increased from 1.4 ng L^{-1} to 30.0 ng L^{-1} at 13.5 pore volumes and then declined to 12.5 ng L^{-1} by the end of the column experiment. Over the duration of the column experiment, the pH increased from an initial value of 7.43 to 7.90 observed at 11 pore volumes and then declined to 7.74. The Eh measurements declined from an initial value of 367 mV to -32 mV. Alkalinity concentrations peaked at 677 mg L^{-1}(as $CaCO_3$) and then stabilized to a range of 445-563 mg L^{-1} (as $CaCO_3$). Aqueous Mn increased to a plateau of 3.2 – 4.6 mg L^{-1}, whereas Fe concentrations eventually reached a maximum of 14.1 mg L^{-1}. Sulfate in the effluent declined to <0.03 mg L^{-1} after the influent switch with H_2S production remaining at or slightly above 5 μg L^{-1}. Ammonia-N peaked at 3.1 mg L^{-1} at 13.5 PV, NO_3^- declined from 537 mg L^{-1} to <0.03 mg L^{-1} and PO_4-P increased to 1.3 mg L^{-1} from an initial value of 0.03 mg L^{-1}. Concentrations of organic acids were observed in the column effluent. Acetate increased from <0.01 mg L^{-1} to a plateau of 100-190 mg L^{-1} and propionate increased from <0.01 mg L^{-1} to a maximum of 367 mg L^{-1} around 9.3 pore volumes and then declined to 181 mg L^{-1}.

The aqueous sample collected from the top port at 12 pore volumes of flow had the highest THg-0.45 value of 12.1 μg L^{-1} (Fig. 2.8). The MeHg concentrations increased along the flow path of the column and then declined in the effluent. The top port had the highest observed MeHg value of 51.1 ng L^{-1} at the port sampling event closest to the end of the column experiment (19.5 PV). The pH in the bottom port increased initially from 7.38 to 7.68 at 6 pore volumes of flow before it declined to 7.30. Sulfate declined to <0.03 mg L^{-1} after the influent switch to the high lactate solution, and H_2S measurements remained close to 5 μg L^{-1}. Manganese concentrations appeared to stabilize by the latter two sampling times,

whereas Fe increased over time to a maximum of 23.4 mg L^{-1} in the top port at the final port sampling time. Organic acids were measured in the ports along the length of the column. Acetate reached a maximum of 160 mg L^{-1} in the bottom port at 11.5 pore volumes of flow after which the concentration declined to 75 mg L^{-1}. Propionate increased from <0.01 mg L^{-1} in the ports to a maximum of 400 mg L^{-1} in the bottom port at 6 pore volumes and then declined to 190 mg L^{-1} at the end of the column experiment.

2.4.4 Lactate-sulfate column aqueous concentrations

After the influent switch, the THg-0.45 concentrations increased in the lactate-sulfate column effluent from an initial 0.87 μg L^{-1} to 5.6 μg L^{-1} at 8.6 pore volumes of flow and then increased again to a maximum of 21.6 μg L^{-1} at 11.6 pore volumes (Fig. 2.9). The aqueous MeHg increased from 0.91 ng L^{-1} to a peak of 1850 ng L^{-1}at 20.5 pore volumes and declined to 894 ng L^{-1} at the time of column sectioning. Over the duration of the column experiment the pH of the effluent increased from 7.48 to 8.46 and Eh declined from 272 mV to -130 mV. Alkalinity concentrations in the effluent reached a plateau of 1033 – 1062 mg L^{-1} (as $CaCO_3$). Manganese concentrations increased from 0.02 mg L^{-1} to a maximum of 6.9 mg L^{-1} at 5.6 pore volumes and then declined to 0.62 mg L^{-1}. Aqueous Fe increased from 0.01 mg L^{-1} to a maximum of 9.2 mg L^{-1} at 8.6 pore volumes of flow and then declined to 1.0 mg L^{-1}. The switch in influent to a high lactate-sulfate solution resulted in concentrations of SO_4^{2-} in the column effluent reaching a maximum of 871 mg L^{-1} at 5.6 PV before declining to 48 mg L^{-1}. The effluent H_2S increased from <5 μg L^{-1} to a maximum of 5320 μg L^{-1} at 20.5 pore volumes and declined to 2200 μg L^{-1} at 23.5 pore volumes. Over the duration of the column experiment NH_3-N concentrations increased from 0.6 mg L^{-1} to 3.3 mg L^{-1}, NO_3^- declined from 307.9 mg L^{-1} to <0.03 mg L^{-1} and PO_4-P increased from 0.04 mg L^{-1} to 12.0 mg L^{-1}. Organic acids were observed in the column effluent. Acetate increased from <0.01 mg L^{-1} to a maximum of 225 mg L^{-1} at 10 pore volumes of flow and then declined to ~12 mg L^{-1} while propionate was only observed >0.03 mg L^{-1} twice at 4.2 and 5.6 pore volumes with concentrations of 10.0 mg L^{-1} and 149.3 mg L^{-1} respectively.

The THg-0.45 concentrations increased along the flow path of the column after the addition of lactate and sulfate (Fig. 2.10). Aqueous MeHg concentrations were consistently higher in the bottom port with the exception of the last port sampling time, where the highest concentration of MeHg of 4910 ng L^{-1} was observed in the top port. The lowest observed Eh value along the length of the column was measured in the bottom port at 21 pore volumes with a value of -188 mV. The aqueous Mn and Fe values declined at a faster rate in the bottom port compared with further along the flow path. Concentrations of H_2S in the ports increased exponentially over time with the greatest value of 55 mg L^{-1} occurring at the bottom port at the last sampling time.

2.4.5 Microbial enumerations

The microbial enumerations at the cessation of the control column (Fig. 2.11-A) showed similar populations of IRB and SRB present in the sediment along the column length with IRB dominating throughout at a consistent population of 10^7 bacterial cells g^{-1} compared with 10^3 for SRB. The microbial enumerations of SRB and IRB of the acetate column sediment (Fig. 2.11-B) indicated an abundant Fe-reducing bacteria population in the order of 10^7 bacterial cells g^{-1} with the highest populations present in the middle of the column at a minimum of 10^{10} bacterial cells g^{-1}. The MPN of bacterial cells g^{-1} of IRB and SRB in the lactate column sediment (Fig. 2.11-C) showed a dominant population of IRB throughout the column at 10^6-10^7 bacterial cells g^{-1} compared with SRB populations on the order of 10^2-10^3 cells g^{-1}. The MPN bacterial enumerations of IRB and SRB at the time of sectioning for the lactate-sulfate column sediment (Fig. 2.11-D) indicated a large viable SRB community observed in the column at the two depths closest to the influent over the IRB with a range from 10^7 at the bottom to 10^5 bacterial cells g^{-1} at the top of the column. The IRB enumerations showed viable populations on the order of 10^6 bacterial cells g^{-1} except at the top of the column where 10^9 bacterial cells g^{-1} were observed.

2.4.6 Deltaproteobacteria

Subsequent analysis of the sediment with PCR indicated the Deltaproteobacteria class for the control column represented 7.21%, 7.64% and 8.17% of the total sequence counts at the 4-6, 8-10 and 12-14 cm intervals of the column respectively. Of the identified Deltaproteobacteria, the majority of the column was dominated by other Deltaproteobacteria which contains sequences that comprised <0.5% of the sequences identified as Deltaproteobacteria, followed by Nitrospinaceae and Geobacteraceae (Fig. 2.12-A). There was no particular pattern evident between the sections of the column with similar sequencing results observed at all three levels of the column. The Deltaproteobacteria class for the acetate column sediment represents 21.91%, 17.84% and 23.47% of the 4-6, 8-10 and 12-14 cm sections of the column respectively. The Geobacteraceae dominated the identified sequences throughout the column accounting for 64-73% of the identified Deltaproteobacteria (Fig. 2.12-B). The Deltaproteobacteria class for the lactate column sediment represented 10.97%, 11.77% and 10.91% of the 4-6, 8-10 and 12-14 cm sections of the column respectively. Of these the Geobacteraceae were again dominant in the column, representing 45- 55% of the identified Deltaproteobacteria (Fig. 2.12-C). The Deltaproteobacteria class for the lactate-sulfate column sediment represented 21.18%, 15.39% and 17.06% of the 4-6, 8-10 and 12-14 cm sections of the column, respectively. There was a gradient present in the Deltaproteobacteria community observed over the different column levels (Fig. 2.12-D). Geobacteraceae increased along the flow path of the column from 32% to 50% while Desulfovibrionaceae decreased from 17% to 1.0%.

2.4.7 Identified Hg methylators

Comparison of species identified by PCR from the sediments with a table of predicted methylators updated June 28, 2013 (ORNL, 2013) there are four species that can be identified in the columns that are Hg methylators (Fig. 2.13). The lactate-sulfate column had the highest counts of known methylating bacteria at 23.5% of identified species in the sediment or 1.64% of all column sequences. The acetate column had the second highest counts of known methylators at 4.9% of identified species and 0.89% of

all column sequences. Known or suspected Hg methylators made up 2.7% of the identified species and 0.56% of all column sequences for the lactate column. Finally, in the control column, 0.67% of the identified species and 0.13% of all sequences represented known or predicted Hg methylators.

The only Hg methylating species identified in the control column sediment was *Geobacter spp.* whose counts decreased along the flow path of the column from 1.15% of identified species to 0.23% (Fig. 2.13-A). In the acetate column *Geobacter spp.* comprised 4.4-5.2% of identified species and *Desulfovibrio putealis* was observed in only one sediment interval (closest to the influent) at 0.18% (Fig. 2.13-B). *Geobacter spp.* in the lactate column comprised 1.9-2.2% of identified species with *Desulfovibrio putealis* present closest to the influent and in the mid-section of the column at 0.47% and 0.13% respectively and *Desulfosporosinus spp.* present closest to the influent at 0.11% (Fig. 2.13-C). In the lactate-sulfate column *Desulfovibrio putealis* had the highest counts decreasing along the flow path of the column from 25.9% to 1.5% of the species identified (Fig. 2.13-D). *Geobacter spp.* was also observed with counts that comprised 6.9-10.1% of identified species. *Desulfobacterium spp.* and *Desulfosporosinus spp.* were also present at counts that comprised less than 0.5% of the column sediment.

2.4.8 Solid-phase Hg extractions

The THg present in the sediment of all of the column intervals was 183 $\mu g\ g^{-1}$ ±13, a similar value to the original sediment which was 213 $\mu g\ g^{-1}$ (Fig. 2.14). Sequential extraction analyses targeting the water soluble (F1), weak acid extractable (F2), organo-complexed (F3), strongly complexed (F4) and sulfide/residual (F5) Hg fractions showed an increase in the F2 and F4 fractions and a loss of the F5 fraction in the control column relative to the original sediment (Fig. 2.14-A). A loss of the F5 fraction was observed along the length of the acetate column sediment (Fig. 2.14-B) with the exception of the 8-10 cm interval which contained a similar concentration of F5 fraction compared to the original sediment (125 $\mu g\ g^{-1}$ versus 132 $\mu g\ g^{-1}$). The lactate column (Fig. 2.14-C) had Hg in fractions similar to the original sediment extraction values with the exception of the 12-14 cm interval. The 12-14 cm interval of

the lactate column had a loss of the F5 fraction and gain in the strongly complexed/elemental F4 fraction and the F2 weakly acid extractable fraction. The lactate-sulfate column (Fig. 2.14-D) had a consistent loss of the F5 fraction from 132 μg g^{-1} in the original sediment to 105 μg g^{-1}± 10.0 in the column sections. The lactate-sulfate column also had the greatest concentration of the F3 organo-complexed fraction of all the columns, with the top and bottom sections containing 14 and 15 μg g^{-1} respectively.

2.4.9 Solid-phase MeHg

The control, acetate and lactate columns all contained <0.02% of the Hg as MeHg on the column sediments after sectioning (Fig. 2.15). The acetate and lactate columns (Fig. 2.15-B and Fig. 2.15-C respectively) contained similar concentrations of MeHg on the solid phase, with both reaching a maximum of 29 ng g^{-1} dry weight of MeHg at the 4-6 cm interval and overall average concentrations of 26 ng g^{-1} ± 3.4 and 27 ±1.9 ng $^{-1}$ respectively. The control column material (Fig. 2.16-A) contained a lower concentration of MeHg with 17 ng g^{-1} ±1.8 observed on the sediments. The lactate-sulfate column (Fig. 2.16-D) contained the highest concentrations of MeHg of all the column experiments. A maximum of 529 ng g^{-1} ±103 (dry wt.) was observed at the 4-6 cm interval and lower values of 182 and 174 ng g^{-1} were observed in the 8-10 and 12-14 cm intervals respectively. The lactate-sulfate column MeHg observed in the sediments at the end of the column experiment represented 0.33%, 0.094% and 0.090% of the THg in the 4-6, 8-10, and 12-14 cm intervals respectively.

2.5 Discussion

2.5.1 Pore water chemistry

The main reactions controlling the microbial and chemical composition in the control column were likely derived from the natural breakdown of organic matter already present in the sediment stimulated by the isolation of the system from atmospheric oxygen under the saturated conditions. After 18.4 PV there were concentrations of acetate and propionate detected in the influent (2.2 mg L^{-1} and 0.3 mg L^{-1} respectively) which may have led to the increase in MeHg concentrations observed towards the termination of the experiment. The natural organic carbon in the sediment as well as added organic carbon (e.g. acetate, lactate), can be oxidized through bacterially mediated processes by coupling with terminal electron acceptors such as Mn(IV) oxides or Fe(III) oxyhydroxides (Eq.1, 2).

$$CH_3COO^- + 4MnO_2 + 7H^+ \leftrightarrow 4Mn^{2+} + 2HCO_3^- + 4H_2O \qquad \text{Eq. 1}$$

$$CH_3COO^- + 8FeOOH + 15H^+ \leftrightarrow 8Fe^{2+} + 2HCO_3^- + 12H_2O \qquad \text{Eq.2}$$

The oxidation of organic matter under anoxic conditions produces alkalinity, which was observed in all columns to different extents, together with an increase in the aqueous concentrations of reduced Fe and Mn. There also were indications of NO_3^- reduction and SO_4^{2-} reduction occurring in all columns as NO_3^- decreased to below the analytical detection limits after the first two pore volumes of flow and SO_4^{2-} concentrations decreased below influent levels. The decline observed in NO_3^- and SO_4^{2-} concentrations indicate that SO_4^{2-} and NO_3^- were likely consumed through organic carbon oxidation reactions. A variety of bacteria have the ability to reduce nitrate, including species from the genus *Clostridia* and genus *Pseudomonas* (Burgin and Hamilton, 2007). Denitrifying bacteria including species from the genus *Thiobacillus* (Atlas, 1984) that may have contributed to the decline in NO_3^- were present in all columns.

Dar et al. (2008) observed fermentation of lactate in batch reactor experiments at a lactate to SO_4^{2-} molar ratio of 20.9:1. The higher lactate to SO_4^{2-} molar ratio (50:1) induced in the lactate column influent solution was anticipated to promote the fermentative pathway (Eq. 3).

$$3CH_3CH(OH)COO^- \leftrightarrow CH_3COO^- + 2CH_3CH_2COO^- + HCO_3^- + H^+ \qquad \text{Eq.3}$$

Complete removal of lactate was observed by the first sampling port. Degradation of lactate to form acetate and propionate at a 1:2 ratio is expected (Oyekola et al., 2012), and was observed at the last port sampling time with an acetate to propionate ratio of 1:2.01 observed in the first port. The acetate to propionate ratio declined along the length of the column, possibly due to consumption of these by-products by acetate and propionate-utilizing bacteria (e.g. some members of genus *Desulfobulbus*) that were identified in the column sediment at the termination of the experiments (Hansen, 1993). Acetate and propionate can be produced by specific strains of SRB such as *Desulfobulbus propionicus* (Oyekola et al., 2009; Widdel and Pfennig, 1982) which are from the Desulfobulbaceae family. Species related to Desulfobulbaceae (Fig. 2.11-D) were observed in the lactate column, thus *Desulfobulbus propionicus* or a similar species could be responsible for the formation of the observed by-products.

The addition of excess SO_4^{2-} in the lactate-sulfate column provides an exogenous electron acceptor and the lactate should be fully oxidized. The high concentration of H_2S in this column should allow the lactate oxidizers to outcompete the fermenters (Oyekola et al., 2010). Acetate was observed in the effluent after the influent was switched to lactate-sulfate and continued to be measured until approximately 13 pore volumes of flow. The presence of acetate indicates incomplete oxidation of lactate by SRB (Hansen, 1993), possibly by *Desulfovibrio* which were identified in this column. The absence of organic acids after 13 PV suggested the growth of SRB that are capable of complete oxidation of lactate (e.g. *Desulfobacter*) which was identified in the column sediment. The oxidation of lactate coupled with the reduction of SO_4^{2-} (Eq. 4) in the lactate-sulfate column produces H_2S and carbonate alkalinity through (Postgate, 1984):

$$2CH_3 3CH(OH)COO^- + SO_4^{2-} \leftrightarrow 2CH_3COO^- + HS^- + 2HCO_3^- \qquad \text{Eq. 4}$$

A comparison of the consumed SO_4^{2-} observed in the lactate-sulfate column ports to produced HCO_3^- correlated strongly with a ratio of SO_4^{2-}:HCO_3^- of 1:1.65 (adjusted R^2 of 0.932, p-value <0.001). The ratio of SO_4^{2-}:HCO_3^- (1:2.17) was closer to the stoichiometric ratio when the focus was narrowed to the observations from the last two port sampling events and had a stronger correlation (adjusted R^2 of 0.942, p-value <0.001). This stronger correlation at the later column lifetime was a closer ratio to the theoretical ratio of SO_4^{2-} to HCO_3^- and is consistent with the predominance of SO_4^{2-} reduction by lactate.

Formation of H_2S can lead to sequestration of metals from solution (Eq. 5).

$$Me^{2+} + HS^- \rightarrow MeS + H^+ \qquad \text{Eq. 5}$$

The reaction in Eq.5 is between divalent metals (Me^{2+}) such as Fe, Hg, Zn which then lowers pH through the release of hydrogen ions. The reaction in Eq.5 was most recognizable in the port of the column closest to the influent, which reached a pH of 7.83 by the last port sampling time, compared with a pH of 8.4 in the effluent. There was a consistently lower amount of H_2S measured than what should be theoretically produced from Eq. 4 suggesting binding with divalent metals or other substrates. The decline in THg concentrations observed in the column effluent could be a result of the reaction in Eq. 5 where a maximum THg value of 21.6 μg L^{-1} declined to 14.3 μg L^{-1}, the latter value corresponding to the maximum H_2S concentration of 5.3 mg L^{-1}.

2.5.2 Nutrient release

The release of NH_3-N and PO_4-P in all columns suggests a breakdown of organic matter containing P and N (Waybrant et al., 2002) present in the sediment and not related to the organic carbon additives. The rate of organic carbon degradation stimulated by bacteria growth enhanced the release of these products from the sediment itself. The release of NH_3-N and PO_4-P combined with the increase observed in HCO_3^- in the organic amended columns could indicate the faster relative rates of organic matter degradation (van

der Heide et al., 2010). The lactate-sulfate column had the largest amount of nutrient release and also the greatest increase in carbonate alkalinity suggesting this column had the greatest rate of organic carbon degradation.

2.5.3 Mercury mobilisation

An initial high release of THg-0.45 in the control column effluent could be attributed to the system equilibrating to the induced flow conditions and potential transport of particles. The THg-0.45 concentrations in the acetate amended column were consistently higher than both the control and lactate columns. Acetate does not increase the dissolution of HgS particles nor does it bind to Hg as strongly as sulfur-containing ligands do (Ravichandran, 2004) and should not be directly correlated to the mobilization of Hg observed in the effluent. The presence of acetate and propionate produced from the incomplete oxidation of lactate in the lactate-amended column did not result in a similar mobilization of Hg.

2.5.4 Pore water MeHg production

The MeHg concentrations in the control column effluent were correlated with both Fe concentrations and the mass of SO_4^{2}-consumed with adjusted R^2 of 0.862 and 0.903 respectively and p-values <0.001. Geochemical speciation calculations of the column effluent using MINTEQA2 indicated the majority of the Fe at the end of the column life was present as the reduced species Fe^{2+}. The simultaneous reduction of Fe and SO_4^{2-} is not unusual (Postma and Jakobsen, 1996) as bacteria can use multiple sources as terminal electron acceptors; various SRB also have the capability of using Fe(III) during anaerobic respiration (Barns and Nierzwicki-Bauer, 1997). Both IRB and SRB are thought to contribute to MeHg production at this site and these findings may provide further support to the contributions of both bacterial groups (Yu et al., 2012).

The MeHg production in the lactate and acetate columns was similar when compared on a percentage of THg basis, but differ with respect to the mass of MeHg produced. Concentrations of MeHg were observed in greater concentrations in the acetate column compared to the lactate column. As SO_4^{2-} concentrations were below analytical detection limits (0.01 mg L^{-1}), a correlation between MeHg and SO_4^{2-} consumed could not be determined. The MeHg concentrations in the acetate column were correlated with both H_2S and Fe concentrations (p-values <0.05). No correlation in the lactate column was observed between MeHg and the SO_4^{2-} consumed, H_2S produced or Fe concentrations.

A positive correlation was observed in the lactate-sulfate column between MeHg and H_2S concentrations in the effluent (adjusted R^2 of 0.818, p-value <0.001). The highest percentage observed of MeHg in the effluent corresponded to the greatest concentration of H_2S. The decline in MeHg at the end of the column life independent of THg output may be due to reductive demethylation by microbes producing methane which is known to take place in the riverbank sediments of the South River (Yu et al., 2012). The addition of 10 mM SO_4^{2-} into this column and high concentrations of H_2S which developed did not appear to inhibit methylation as was proposed and observed in the literature (Gilmour & Henry, 1991; Harmon et al., 2007). This study involved working with a sediment that already contained elevated concentrations of Hg and was not spiked with $HgCl_2$ or $HgNO_3$ as in Gilmour & Henry (1991) or Harmon et al., (2007) in their respective studies. Harmon et al. (2007) ended the experimental time of their study after 35 days, which may have been too short of a time to observe methylation of Hg. The lactate-sulfate column experiment explored in this study obtained maximum MeHg production after 48 days. It is likely the Hg was mainly in the form of HgS in the South River sediment used in the column experiments, which is the case at another location of the South River site (Desrochers, 2013). The increase in labile organic carbon through influent amendments may have increased the nanoparticulate portion of HgS through enhanced dissolution (Slowey, 2010) and made the HgS available for methylation (Zhang et al., 2012). The highest percentage of aqueous MeHg (41% of the THg) occurred in the bottom port which also had concentrations of 55.0 mg L^{-1} of H_2S. The presence of high concentrations of H_2S at this column location

with high conversion to MeHg may indicate that H_2S accumulation did not inhibit MeHg formation in this study. The greatest conversion of THg to MeHg was found at the column location closest to the influent and declined along the length of the column, mirroring the trend of the *Desulfovibrio*-related sequences identified in the sediment.

2.5.5 Column redox conditions at time of sectioning

The late-time pore water chemistry of the column effluents were compared to parameters (Table 2.3) which suggested that at termination of the columns the control column was entering mixed Mn(IV)- and Fe(III)-reducing conditions, the acetate and lactate columns were in dominant Fe(III)-reducing conditions, and the lactate-sulfate column was the only column that firmly established SO_4^{2-}-reducing conditions (Chappelle et al., 2009). The sharp decline in H_2S and further decline in SO_4^{2-} concentrations at the end of the lactate-sulfate column experiment could indicate the beginning of methanogenesis (Stumm & Morgan, 1996).

Due to the low concentrations of SO_4^{2-} in the SRW (~0.11 mM) with subsequently little to no H_2S production, the acetate and lactate columns did not transition from predominantly Fe(III)-reducing to SO_4^{2-}-reducing conditions. This shift from Fe(III)-reducing to SO_4^{2-} -reducing processes was observed by Anderson et al. (2003) using acetate as an organic carbon source for U(VI) reduction. It is likely that in both the acetate and lactate columns SO_4^{2-} reduction occurred very close to the influent as SO_4^{2-} concentrations declined immediately in the bottom ports after the influents were switched. The organic carbon amended columns therefore likely became SO_4^{2-}-limited quickly.

2.5.6 Changes in bacterial community and Hg methylators

There were relatively low viable populations of both SRB and IRB present in the control column as determined through MPN enumerations when compared with the three organic amended columns. The control column sediment had IRB present in greater numbers than SRB. The greatest viable populations

of IRB were enumerated in the acetate column but not in the lactate column even though both had similar reduced Fe concentrations in the effluent. The difference in enumerated IRB and SRB in the acetate and lactate columns may suggest that Fe(III) reduction in the lactate column followed a different pathway other than through the IRB that could be enumerated. The significant accumulation of reduced Fe in both the acetate and lactate columns suggested dissimilatory Fe(III) reduction was taking place (Lovley, 1991). The viable populations of SRB were highest in the lactate-sulfate column and outnumbered the IRB except for the sediment closest to the effluent, indicating a possible switch from IRB to SRB as some SRB have a slower growth rate. This switch from IRB to SRB over time was similar to an observation by Druhan et al. (2012) under field conditions.

The Deltaproteobacteria in the column show distinct differences in the bacterial communities between the columns. Mosher et al. (2012) found correlations between the *Desulfobulbus* population and MeHg production at a Hg contaminated site, while in the South River bank sediment evaluated in this study no correlation was observed between this particular genus and MeHg production. There were a higher proportion of *Desulfobulbus*-related sequences in the control column compared with the lactate column but a lower concentration of MeHg was observed in the effluent. Sequences identified as *Desulfobulbu*s were also higher in the acetate amended column than the lactate column, yet both had a similar percentage of MeHg in the effluent. Research by King et al. (2000) suggests that acetate enhances Hg methylation through growth of acetate-utilizing SRB such as *Desulfobacter* in slurries. *Desulfobacter* did not appear to have the same correlation with MeHg as in King et al. (2000) as the four column experiments had no observable trend between % of identified species of *Desulfobacter* and mass of MeHg in the column effluent.

Geobacter spp., the only known/predicted methylator identified in the control column through PCR, may be responsible for the MeHg observed in the column effluent, though it is possible that another bacteria or groups of bacteria yet to be identified may be responsible. Comparing the lactate and acetate columns, even though there is a greater percentage of *Desulfovibrio putealis* and species related to

Desulfosporosinus in the lactate column than the acetate, there was no associated rise in MeHg observed in the effluent. *Desulfovibrio putealis* dominated the sequence counts of the methylating bacteria in the lactate-sulfate column, with the greatest counts nearest to the influent coinciding with the greatest MeHg concentrations. It is likely that this species was responsible for the majority of the MeHg production in this column.

2.5.7 Solid-phase Hg and MeHg

The majority of the Hg present in the column sediments after sectioning was in the F4 or F5 fraction in comparison to the South River sediment prior to use in these experiments, where the Hg was found to be mainly in the F5 fraction. This loss of F5 to F4 fraction in the column sediments may be due to the induced anaerobic and saturated flow conditions. There was also no significant loss of Hg in the sediment from the columns due to leaching over the course of the experiment. The consistently higher values obtained from the THg extractions compared to the sum of the Hg sequential extractions could be due to the longer reaction time with aqua regia during the THg extraction and/or loss during the Hg sequential extraction process.

Solid-phase MeHg concentrations present in the column sediments accounted for <1% of the THg, which is consistent with the range of 0.01-1% of the THg in sediments in Bloom et al. (2003). The greatest accumulation of solid-phase MeHg and % of THg observed in the lactate-sulfate column sediment interval closest to the influent corresponded to the highest % MeHg concentrations measured in the pore water.

2.6 Conclusions

The organic amendments in the three columns promoted an increase in net Hg methylation to different degrees relative to the control column. The bacterial communities in the sediment responded quickly to changes in their environment under saturated flow. It is possible that the MeHg concentrations produced in the acetate and lactate column effluents were linked to both IRB and SRB in these sediments. The aqueous MeHg produced in the lactate-sulfate column corresponded to greater numbers of *Desulfovibrio putealis* and may indicate that this species may be the main contributor to Hg methylation in this column. There was no observed suppression of methylation with either high H_2S or SO_4^{2-} conditions as has been reported previously, with the only control on methylation in the lactate-sulfate column possibly being bacterial demethylation and subsequent movement from sulfidic conditions to methanogenic. It appeared as though acetate increased the mobilization of Hg, though the mechanisms behind this mobilization need to be explored in more detail. The high H_2S present in the lactate-sulfate column effluent did not appear to inhibit MeHg formation and strongly correlated to aqueous MeHg.

Table 2.1: Solid-phase chemical composition of South River sediment used in column studies.

	($\mu g\ g^{-1}$) dry weight						
Sample Location	**Hg**	**Fe**	**Mn**	**TOC**	**TIC**	**Total C**	**Total S**
RRM 3.5 - D	167	16 000	230	17 600	3 200	19 300	300

Table 2.2: Chemical composition of column influent solutions with error reported as one standard deviation from the mean.

	Influent Solution			
Parameter	SRW	Acetate	Lactate	Sulfate-Lactate
pH	8.53 (±0.06)	8.04 (±0.04)	7.95 (±0.09)	7.85 (±0.11)
Eh (mV)	281.8 (±30.9)	334.6 (±37.4)	320.6 (±34.6)	191.5 (±201.5)
Alk (mg L^{-1} as $CaCO_3$)	121.5 (±14.2)	368.4 (±31.7)	254.1 (±39.3)	247.4 (±44.7)
Hg (ng L^{-1})	6.5 (±2.1)	5.2 (±4.1)	5.0 (±2.7)	7.3 (±6.4)
Cl^- (mg L^{-1})	6.0 (±0.3)	5.8 (±0.6)	5.5 (±0.3)	5.4 (±0.2)
NO_3^- (mg L^{-1})	0.8 (±1.0)	1.3 (±1.3)	1.3 (±1.2)	1.2 (±1.0)
SO_4^{2-} (mg L^{-1})	11.6 (±0.3)	10.9 (±0.8)	11.1 (±1.0)	970.6 (±2.0)
Ca (mg L^{-1})	26.4 (±0.8)	29.7 (±2.4)	27.0± (1.8)	28.7 (±1.9)
K (mg L^{-1})	2.7 (±0.4)	2.6 (±0.1)	3.0± (0.3)	4.2 (±1.2)
Mg (mg L^{-1})	10.6 (±0.5)	11.5 (±0.9)	10.4 (±0.5)	11.0 (±0.9)
Na (mg L^{-1})	6.2 (±0.1)	151.0 (±6.3)	141.6 (±0.6)	600.2 (±12.8)
Si (mg L^{-1})	3.7 (±0.1)	3.6 (±0.7)	3.5 (±0.2)	4.2 (±0.5)
Mn (μg L^{-1})	2.1 (±3.1)	<0.4	<0.4	<0.4
Fe (μg L^{-1})	6.4 (±2.2)	7.0 (±5.1)	9.7 (±8.66)	39.5 (±39.0)
Lactate (mg L^{-1})	<0.03	<0.03	512.0 (±16.4)	511.3 (±11.3)
Acetate (mg L^{-1})	0.75 (±1.3)	341.9 (±27.7)	<1.0	<1.0

Table 2.3: Distinguishing anoxic reduction zones.

General Criteria for Distinguishing Between Redox Processes: Modified from Chappelle et al. (2009)								
		Water Chemistry (mg L^{-1})						
General Redox Category	**Dominating Process**	O_2	NO_3^-	Mn^{2+}	Fe^{2+}	SO_4^{2-}	Fe^{2+}/H_2S Ratio	Notes
Anoxic	NO_3^- Reduction	<0.5	≥0.5	<0.05	<0.1			
	Mn(IV) Reduction	<0.5	<0.5	≥0.05	<0.1			
	Fe(III) Reduction	<0.5	<0.5		≥0.1	≥0.5	>10	
	Mixed Fe(III)/SO_4^{2-} Reduction	<0.5	<0.5		≥0.1	≥0.5	≥3≤10	
	SO_4^{2-} Reduction	<0.5	<0.5		≥0.1	≥0.5	<3	
Mixed								Criteria are met for more than one process

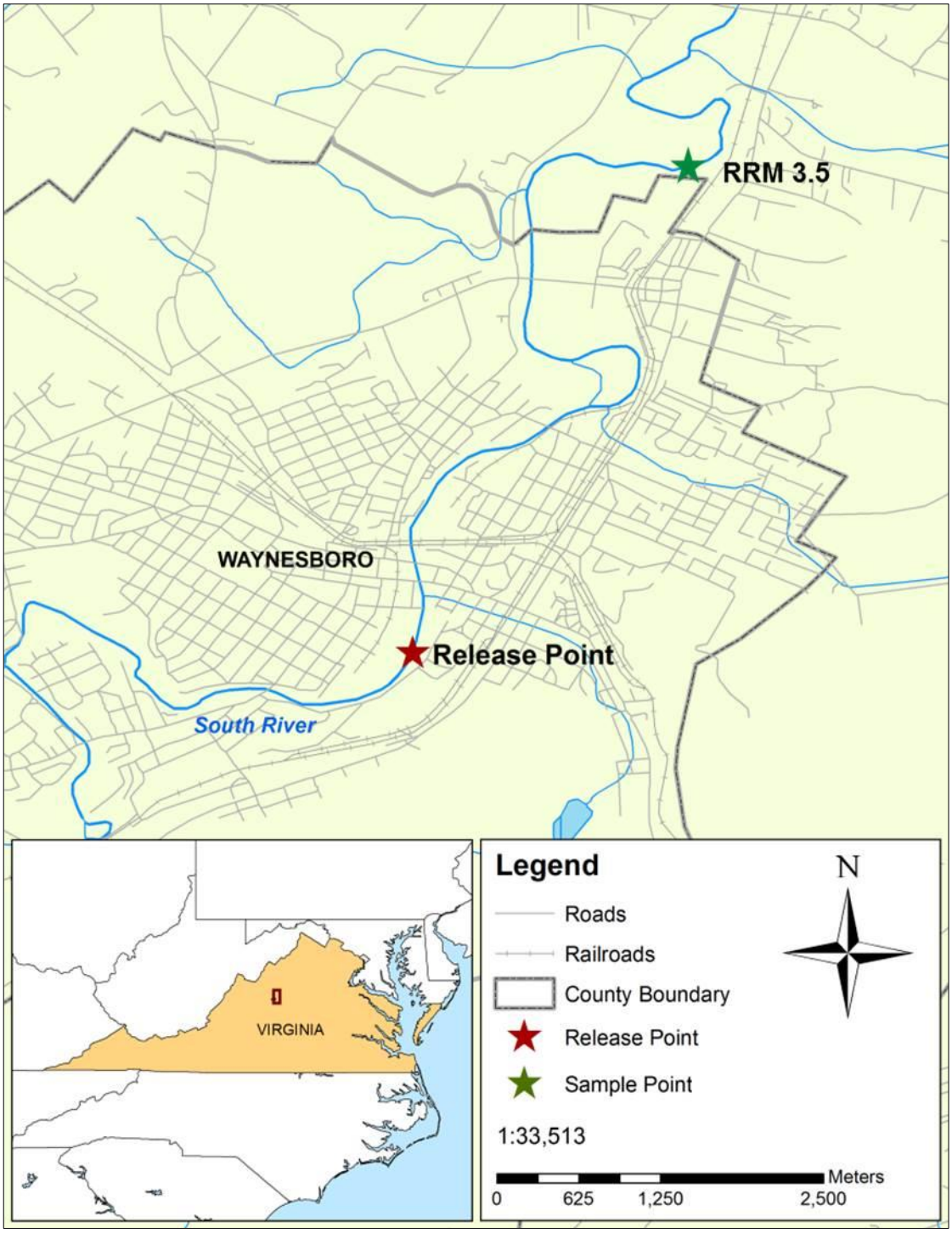

Fig. 2.1: Location of sediment D at RRM 3.5 relative to the point of historical Hg release.

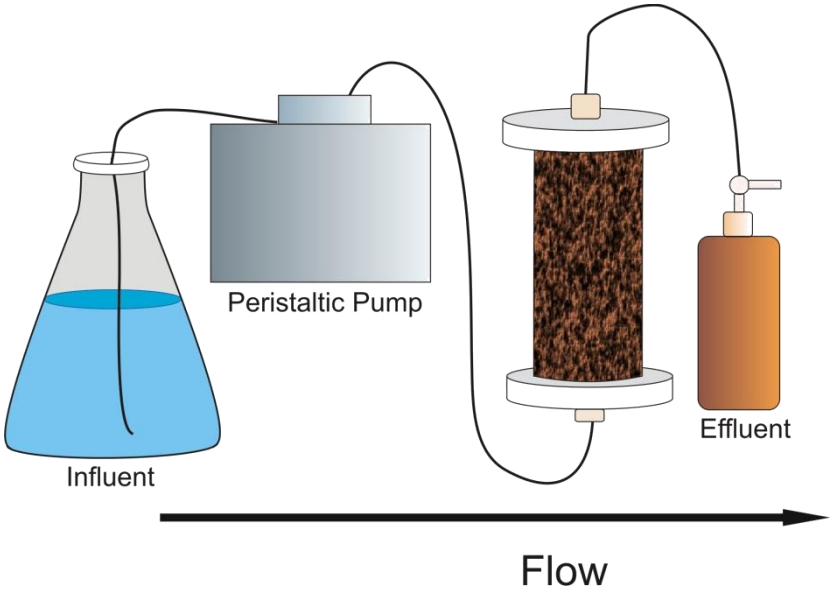

Fig. 2.2: Schematic diagram showing experimental set-up and column design.

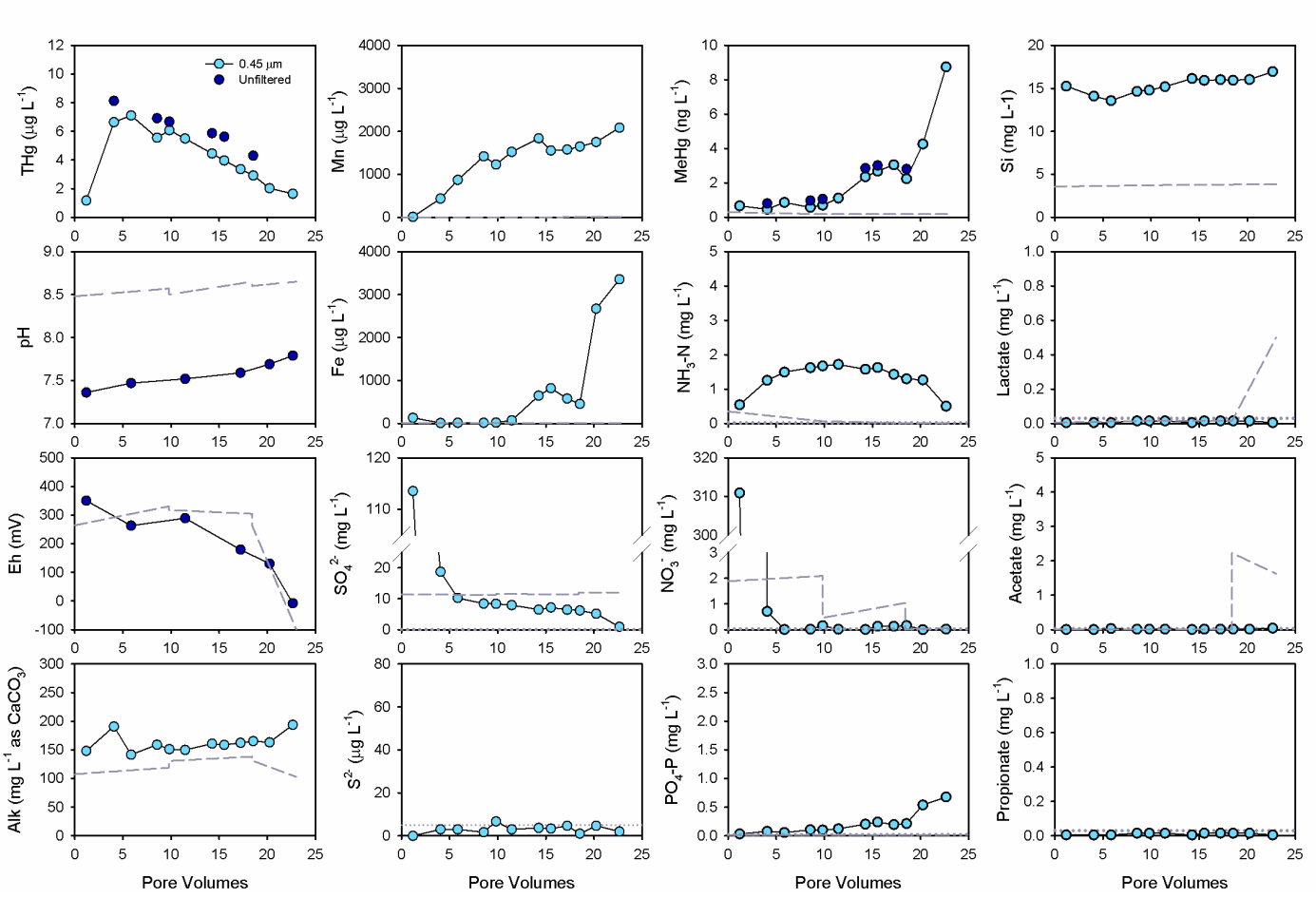

Fig. 2.3: Inorganic and organic concentrations monitored over time in the control column effluent. Note dashed lines represent the influent concentrations, while dotted lines indicate analytical detection limits.

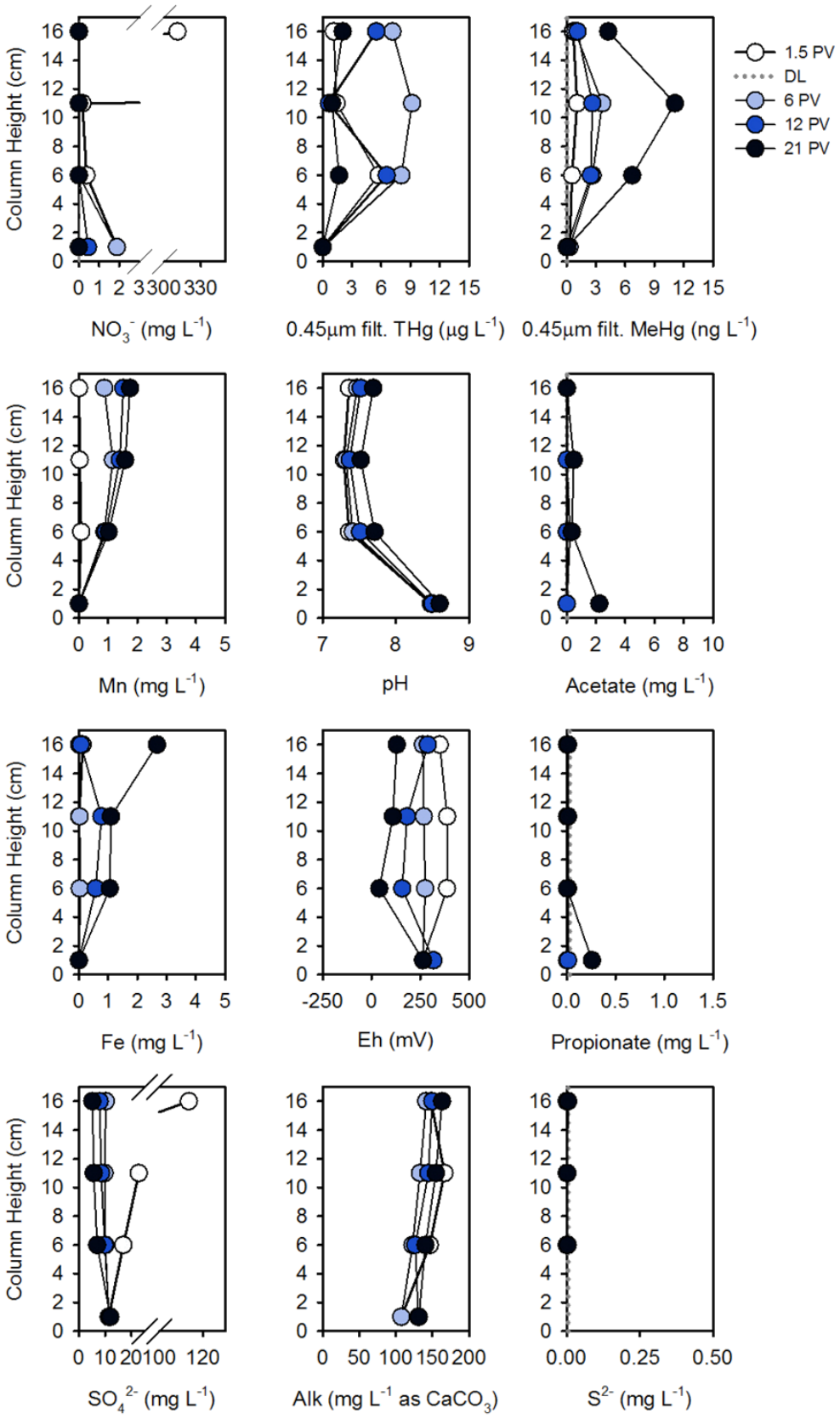

Fig. 2.4: Concentrations of Hg, MeHg, pH, alkalinity and redox indicators for aqueous samples collected along the control column length.

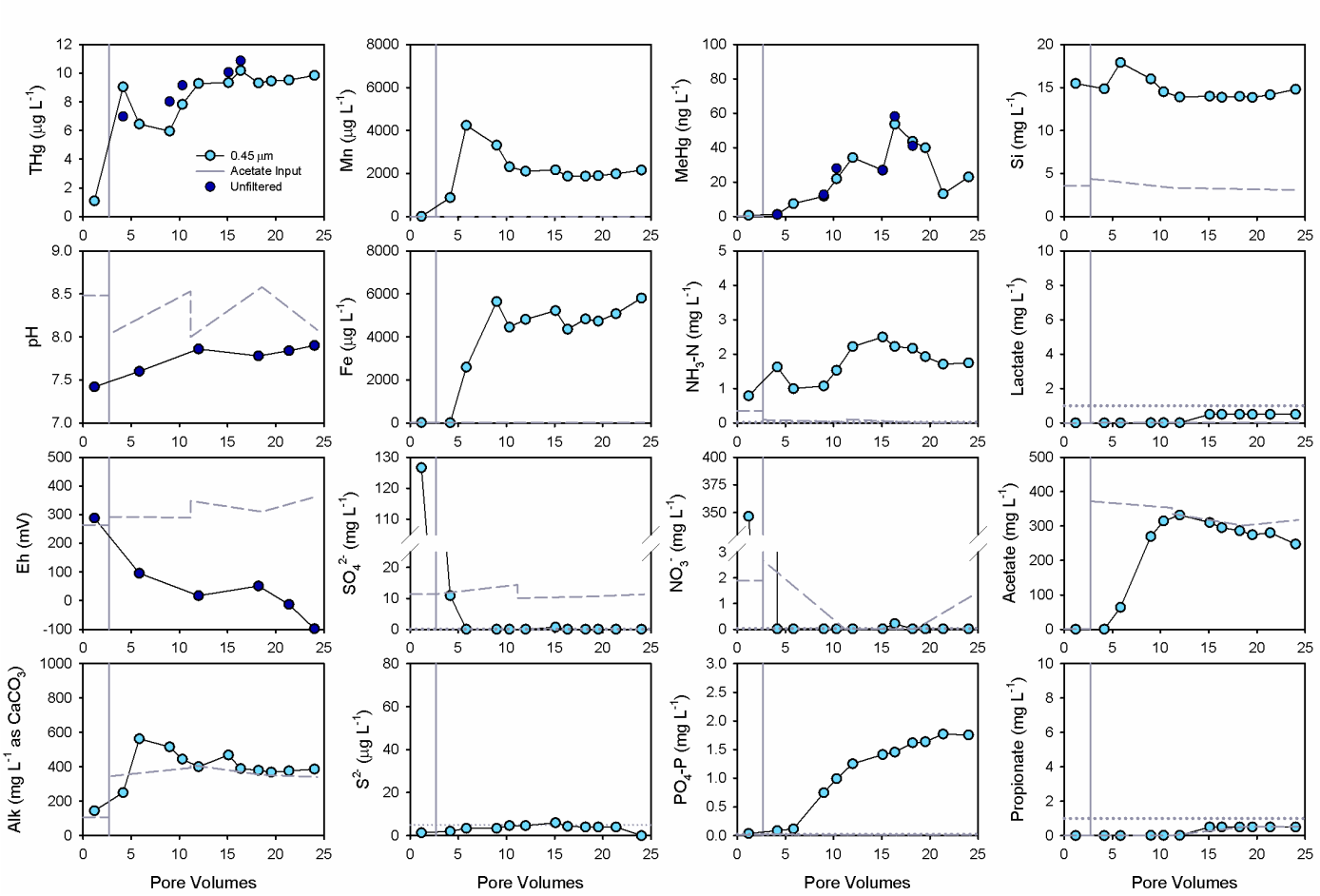

Fig. 2.5: Concentrations of inorganic and organic constituents versus time in the acetate column effluent. Dashed lines indicate influent concentrations while dotted lines indicate analytical detection limits.

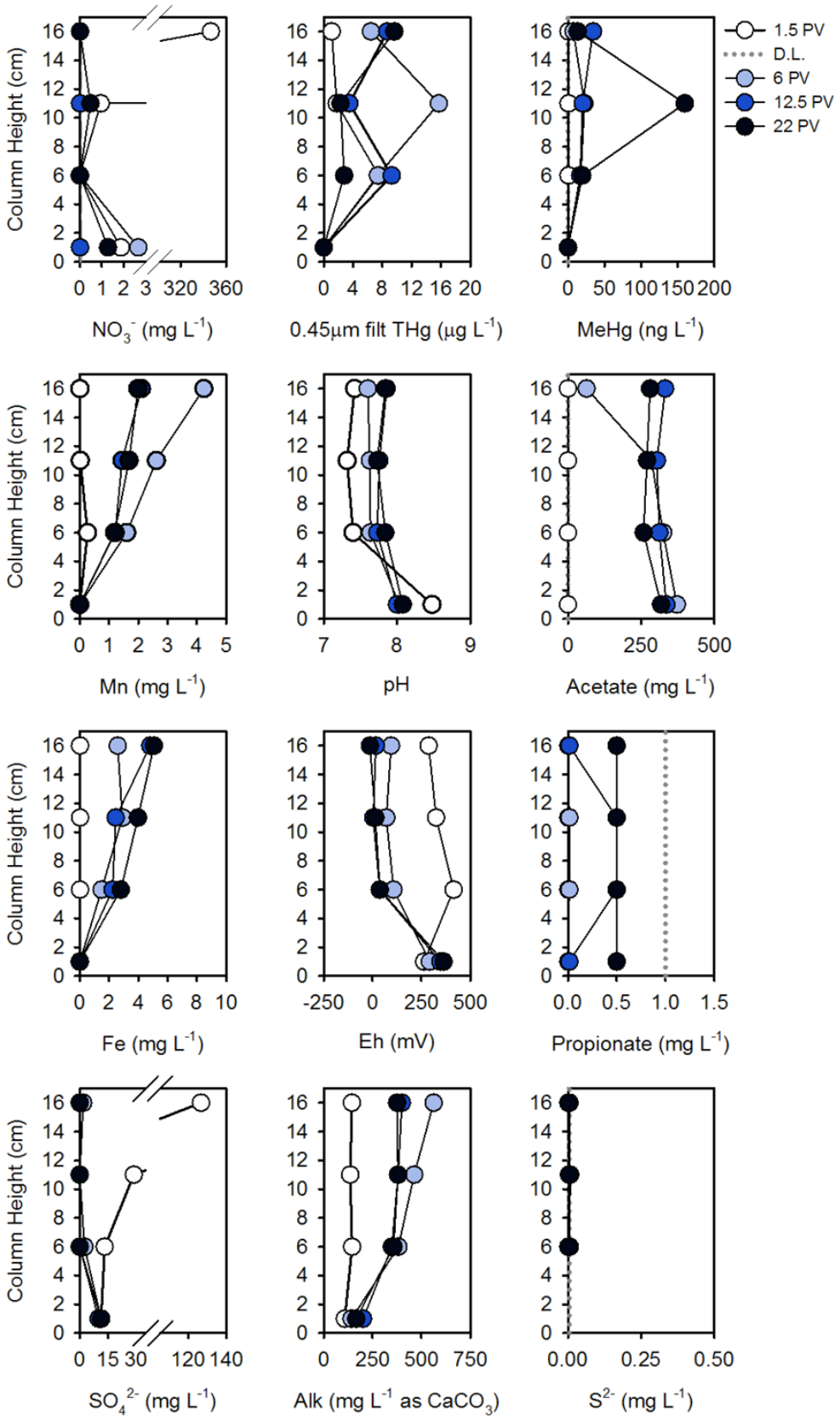

Fig. 2.6: Concentrations of Hg, MeHg, pH, alkalinity and redox indicators for aqueous samples collected along the acetate column length.

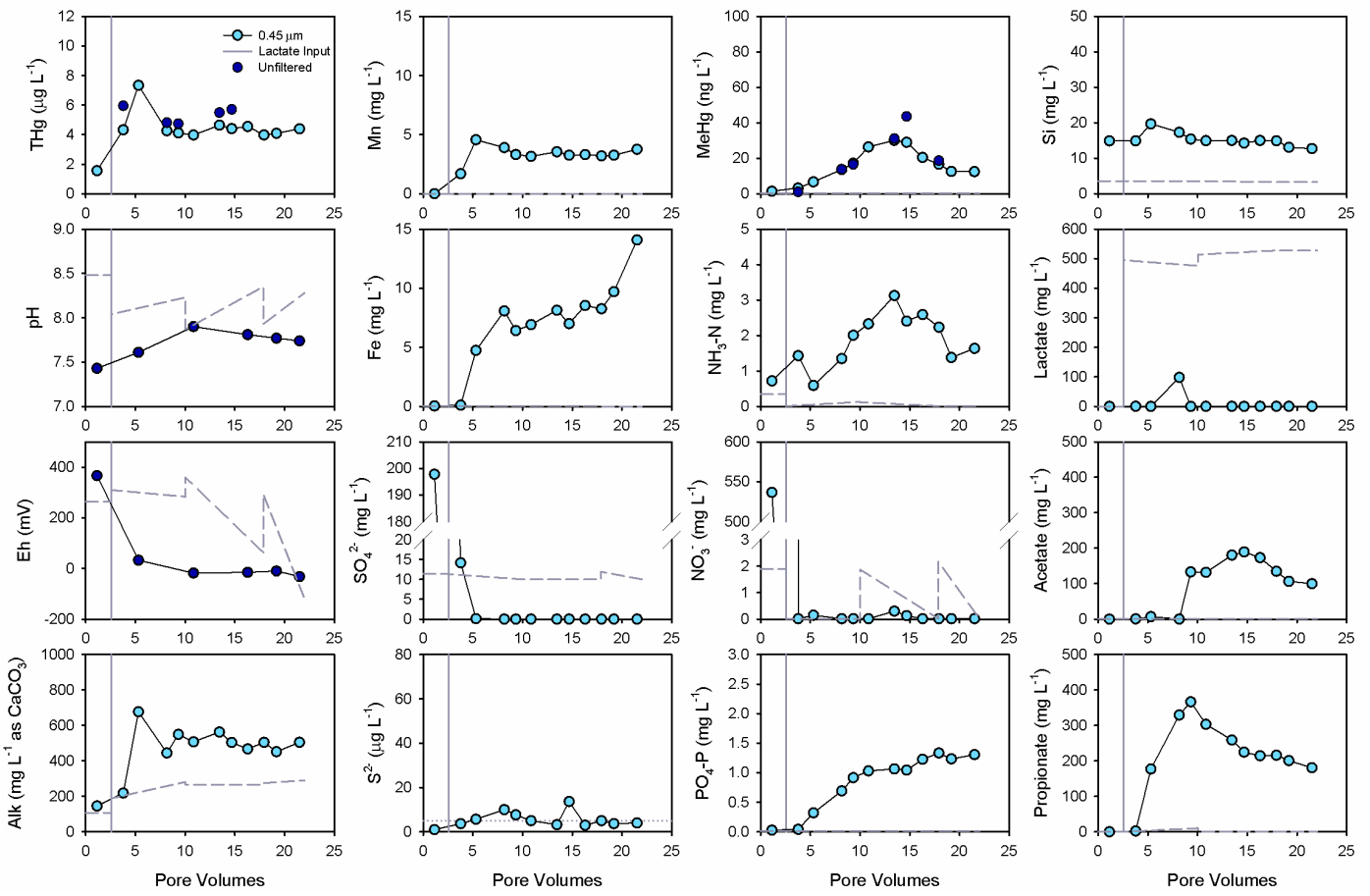

Fig. 2.7: Inorganic and organic concentrations monitored over time in the lactate column effluent. Note dashed lines represent the influent concentrations, while dotted lines indicate analytical detection limits.

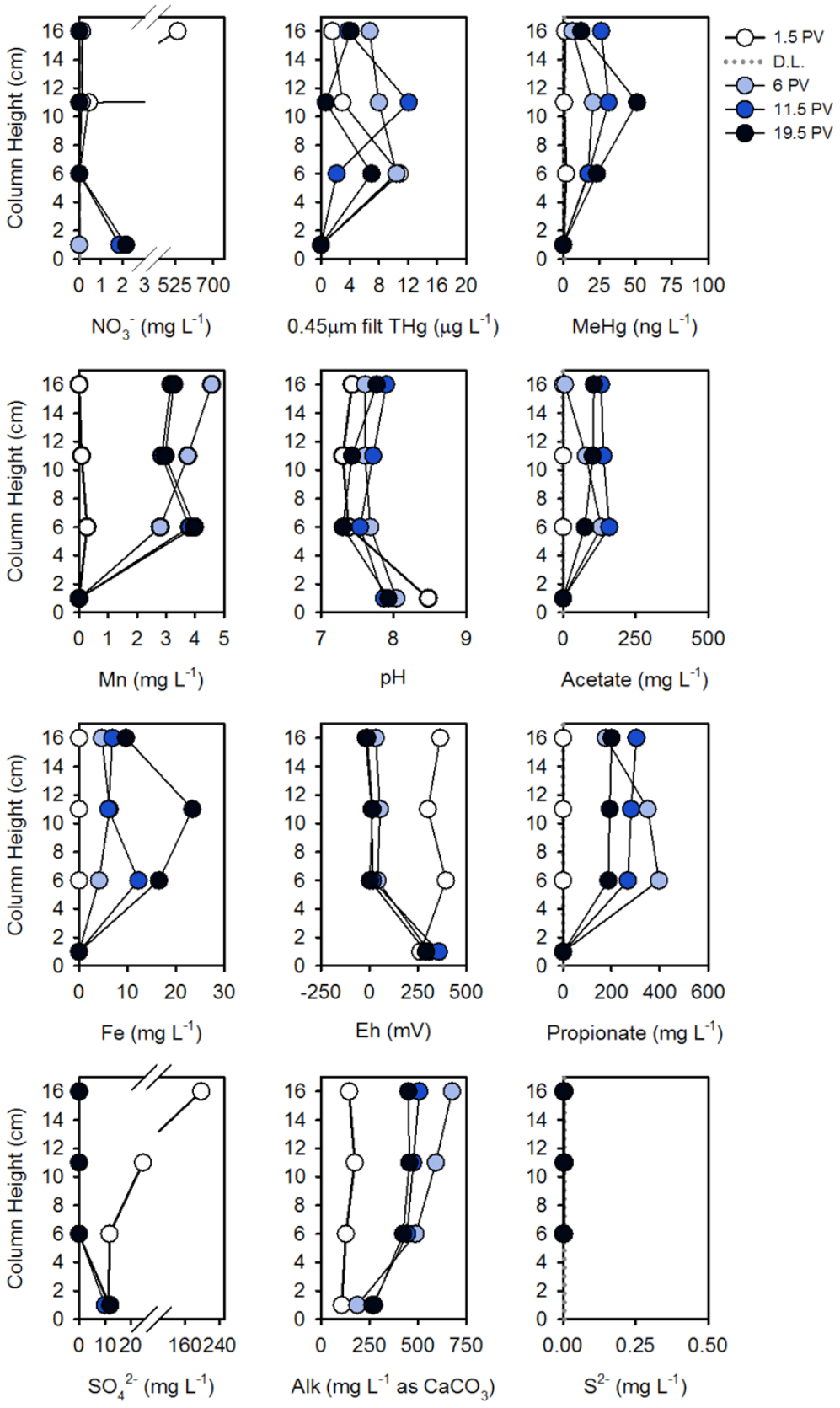

Fig. 2.8: Concentrations of Hg, MeHg, pH, alkalinity and redox indicators for aqueous samples collected along the lactate column length.

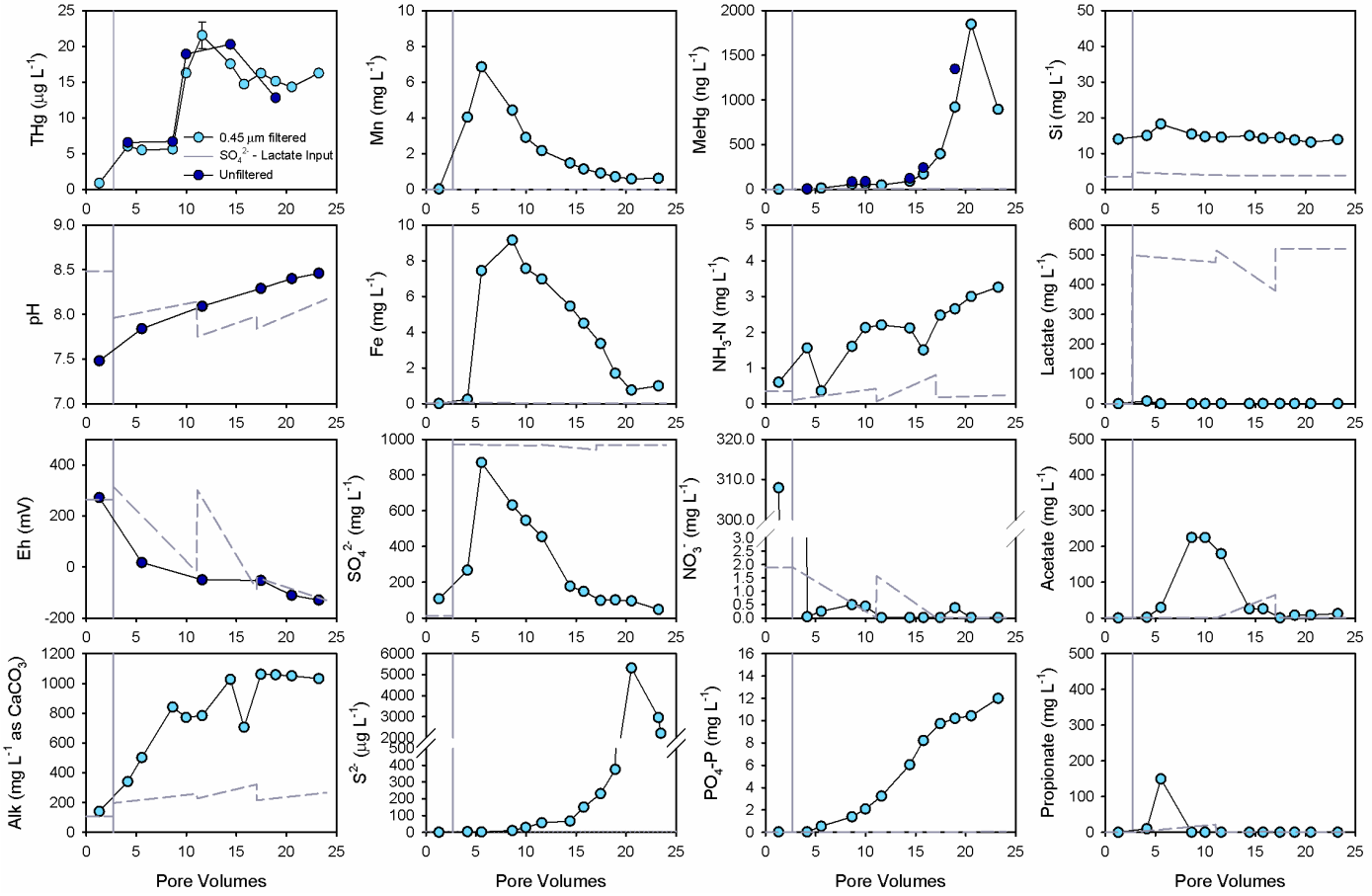

Fig. 2.9: Inorganic and organic concentrations monitored over time in the lactate-sulfate column effluent. Note dashed lines represent the influent concentrations, while dotted lines indicate analytical detection limits.

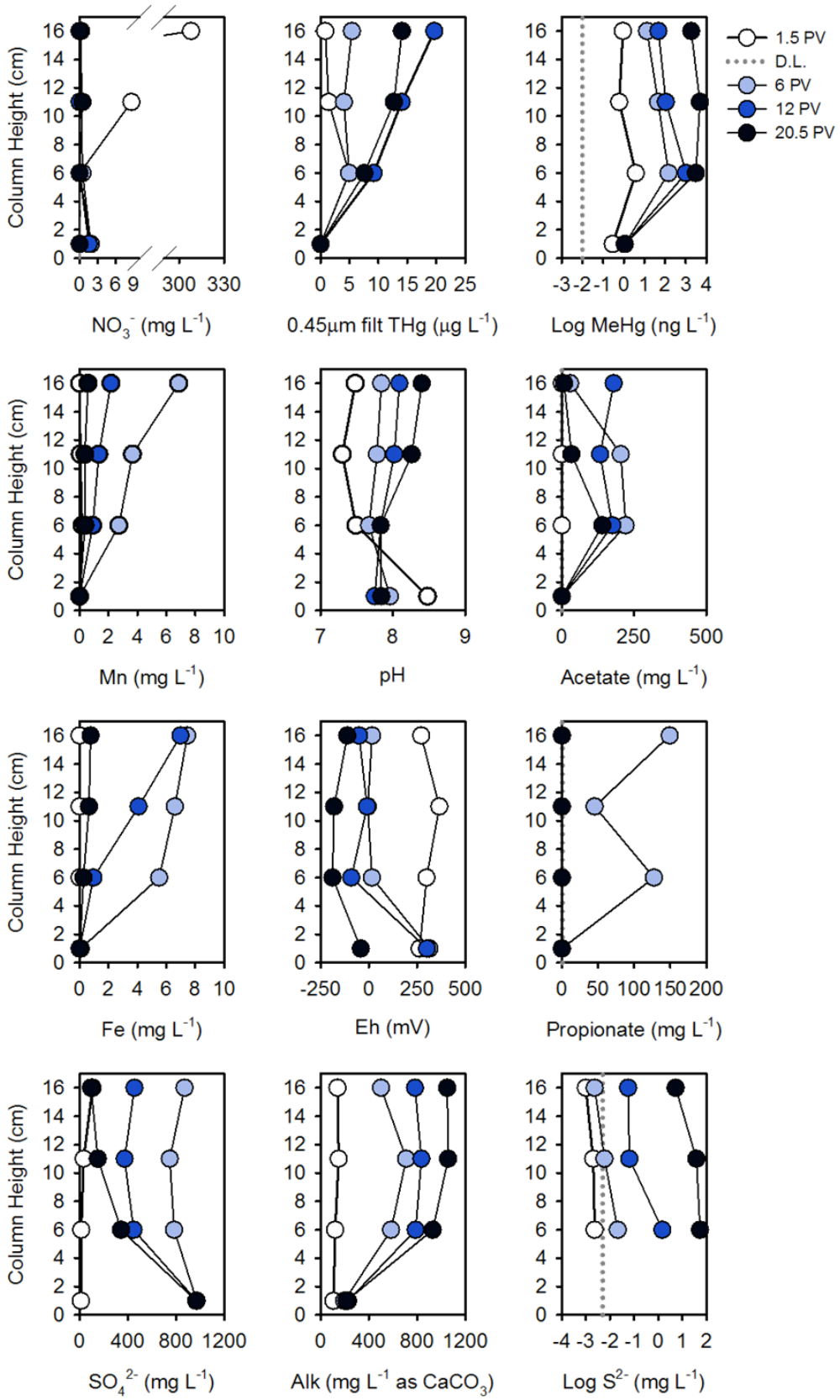

Fig. 2.10: Concentrations of Hg, MeHg, pH, alkalinity and redox indicators for aqueous samples collected along the lactate-sulfate column length. Note change in scale for sulfide.

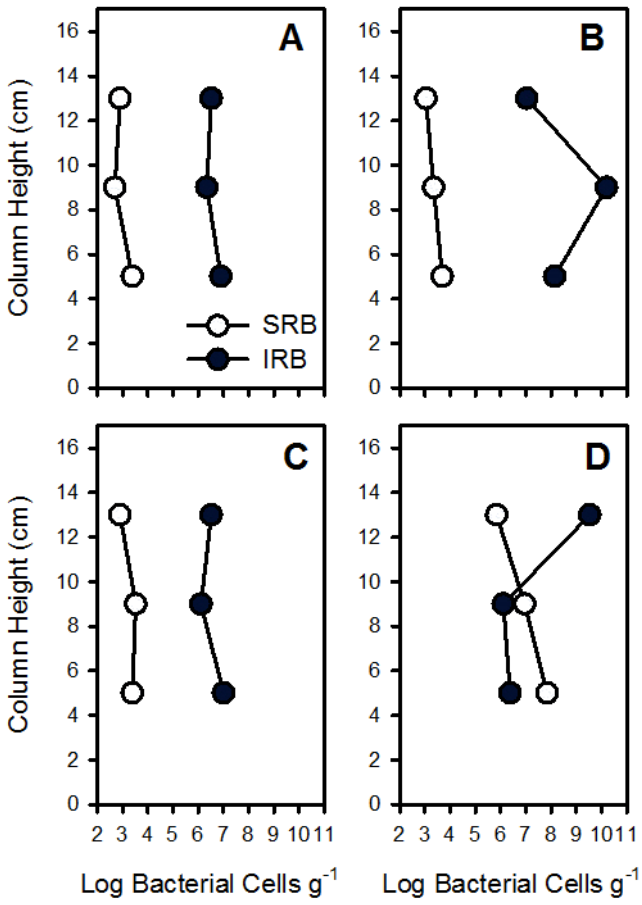

Fig. 2.11: MPN enumeration results for solid-phase samples collected at different locations along the length of the columns. The letters A, B, C and D refer to the control, acetate, lactate and lactate-sulfate columns respectively.

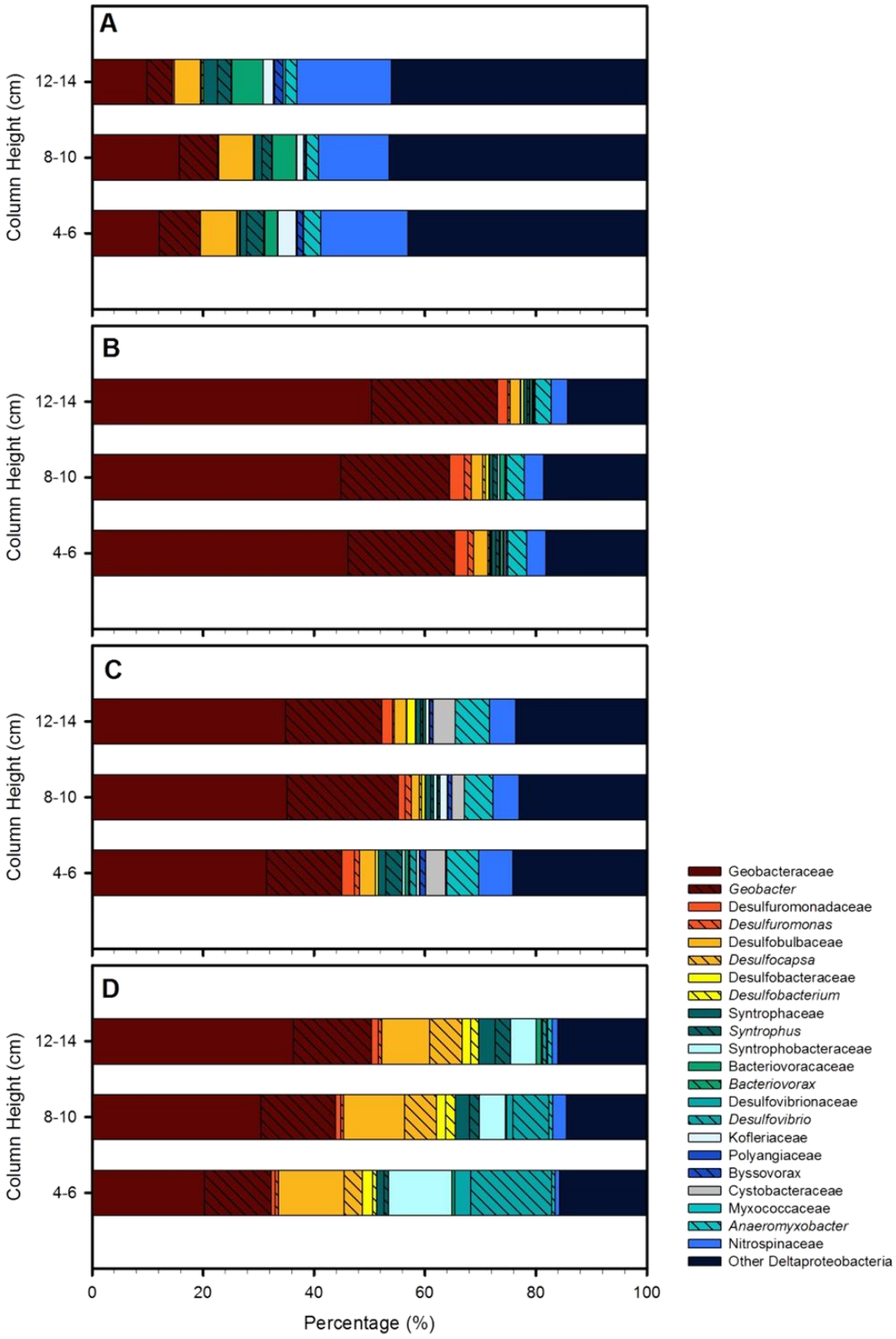

Fig. 2.12: Deltaproteobacteria identified from PCR analysis for all columns at time of sectioning, with the letters A, B, C, and D representing the control column, acetate column, lactate column and lactate-sulfate column respectively. Colours represent Family while added patterns highlight the dominant genus identified.

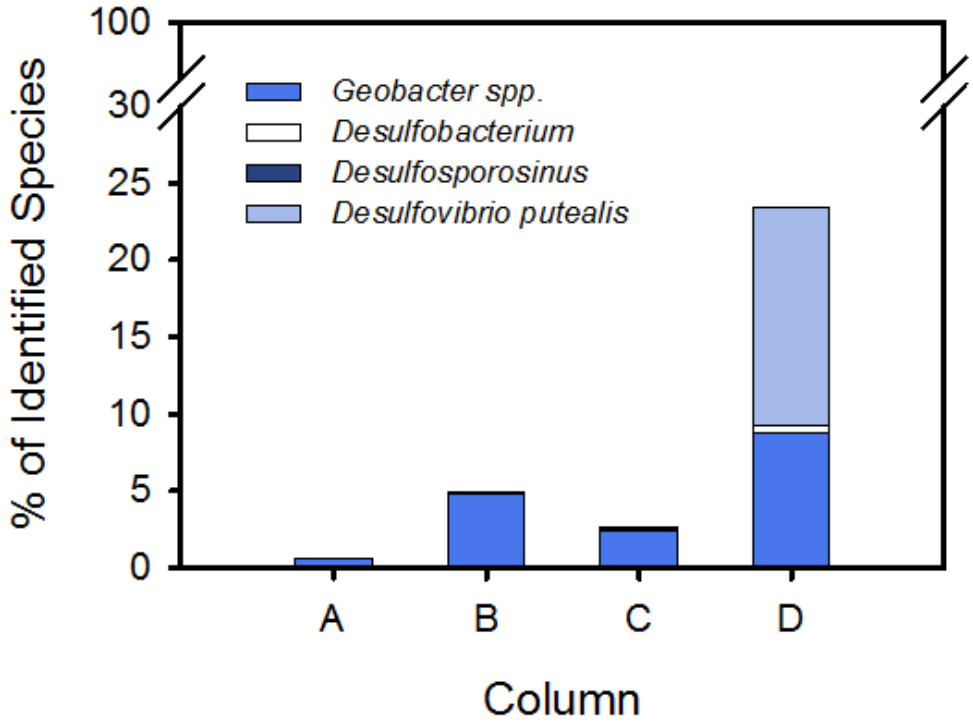

Fig. 2.13: Percentage of species identified as known Hg methylators averaged over the length of the columns. The letters A, B, C and D represent the control, acetate, lactate and lactate-sulfate columns respectively.

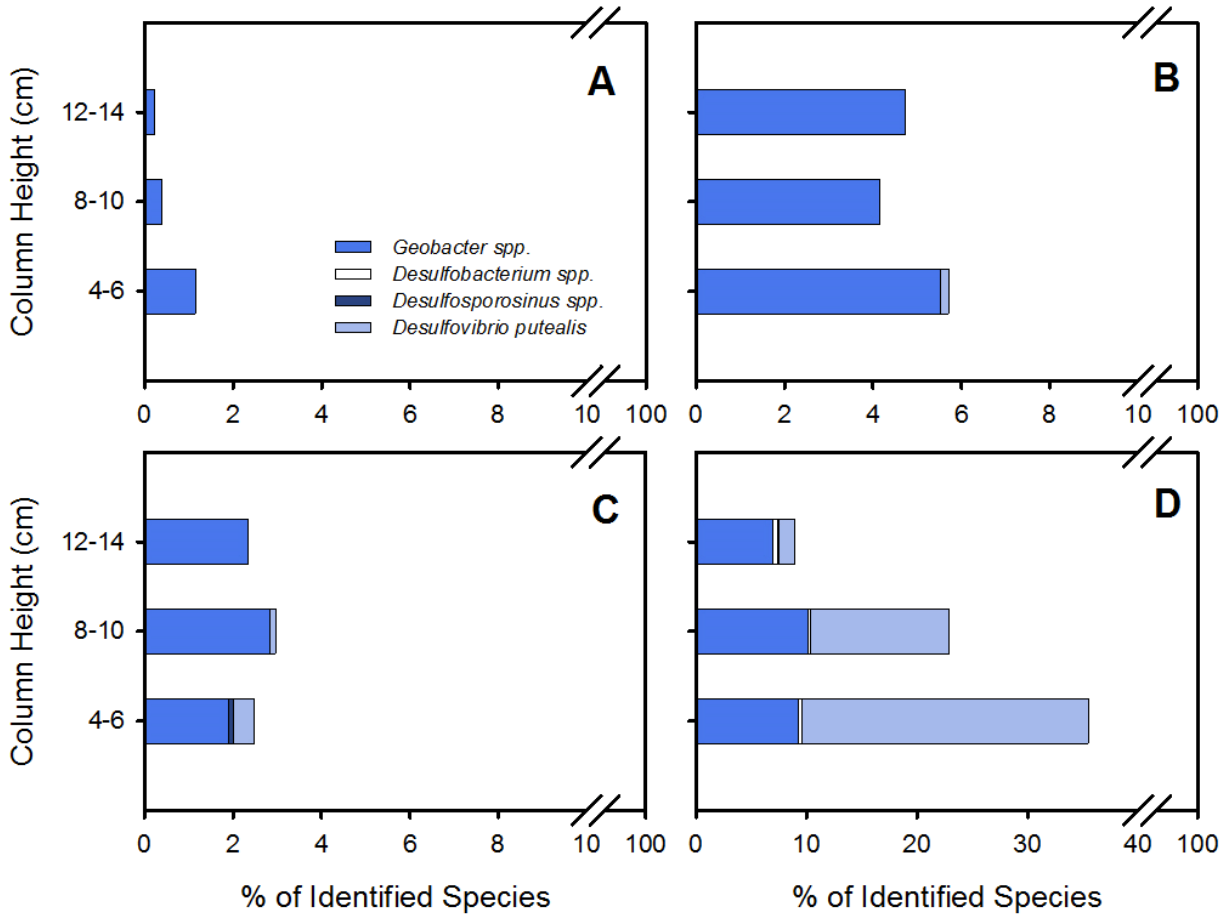

Fig. 2.14: Percent of known Hg methylators identified at different distances along the column through PCR analysis. The letters A, B, C and D refer to the control, acetate, lactate and lactate-sulfate columns respectively.

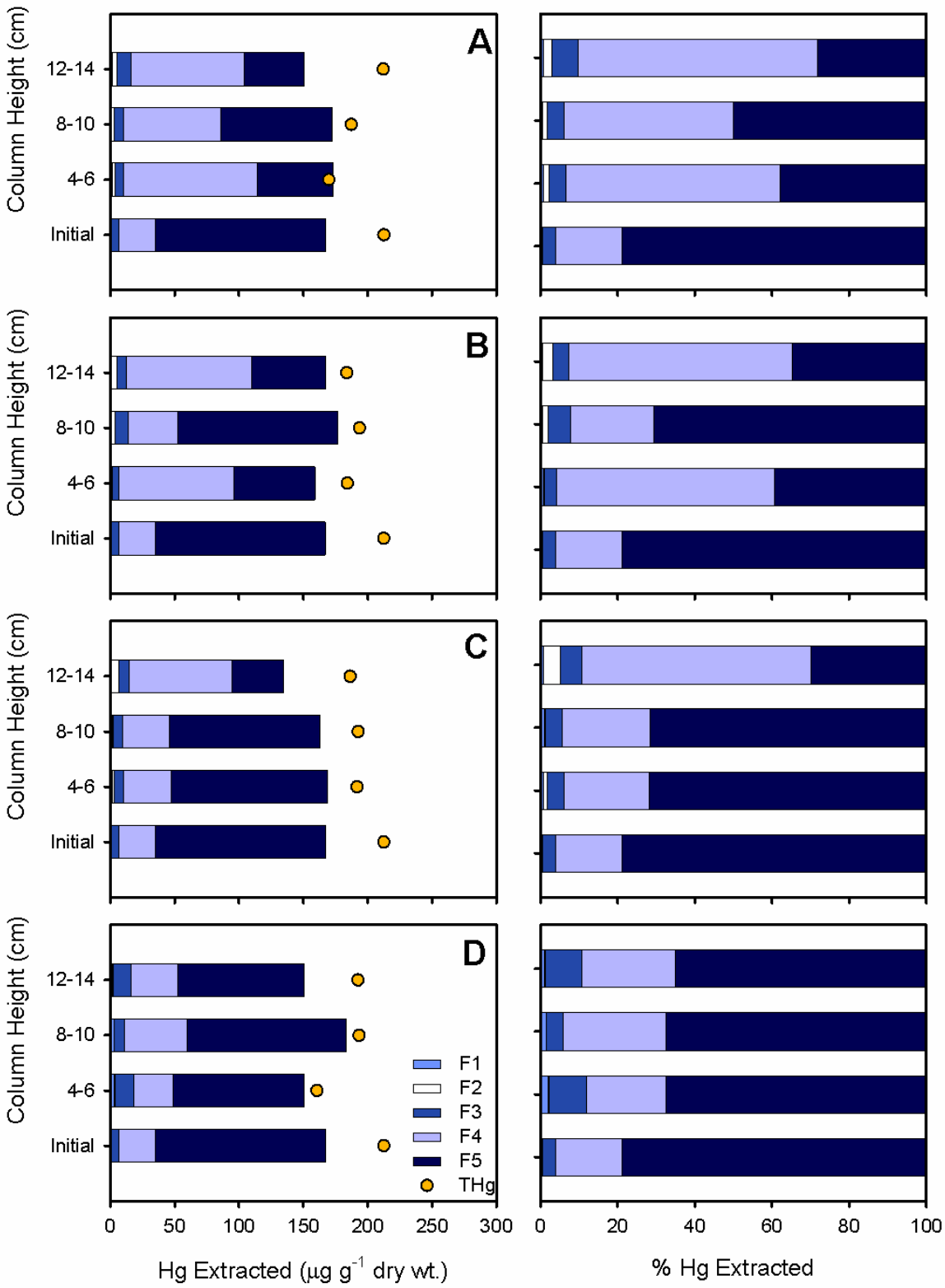

Fig. 2.15: Mass and percent of THg and Hg obtained through sequential extraction analyses present in the column sediments at the termination of the experiment. The F1 fraction targets water soluble Hg, F2 weak acid extractable, F3 organo-complexed, F4 elemental/strongly complexed and F5 the Hg-sulfide fraction. The letters A, B, C and D refer to control, acetate, lactate and lactate-sulfate column respectively.

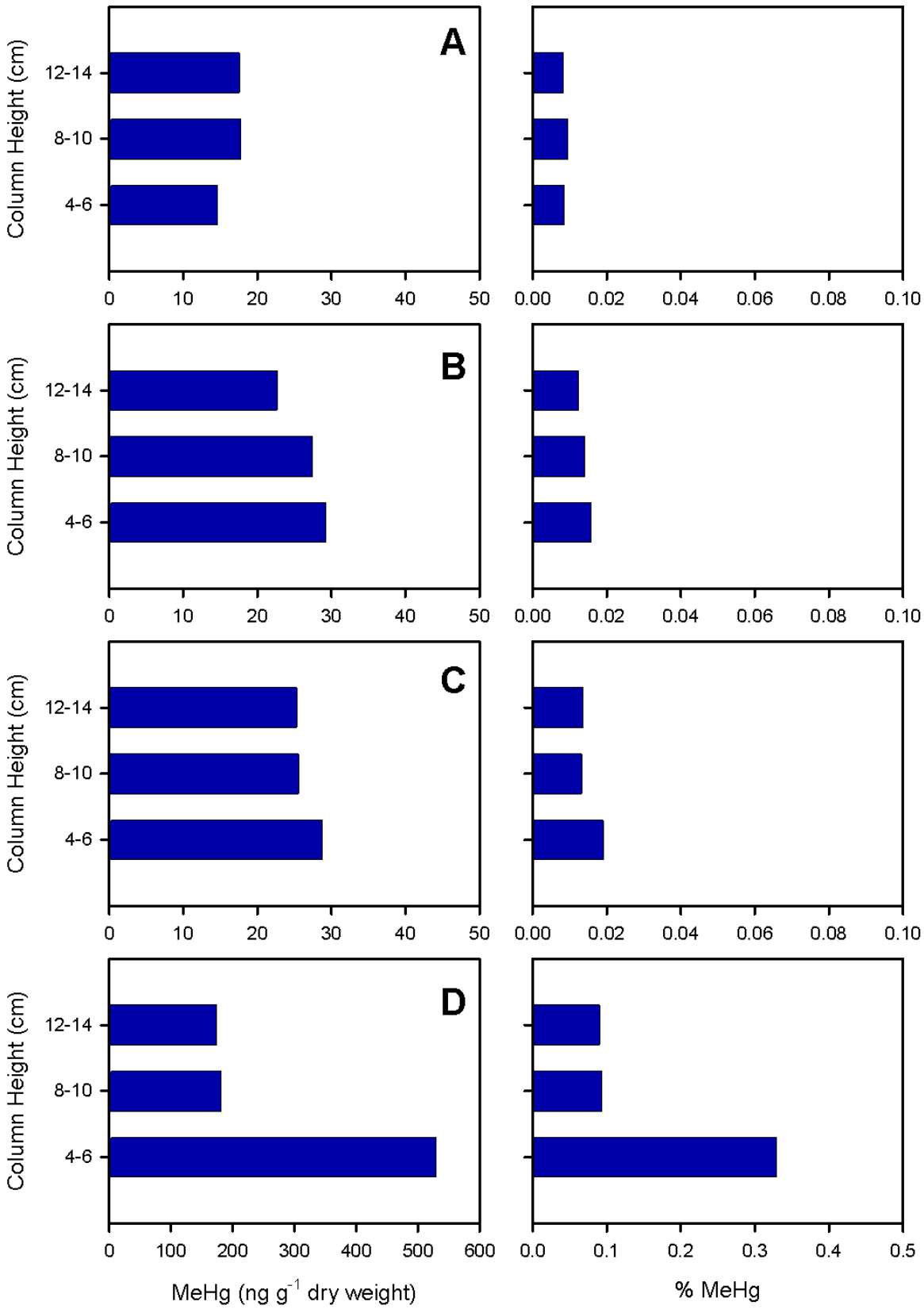

Fig. 2.16: Concentrations of MeHg in the sediment at the termination of the experiment. The letters A, B, C and D refer to control, acetate, lactate and lactate-sulfate column respectively.

Chapter 3: *Assessment of Biochar as a Treatment Material for Mercury under Saturated Flow Conditions*

3.1 Executive Summary

Remediation of mercury (Hg) in riverbank sediments involves complexities that arise from the typically large area and dynamic nature characteristic of river systems. If a treatment material is applied in remediation efforts it must be stable under variable environmental conditions, and also must not promote increases in Hg bioavailability. Elevated concentrations of Hg are present in riverbank sediments and floodplain soils along the South River, near Waynesboro, VA, USA. Previous studies focused on biochar as a treatment material which potentially could be applied to remove Hg released from riverbank sediments. A column experiment was conducted to evaluate the release of Hg from riverbank sediments under continuous flow conditions. The effluent from the sediment column was then passed through a second column containing biochar to evaluate the removal of Hg. A decline in the dissolved Hg concentrations from 399 ng L^{-1} ±91 to < 6.2 ng L^{-1} ±1.9 (representing >98% removal of 0.45 μm filtered total Hg) was observed in the biochar column, with the removal occurring mainly within the first few cm of material. After 1.4 years of treating Hg, the influent to the biochar column was switched to low-Hg river water, followed by an influent of simulated acid rain water (regional pH of ~4.6), to evaluate the stability of the Hg. With low-Hg river water as the influent solution, there was no observed release of unfiltered and filtered Hg from the biochar with concentrations remaining near background values. With simulated acid rain water as an influent solution, there was a brief increase of unfiltered and 0.45 μm filtered Hg (78.5 ng L^{-1} and 56.6 ng L^{-1}) before returning to background levels. These results suggest that Hg-binding to the biochar was sufficiently strong to prevent release of Hg under aqueous chemistry conditions representative of clean river water and simulated acid rain water.

3.2 Introduction

3.2.1 Mercury

Mercury (Hg) is a toxic element which occurs as the reduced (Hg^0), ionic (Hg^{1+} and Hg^{2+}) and the highly toxic organic (CH_3Hg, $(CH_3)_2Hg$) forms. Mercury tends to associate with soft bases such as thiol compounds, involving mainly covalent bonding mechanisms as opposed to electrostatic (Schuster, 1991). The bioaccumulation of CH_3Hg (MeHg) in aquatic systems poses a threat to ecosystem and human health. Concentrations of Hg have been observed to reach 4.5 ppm in large aquatic species such as shark (FDA, 2013) and even higher concentrations in organs of polar bears, arctic birds and other species (Dietz et al., 2013).

3.2.2 Contaminated sites: Rivers

Examples of anthropogenic source of Hg to river systems include chlor-alkali plants and the gold mining process which are the sources of Hg in a branch of the coastal lagoon Ria de Aveiro in Portugal (Ramalhosa et al., 2006) and the Cuyuní river basin in Venezuela respectively (Santos-Francés et al., 2011). A Hg mine that was in operation for over 500 years in Slovenia resulted in generation of tailings and loss of Hg into the river system that continue to be a large source of high levels of Hg into the Idrija River and the Gulf of Trieste (Hines et al., 2000).

Riverbank sediments containing elevated concentrations of Hg present unique challenges for remediation. Erosion, transport and deposition of Hg contaminated particles can spread from the initial source to result in new, secondary sources of Hg. Sediments act as persistent sources for Hg as observed in Honda Bay, Philippines where HgS was transformed within 100 m of its cinnabar mine tailings source and distributed in the sediments kilometres downstream (Benoit et al., 1994). The release of particulate Hg that accompanies disturbances from activities such as dredging should be taken into account when developing plans for remediation (Wang et al., 2004).

3.2.3 Site description

The South River that passes through Waynesboro, VA, USA contains elevated concentrations of Hg in its riverbank and floodplain sediments. The historical release of Hg at this site originated from a textile plant in Waynesboro which used $HgSO_4$ as a catalyst during an acetate production process from the years 1929 to 1950 (Carter, 1977). One of the current approaches for mitigating Hg release at this site is bank stabilization which has been implemented in a pilot study close to the historical release area of the plant (Flanders et al., 2010). One part of an integrated method to remove Hg from water emanating from the riverbanks has been proposed by Desrochers (2013), which incorporates the use of a reactive material installed in reactive mats laid against the riverbanks to passively treat Hg as it discharges, a concept similar to permeable reactive barriers (Blowes et al., 2000).

3.2.4 Mercury treatment material

Biochar refers to biomass that has undergone the process of low-temperature pyrolysis resulting in a biomass with much higher carbon content (Lehmann, 2007). The large surface area, pore size and functional groups (which differ based on the parent material and pyrolysis temperature) make biochar effective at heavy metal removal (Park et al., 2011). The potential of a biochar (Cowboy Charcoal) to be used as a reactive material against the riverbank sediments is being explored in this study. Cowboy Charcoal was packed into a column, loaded with Hg leached from riverbank sediments and then perturbed with different influent solutions to monitor Hg response.

3.2.5 Research objectives

An important aspect of remediation by a material is the ability to resist perturbations from the environment and still effectively treat a contaminant. The local pH of the rain at the South River site is ~4.6 (USGS, 2007), and a treatment material must be able to retain Hg over a pH range that encompasses this value. This study evaluated the stability of Hg bound to biochar during prolonged contact with river

water and simulated acid rain water to assess the influence of perturbations in water chemistry on the long-term effectiveness of biochar as a passive treatment material for Hg.

3.3 Methodology

3.3.1 Materials and collection

Approximately 4-5 L of sediment from the South River was collected in May 2009 at relative river mile (RRM) 0.1 downstream from the site of historical release. The sediment sample was collected at the edge of the river bank from a location close to the baseflow elevation of the river (transect RRM 0.1, sample SR3). This sample was shipped to the University of Waterloo, ON where it was homogenized and separated into 1L wide-mouth Nalgene bottles which were wrapped in aluminum foil and stored at 4°C. The biochar (Cowboy Charcoal) was produced from oak and maple hardwoods that was charred at >500°C in low oxygen conditions before being crushed and sieved to a <2 mm particle size. The South River water (SRW) was collected approximately bimonthly upstream from the textile plant and shipped to the University of Waterloo on ice where it was then stored at 4°C in dark conditions. Simulated acid rain water was prepared using deionized water which was adjusted to a pH of 4.6 with a mixture of 1.14 M H_2SO_4 and 1 M HNO_3. The chemical compositions of the three influent solutions are detailed in Table 3.1.

3.3.2 Column set-up/experimental design

Two custom-made acrylic columns (Columns 1 and 2) with volumes of ~178.9 cm^3 ± 5.0 cm^3 with two side ports were used. A sediment column (Column 1) was initially leached with SRW and then connected to the treatment column (Column 2) which contained biochar treatment media to begin Stage 1 of the experiment (Fig. 3.1A). After Column 2 was loaded with Hg, Column 1 was disconnected and the influent for Column 2 was replaced with solutions consisting of SRW (Stage 2) and then ARW (Stage 3) to evaluate leaching of Hg from the treatment material (Fig. 3.1B). The influent solutions were pumped

from the bottom of the columns to the top at constant flow rates using a high precision peristaltic pump (ISMATEC, Switzerland).

Column 1 was wet-packed with riverbank sediment, which was terminated at both ends by 1 cm of silica sand and two sizes of NITEX filtering mesh screens, a 125 μm size closest to the material followed by a coarse mesh screen. The SRW was pumped through Column 1 at ~3 pore volumes a week (1 pore volume = 86 mL). After Column 1 flowed for 78 pore volumes, Column 2 (treatment column) was attached in series to treat the effluent.

Column 2 was dry packed under atmospheric conditions with a mixture of biochar and silica sand (1:1 by volume or 15.9 wt. % biochar). Column 2 was purged with CO_2(g) for 2 hours and then flushed for 2 pore volumes (1 pore volume = 100.6 mL) with SRW before being attached to Column 1 (Desrochers, 2013).

After loading Hg onto Column 2 for 182 pore volumes, Column 2 was separated and attached to an influent solution containing the low-Hg containing SRW until pore volume 193 and then to ARW until termination of the experiment at 314 pore volumes (Table 3.2). At the termination of the experiment, Column 2 was sectioned in an anaerobic chamber (COY, Mandel Scientific Company, Guelph, CA) containing a 5% H_2/balance N_2 atmosphere. The biochar treatment material from Column 2 was sectioned at 2 cm intervals and placed in 40 mL glass EPA vials, sealed and then frozen at -20°C for further analyses.

3.3.3 Sampling techniques

Effluent from the columns was collected in 200 mL amber bottles and sampled at regular time intervals. Samples collected along the length of Column 2 (port sampling) were completed on four separate occasions, once while the influent solution was obtained from the sediment column (Column 1), once with SRW as an influent solution, and twice with ARW as the influent solution. For reporting purposes,

port sampling locations were plotted relative to the influent which was treated as the 1 cm location, with the bottom and top ports representing 6 cm and 11 cm respectively and finally the effluent representing the 16 cm location. Samples from the ports were collected with 60 mL reusable glass syringes (BD Multi-fit) while maintaining a constant rate of flow into the column. Samples from the column effluent were collected using 20 mL sterile plastic luer-lock syringes (Norm-Ject, Thermo Fisher Scientific, Burlington CA) and where necessary filtered with 32 mm diameter 0.45 μm Supor® membranes (Acrodisc, VWR, Burlington, CA).

Determinations of pH were made immediately on unfiltered samples in a closed-cell apparatus after sample collection using a combination glass bulb/Ross electrode (Orion model 815600, Thermo Fisher Scientific, Burlington, CA). The pH electrode was calibrated prior to each sampling event with pH 7 and 4 buffer solutions and checked against pH 10. Redox measurements (Eh) were conducted immediately on unfiltered samples in a closed-cell apparatus, using a platinum redox electrode with a $Ag/AgCl_2$ reference solution (Orion model 9678 BNWP, Thermo Fisher Scientific, Burlington, CA) that had been checked against both Zobell's and Light's solutions.

Samples for alkalinity were 0.45 μm filtered, and analyzed immediately at the time of collection with bromocresol green-methyl red indicator and the use of a digital titrator with standardized 0.16 N H_2SO_4 (HACH, VWR, Burlington, CA).

Samples for cation and anion analyses were collected, passed through 0.45 μm filters into 15 mL Nalgene bottles and acidified to a pH <2 with ACS grade 69-70% HNO_3 (JT Baker, VWR, Burlington, CA) for cation analysis, and left unacidified for anion analysis prior to storage at 4°C until the time of analysis. Samples for unfiltered and 0.45 μm filtered THg were collected in 15 mL amber vials with PFTE-lined screw caps and acidified to a pH <2 with ACS grade 69-70% HNO_3 (JT Baker, VWR, Burlington, CA) and stored at 4°C until analysis.

3.3.4 Aqueous sample analyses

Cation samples were analyzed using inductively coupled plasma-optical emission spectrometry (ICP-OES) (iCAP 6000, Thermo Scientific) and trace metals using inductively coupled plasma-mass spectrometry (ICP-MS) (XSERIES 2, Thermo Scientific). Anion concentrations were measured using ion chromatography (Dionex IC-OH, DX 600 ED50, Sunnyvale, USA). The THg concentrations were analyzed using cold vapour atomic fluorescence spectroscopy (CVAFS) (Model 2600, Tekran Instruments Corporation. Toronto, CA) and followed EPA method 1631 Revision E (U.S. EPA, 2002).

3.3.5 Solid-phase analyses (THg, MeHg)

The Hg sequential extractions completed on the biochar material followed the method in Bloom et al. (2003) with the F1 fraction targeting the water soluble fraction, F2 the stomach acid soluble, F3 organo-chelated, F4 elemental, and F5 the mercuric sulfide fraction. The following extractants were used: deionized water (F1), 0.1 M CH_3COOH + 0.1 M HCl at pH 2 (F2), 0.1 M KOH (F3), 12 M HNO_3 (F4) and aqua regia (F5). Total Hg was determined through digesting the reactive media for 3 days in aqua regia. The resulting digestates from the sequential and THg extractions were analyzed with CVAFS described previously for aqueous samples.

Solids for MeHg analysis were prepared first using 20% KCl and 8 M H_2SO_4 with an addition of $CuSO_4$ for distillation to improve recovery and displace MeHg from sulfide binding sites (Model 2750, Tekran) before aqueous ethylation and analysis by CVAFS on an automated MeHg analyzer (Model 2700, Tekran) following EPA method 1630 (U.S. EPA, 2001).

3.4 Results

3.4.1 Stage 1: Loading of Column 2 with Hg

3.4.1.1 Temporal monitoring of treatment efficiency

For 182 pore volumes of flow Column 2 received high-Hg water from Column 1 with the effluent from Column 2 being sampled on a regular basis. At the time Column 2 was attached to Column 1 in series, a 0.45 μm filtered THg concentration (THg-0.45) of 1040 ng L^{-1} was observed in the Column 1 effluent. At the time Column 1 was removed the THg-0.45 concentrations had declined to 442 ng L^{-1} ±46 in the effluent of Column 1. The THg-0.45 concentrations in the effluent of Column 2 during this time reached a maximum of 14.3 ng L^{-1} before stabilizing to average concentrations of 6.04 ng L^{-1} ± 1.88 (Fig. 3.2). The THg-0.45 concentrations from Column 1 had declined by >98.6% after passing through the length of Column 2 and THg concentrations declined by >99%. A mass of 8.75 μg of THg-0.45 (0.40 μg g^{-1}) was calculated to have been loaded onto Column 2 during this stage. The THg-0.45 concentrations in the effluent of Column 1 during this stage were previously reported to be ~22-25% of the THg (Desrochers, 2013) which would equate to a total Hg mass of 35.3-40.2 μg (1.6-1.8 μg g^{-1}) on the biochar.

3.4.1.2 Spatial monitoring of treatment efficiency

At 176 PV aqueous samples were collected along the length of Column 2 (Fig. 3.3) when it was still connected in series to Column 1. The influent THg-0.45 concentration of 289 ng L^{-1} declined to 19.1 ng L^{-1} by the first port of Column 2, representing a mass removal of 93.4%. The aqueous THg-0.45 concentrations increased to 76.3 ng L^{-1} in the top port before declining in the effluent to 3.5 ng L^{-1}, which equated to an overall removal of 98.8% of the THg-0.45 over the total length of the biochar treatment column. The pH declined along the length of the biochar treatment material from an influent pH of 7.68 to 6.03 by the top port before it increased to a pH of 7.18 in the effluent. Alkalinity concentrations along the length of Column 2 remained at 81.0 mg L^{-1} ±9.1 as $CaCO_3$. Nitrate concentrations declined from an influent concentration of 0.40 mg L^{-1} to <0.03 mg L^{-1} in the effluent. Aqueous Mn concentrations

increased from 18.3 μg L^{-1} in the influent to 43.2 μg L^{-1} by the top port before it declined to 1.1 μg L^{-1} in the effluent. Aqueous Fe concentrations decreased from the influent value of 71.9 μg L^{-1} to 2.1 μg L^{-1} by the first port then increased slightly in the top port to 9.0 μg L^{-1} before declining again by the effluent at 0.66 μg L^{-1}. Sulfate concentrations declined slightly along the length of the column from an influent value of 5.7 mg L^{-1} to the effluent concentration of 4.5 mg L^{-1}.

3.4.2 Stage 2: Column 2 with SRW influent

3.4.2.1 Temporal monitoring of treatment efficiency

From pore volume 182 to 193 Column 2 was run with an influent of SRW (Fig. 3.2) and the effluent of Column 2 was sampled regularly. The pH in the column effluent during Stage 2 increased from 7.28 ±0.18 prior to the switch in influent solutions to an average of 7.53 ±0.22 while the Eh values increased from 508 mV ±55 to 580 mV±27. The alkalinity concentrations in the effluent of Column 2 declined from 86 mg L^{-1} as $CaCO_3$ to 78 mg L^{-1} during Stage 2 of the experiment. The THg-0.45 concentrations in the effluent averaged 4.3 ng L^{-1} ±0.9 and remained consistent during Stage 2.

3.4.2.2 Spatial monitoring of treatment efficiency

Samples were collected along the length of Column 2 once with an influent of SRW at pore volume 188. During Stage 2 at pore volume 188, the THg-0.45 concentrations increased slightly from an influent concentration of 8.2 ng L^{-1} to 14.0 ng L^{-1} by the top port, and declined to 3.9 ng L^{-1} in the effluent (Fig. 3.4), a decrease of 52.4% over the length of column 2. The influent pH declined from 8.18 to 7.31 ±0.09 along the length of the column. Alkalinity concentrations increased from an influent of 66.2 mg L^{-1} as $CaCO_3$ to 98.7 mg L^{-1} in the top port before declining to 76.5 mg L^{-1} as $CaCO_3$ in the effluent. Nitrate concentrations declined from 2.58 mg L^{-1} in the influent to 0.24 mg L^{-1} by the first port before it declined to <0.03 mg L^{-1}. Aqueous Mn concentrations increased along the length of the column from influent concentrations of <0.04 μg L^{-1} to a maximum of 19.0 μg L^{-1} at the top port while the Fe concentrations

declined from an influent concentration of 6.7 μg L^{-1} to <0.2 μg L^{-1} by the first port. Sulfate concentrations were observed at 7.74 mg L^{-1} ±0.01 across the length of Column 2 and in the effluent.

3.4.3 Stage 3: Column 2 with ARW influent

3.4.3.1 Temporal monitoring of treatment efficiency

From pore volume 193 to the time of column sectioning at 314 pore volumes Column 2 flowed with an influent solution of simulated ARW with a pH of ~4.6 (Fig. 3.2). During Stage 3 of the experiment the pH of the Column 2 effluent declined from 7.53 ±0.22 to a pH of 5.41and the Eh of the effluent increased from 580 mV±27 to 641 mV ±45 at the termination of the experiment. Alkalinity concentrations in the effluent of Column 2 declined from 78 mg L^{-1} to 2.45 mg L^{-1} as $CaCO_3$. The aqueous concentrations of unfiltered and THg-0.45 in the Column 2 effluent averaged 6.6 ng L^{-1} ±0.7 and 6.6 ng L^{-1} ±1.0 respectively at the onset of ARW. After 4 pore volumes of flow with ARW as an influent solution the unfiltered THg concentration increased to 78.5 ng L^{-1} while the THg-0.45 concentration increased to 56.6 ng L^{-1}. This increase was not sustained and concentrations of THg-0.45 declined in the effluent and remained at 5.0 ng L^{-1} ±1.5, and unfiltered THg concentrations also remained low at 5.4 ng L^{-1} ±1.5.

3.4.3.2 Spatial monitoring of treatment efficiency

Samples were collected along the length of Column 2 twice with an influent of ARW, once at 202 pore volumes of flow and again at pore volume 210. During Stage 3 of the experiment at pore volume 202, the THg-0.45 concentrations increased relative to the values observed during Stage 2 to 20.5 ng L^{-1} and 82.9 ng L^{-1} in the bottom and top ports of Column 2 respectively (Fig. 3.5). Nitrate concentrations had declined from an influent value of 0.5 mg L^{-1} to 0.06 mg L^{-1} by the bottom port. Aqueous Fe concentrations increased from an influent concentration of <0.2 μg L^{-1} to 12 μg L^{-1} by the bottom port before declining to 1.6 μg L^{-1} in the effluent.

At pore volume 210 (Fig. 3.6) the THg-0.45 concentrations at the bottom port were 32.3 ng L^{-1} and increased to 71.4 ng L^{-1} by the top port and declined to 5.7 ng L^{-1} in the effluent. The alkalinity concentrations increased along the column length with values of 11.3 mg L^{-1} and 19.8 mg L^{-1} as $CaCO_3$ in the bottom and top ports respectively and declined to 7.5 mg L^{-1} in the effluent.

3.4.4 Solid-Phase Analyses

At the termination of the column experiment at 314 pore volumes, the solid-phase concentrations of THg in the biochar material of Column 2 indicated the majority of Hg was present within the first 2 cm of biochar at a concentration of 0.26 μg g^{-1} dry wt. (Fig. 3.7). The solid-phase THg concentration reached a minimum of 0.04 μg g^{-1} at the 8-10 cm interval of material. Sequential Hg extractions of the first 2 cm of biochar material indicated that the majority of the Hg was present in the F4 fraction at 67%, followed by the F3 fraction at 31% (Fig. 3.8). The concentrations of MeHg on the biochar at the 0-2cm interval were 0.20 ng g^{-1} dry wt., representing 0.08% of the THg.

3.5 Discussion

3.5.1 Stage 1: Conditions during Hg loading

Sampling of the pore water along the length of Column 2 at pore volume 176 during Stage 1 revealed that the majority of the 0.45 μm filtered THg concentrations from the influent had declined within the first few cm of material in Column 2. The accumulation of Hg at the top port during this stage may indicate the presence of a preferential flow path within the column, or an unevenness of the biochar material during column packing. Another biochar treatment column (results not shown) did not have the same increase in aqueous concentrations of THg along the length of the column (Desrochers, 2013). The decline in aqueous Fe concentrations at the bottom port may indicate the ability of biochar to remove other metals parallel with Hg. There is also little evidence for SO_4^{2-} reduction with the biochar material along the length of the column as the concentrations deviated little from the influent. The functional groups of biochar that are the source for electrostatic metal removal, such as the oxygen-containing carbon bonds in carboxyl groups (Zimmerman, 2010), could be the mechanism for the decline in Hg concentrations observed in the effluent in combination with physical filtration.

3.5.2 Stage 2: Conditions with an influent of SRW

The ingress of SRW may have promoted the reduction of NO_3^- through denitrification (Eq. 1), in Column 2 which may explain the decline in NO_3^- concentrations.

$$NO_3^- + 5e^- + 6H^+ \rightarrow 0.5N_2 + 3H_2O \qquad \text{Eq. 1}$$

The SO_4^{2-} concentrations along the column length remain unchanged providing no indication for SO_4^{2-} reduction (Eq. 2) during this stage of the experiment. There were observable NO_3^- concentrations present along the length of Column 2 which would inhibit SO_4^{2-} reduction (Achtnich et al., 1995).

$$SO_4^{2-} + 8e^- + 9H^+ \rightarrow HS^- + 4H_2O \qquad \text{Eq. 2}$$

The biochar material in Column 2 lowered the pH of the river water along the length of the treatment column from 8.18 to approximately 7.3. The aqueous THg-0.45 concentrations declined along the length of Column 2 and had no significant increase in the effluent. The lack of increase in THg-0.45 concentrations in the effluent suggested that the biochar retained the Hg that had been previously loaded onto the material under continued saturated flow conditions after being exposed to higher pH conditions induced by the SRW influent.

3.5.3 Stage 3: Conditions with an influent of ARW

The brief increase in THg-0.45 concentrations observed in Stage 3 in the effluent of Column 2 followed by concentrations at influent level suggested the biochar material can retain Hg under long-term acidic conditions. This finding of biochar retaining Hg under lower pH conditions is consistent with studies on adsorption of Pb^{2+} to biochar by Jiang et al. (2012) where the main mechanism for removal is attributed to removal mechanisms unaffected by pH (Jiang et al., 2012). The slight increase observed in aqueous THg-0.45 concentrations along the length of the column over time could be explained by the decline in electrostatic adsorption of the biochar material caused by the lower pH. The functional groups of biochar (e.g. carboxyl) may have been responsible for increasing the pH of the pore water (Eq. 3) along the length of the column and are indicative of its buffering capacity (Uchimiya et al., 2011).

$$R - COO^- + H^+ \leftrightarrow R - COOH \qquad \text{Eq. 3}$$

The functional groups on the biochar may still be able to adsorb metals such as Hg under the lower pH conditions (Uchimiya et al., 2011). The functional groups of this particular biochar need to be further characterised to determine its buffering capacity. As the ARW was acidified DI water, the influent solution was a change not only in pH from the previous influent, but a change in the ionic strength, inferring an ability of the biochar to retain Hg under low ionic strength conditions as well.

3.5.4 Termination of the column: Effects of long-term leaching and perturbations

After 121 pore volumes of saturated flow under acidic conditions the majority of the solid-phase Hg on the biochar material from Column 2 was contained within the first 2 cm of material. These high concentrations of solid-phase Hg near the influent indicate the strength of the Hg-biochar complex.

The Hg sequential extractions were developed for sediments and not biochar material (Bloom et al., 2003), but the results can still represent the ease by which Hg can be extracted from the biochar. The sequential extraction results indicated that the mechanisms controlling Hg binding onto biochar were relatively strong, given that that Hg was primarily released with a very strong acid extraction step (12 M HNO_3) and not with milder reagents. The difference between the THg extracted and the sum of the Hg sequential extractions on the biochar material is likely due to the uneven distribution of the Hg on the biochar material.

The very low concentration of solid-phase MeHg on the biochar material suggested that the biochar used in this study did not promote Hg methylation or increase the bioavailability of the Hg retained on the material. The solid-phase MeHg results corresponded to the low pore water MeHg concentrations determined in the effluent of Column 2 during treatment of the sediment column (Desrochers, 2013). The bioavailability of metals bound to biochar appears to be lower than for free metals in incubation studies involving metals other than Hg such as Cu, Cd and Pb with plants (Park et al., 2011). As the biochar used was hardwood which underwent pyrolysis at >500°C it should be less prone to degradation and should still retain its ability to perform as an effective metal removal material (Liu et al., 2013). One of the potential risks with biochar degradation, if it occurs, is the formation of a labile carbon source for bacteria. The level to which biochar may suppress or at least not result in an increase in Hg methylation over different conditions should be studied further.

3.6 Conclusions

Under saturated flow conditions the mixture of biochar and silica sand removed >98% of the THg-0.45 mass from the pore water. The switch of influent solution to SRW resulted in a negligible increase in THg-0.45 concentrations in the effluent, though there was a decrease in THg-0.45 concentrations within the column pore water itself. A switch to a simulated ARW influent resulted in a brief release of Hg in the effluent and a rise within the column, though the THg concentrations remained consistently low under long term flow conditions.

Solid-phase extractions revealed the majority of the Hg was retained within the first 5 cm of material with the majority only being extracted from the biochar material under strongly acidic conditions. There was no specific increase in MeHg observed on the biochar solids. The results of this study suggest that biochar has potential for removing Hg from pore water under saturated flow conditions and is not expected to release significant amounts of Hg during long term leaching with low-Hg river water and simulated ARW.

Table 3.1: Chemical compositions of the three influent solutions for Column 2 (treatment column). Error is represented as 1 standard deviation from the mean.

	Influent Solution		
Parameter	Column 1	SRW	ARW
pH	7.35 (±0.24)	8.15(±0.15)	4.80 (±0.08)
Eh (mV)	532 (±55)	545 (±32)	783 (±55)
Alk (mg L^{-1} as $CaCO_3$)	81 (±14)	80 (±15)	3.9 (±1.3)
Hg (ng L^{-1})	1225-231	2.9 (±2.4)	5.0
Cl (mg L^{-1})	5.8	5.8 (±0.2)	0.39
NO_3^- (mg L^{-1})	0.2	3.2 (±0.3)	0.50
SO_4^{2-} (mg L^{-1})	5.6	8.4 (±2.3)	1.0
Ca (mg L^{-1})	19.3 (±0.0)	25.2 (±5.7)	0.03
K (mg L^{-1})	1.9 (±0.2)	2.1 (±0.3)	0.47
Mg (mg L^{-1})	7.2 (±0.0)	9.8 (±2.5)	0.004
Na (mg L^{-1})	4.0 (±0.3)	4.8 (±0.5)	0.003
Si (mg L^{-1})	3.9 (±0.0)	4.5 (±0.3)	<0.009
Mn (μg L^{-1})	11.6 (±9.5)	<0.04	<0.01
Fe (μg L^{-1})	66.2 (±8.0)	3.2 (±2.0)	<0.2

Table 3.2: Description of Column 2 experimental stages.

Stage	1	2	3
Influent	Column 1	SRW	ARW
Start (PV)	0	182	193
End (PV)	182	193	314
Port sampling times (PV)	176	188	202, 210

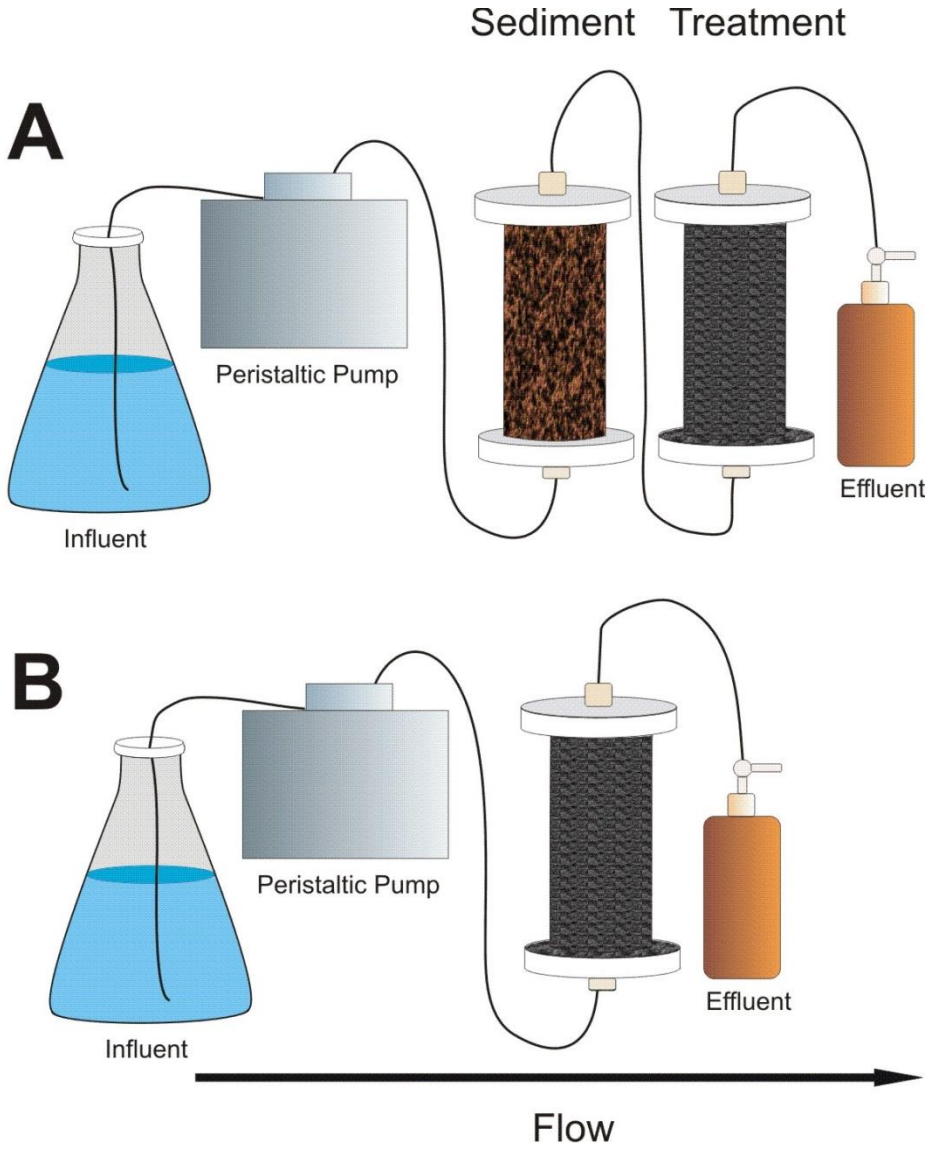

Fig. 3.1: Schematic diagrams of the experimental column design for treatment of Hg under saturated flow conditions. The letter A represents loading with Hg from a sediment column (Stage 1). The letter B represents the isolation of the treatment column (Column 2) subjected to different influent solutions (Stages 2 and 3).

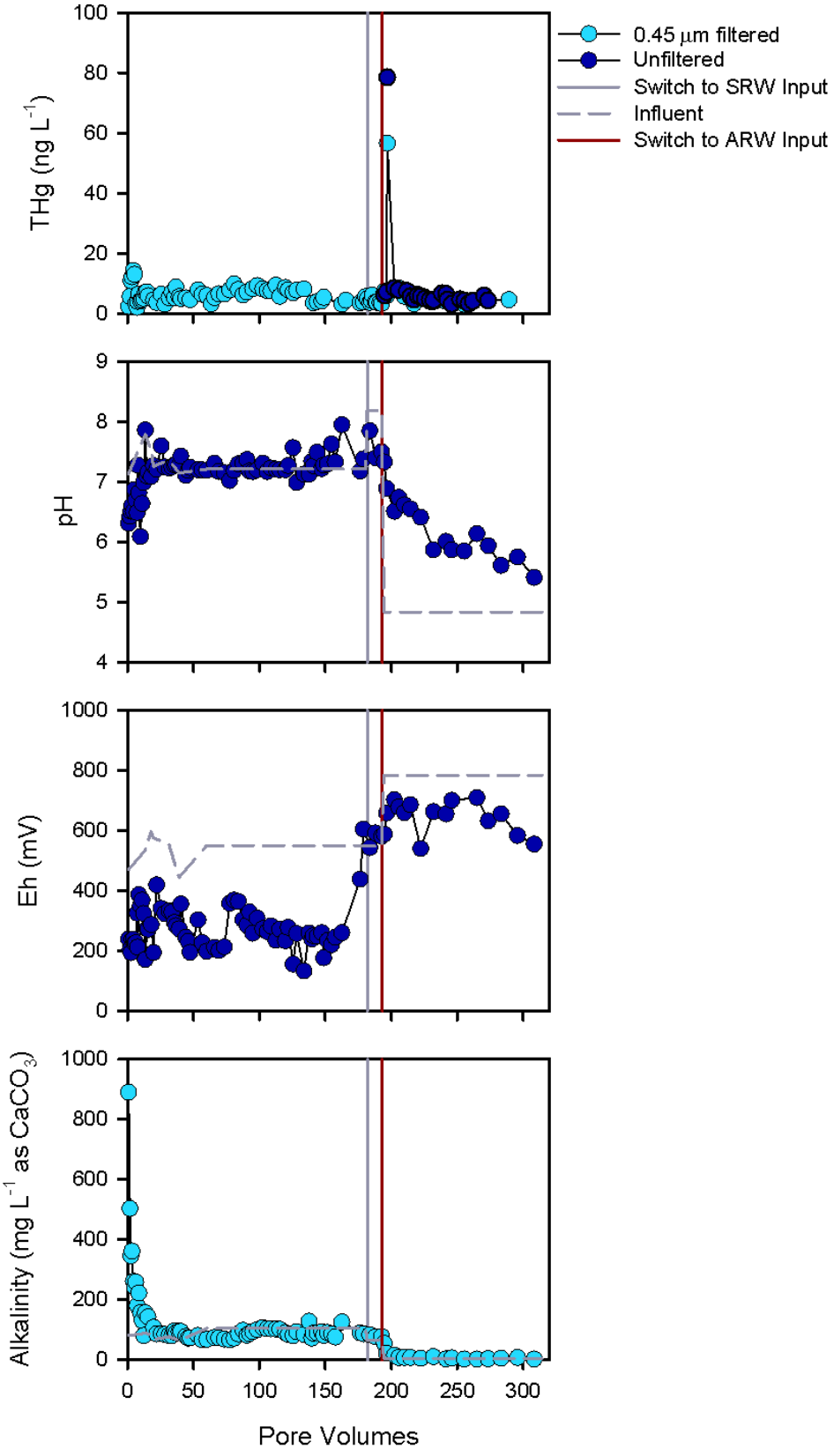

Fig. 3.2: Concentrations of inorganic constituents versus time of the Column 2 effluent.

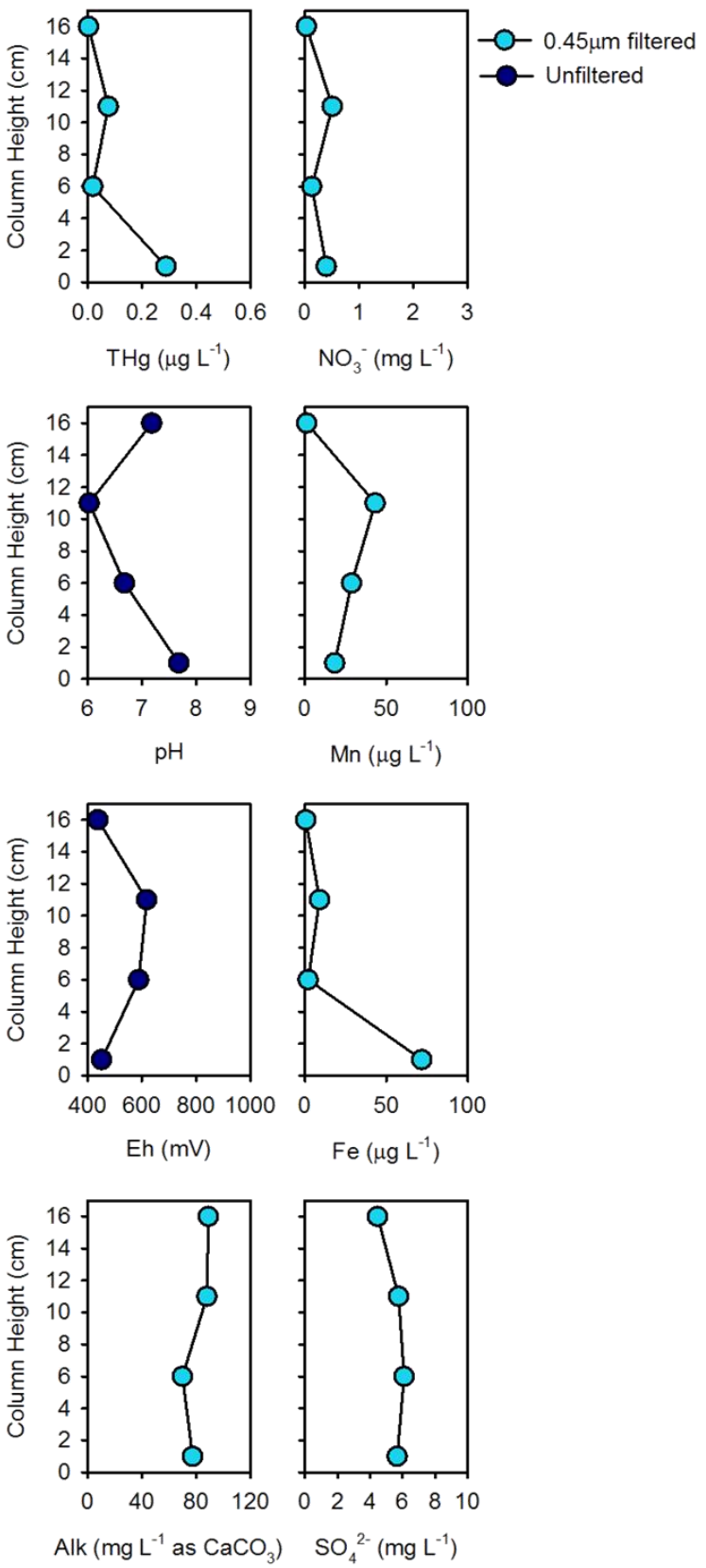

Fig. 3.3: Concentrations of Hg, pH, alkalinity and redox indicators for aqueous samples collected along the length of Column 2 with influent from Column 1 at pore volume 176.

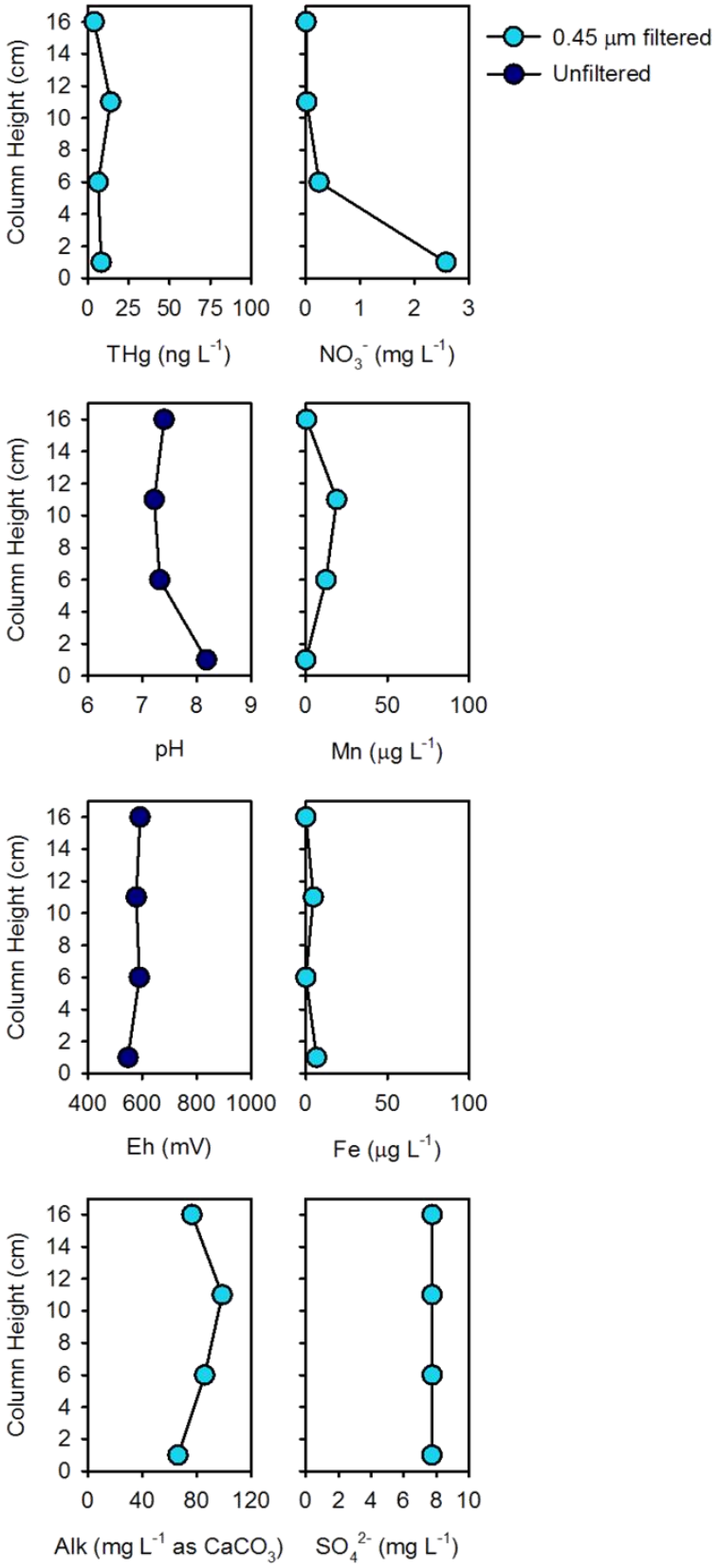

Fig. 3.4: Concentrations of Hg, pH, Eh, alkalinity and redox indicators for aqueous samples collected along the length of Column 2 at pore volume 188 with SRW influent.

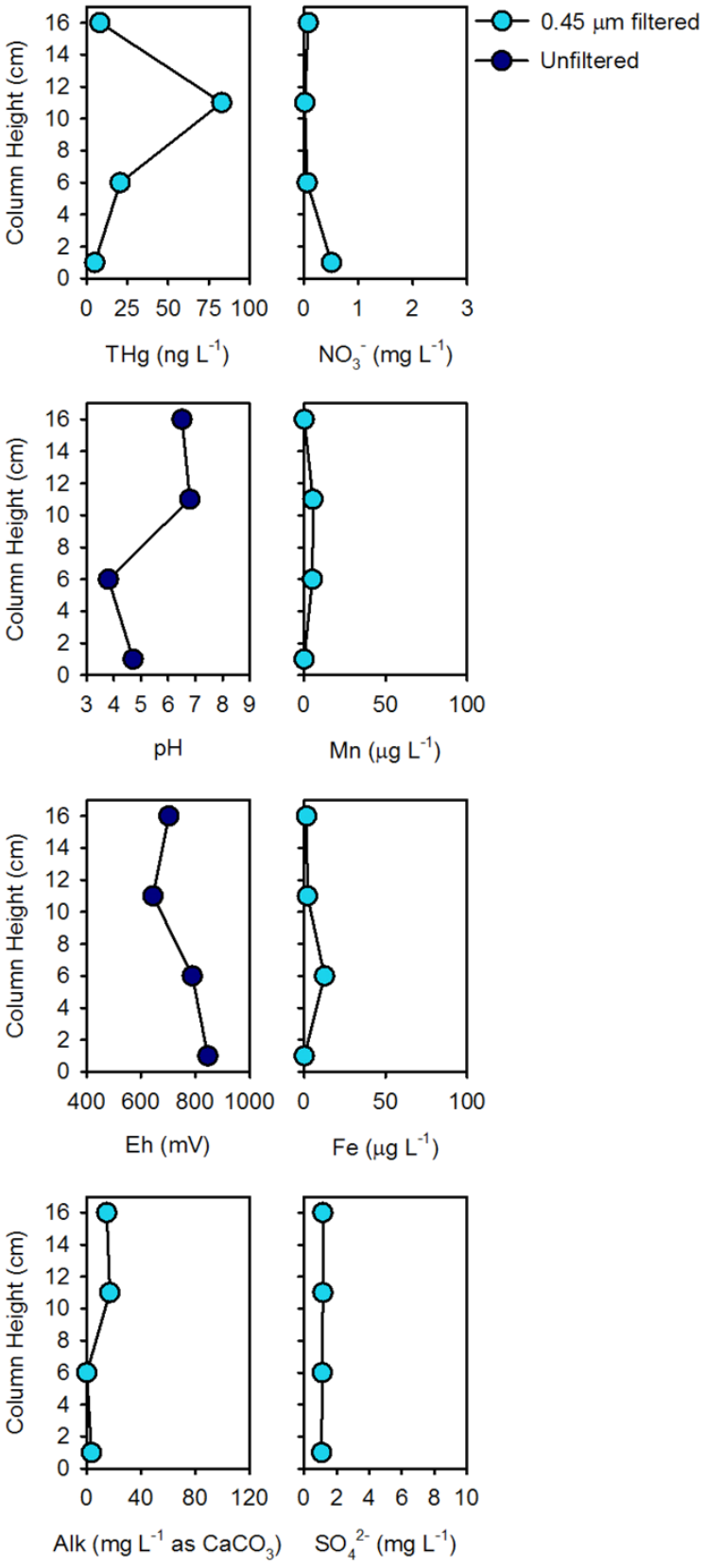

Fig. 3.5: Concentrations of Hg, pH, alkalinity and redox indicators for aqueous samples collected along the length of Column 2 at pore volume 202 with ARW influent.

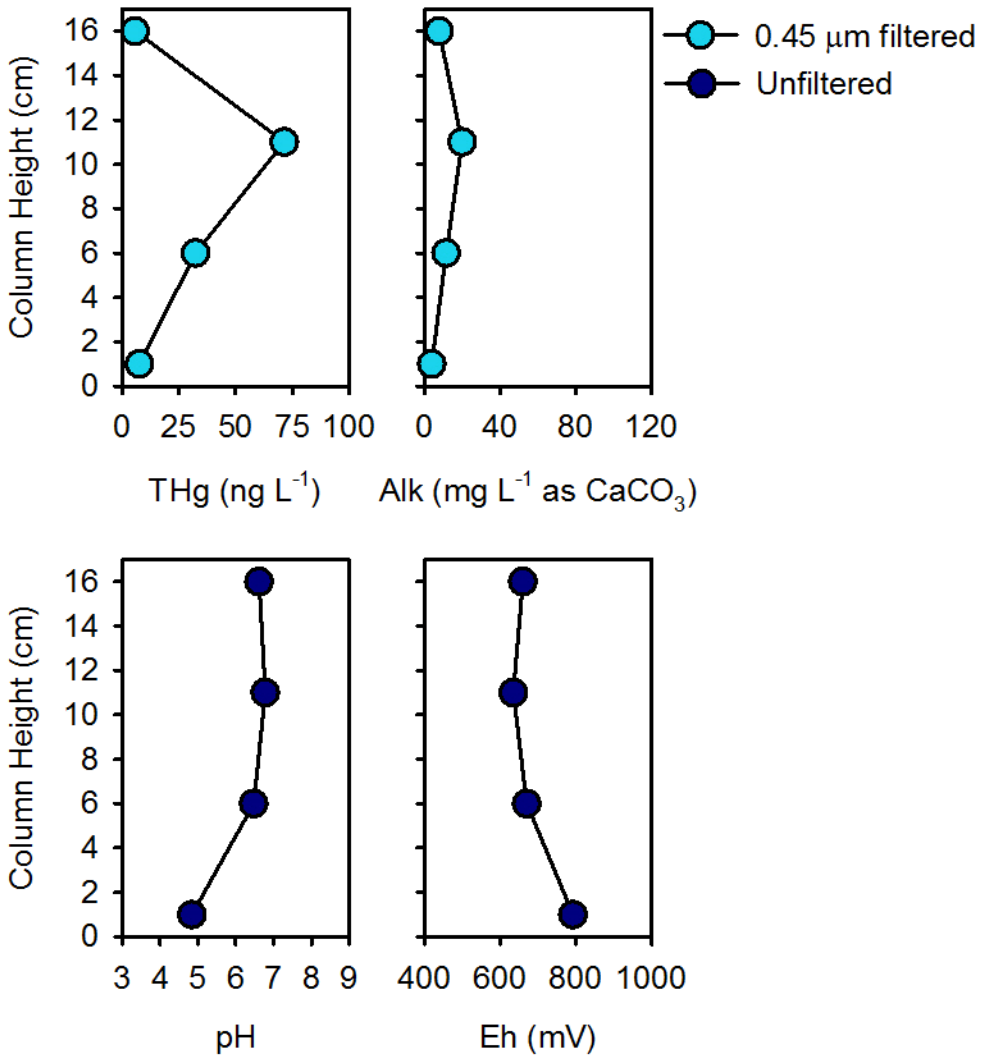

Fig. 3.6: Concentrations of Hg, pH, alkalinity and Eh for aqueous samples collected along the length of Column 2 at pore volume 210 with ARW influent.

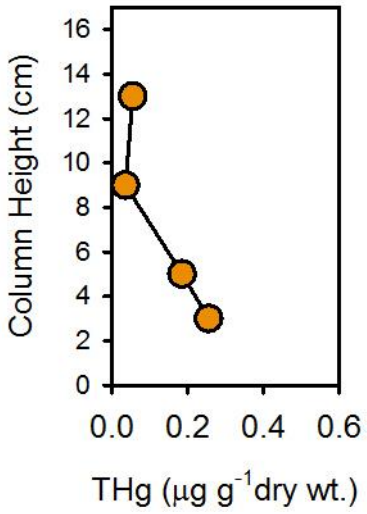

Fig. 3.7: Solid-phase THg concentrations in the biochar material at the termination of Column 2.

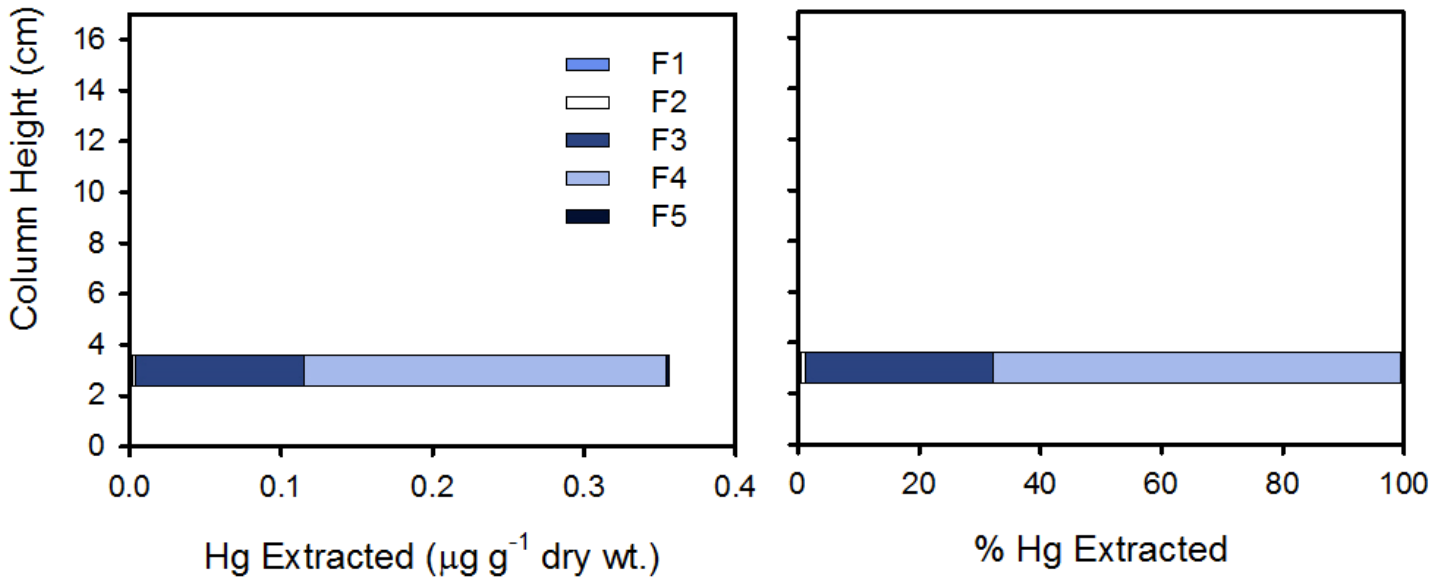

Fig. 3.8: Hg sequential extractions of the first 2 cm of biochar material closest to the influent of Column 2 expressed as total concentration (left) and a percentage (right).

Chapter 4: *Conclusions and Recommendations*

The saturated column studies in Chapter 2 evaluated differences in net MeHg production in sediments containing Hg by amending the influent river water with different organic carbon and SO_4^{2-} concentrations. Research by Gilmour and Henry (1991) hypothesized that concentrations of SO_4^{2-} in excess of 500 μM should inhibit methylation rates, though in the column experiments described in Chapter 2 the greatest percentage and mass of MeHg produced was observed with an influent of lactate with an excess of SO_4^{2-}. Sulfide production, which had reached 55 mg L^{-1} in the port closest to the influent solution in the lactate-sulfate column, did not appear to limit MeHg production. The SRB are known to have a high tolerance for H_2S (Isa et al., 1986) and may only be inhibited by a sheathing effect of FeS around the bacteria over time (Postgate, 1984; Utgikar et al., 2002).

The decline in MeHg concentrations in the effluent at the termination of the lactate-sulfate column experiment may indicate the presence of demethylation. Whether the demethylation process was oxidative or reductive could be determined through monitoring of the relationship of $CO_{2(g)}$ and CH_4 which is done in culture experiments by Oremland et al. (1991). It is possible that the lactate-sulfate column experiment had reached methanogenic conditions or the SRB activity was being inhibited through FeS accumulation. It should also be noted that the lactate-sulfate column had the greatest viable population of SRB in the sediments at the termination of the experiment compared to the other columns.

In the acetate column there was little deviation observed between the influent concentrations of acetate to the effluent concentrations. The acetate column had the greatest enumerable IRB populations over the control column as revealed through the microbial enumerations. The degradation pathway of acetate in the pore water could potentially be determined through isotopic analyses on archived samples. The acetate column exhibited a greater mobilisation of THg perhaps through free Hg(II) complexing with acetate, though this should be addressed with further research. There were differences in the mobilisation of the THg in the effluent between the lactate column compared with the acetate column, even though the

lactate column effluent contained high concentrations of acetate in the pore water from lactate fermentation. The mobilisation of Hg is linked to dissolved organic carbon and dissolved organic matter which impact the aggregation of HgS nanoparticles (Ravichandran et al., 1999; Slowey, 2010). It is recommended that archived samples for DOC and total organic carbon in the pore water be analyzed and compared to Hg mobilisation observed for the different columns in the near future.

In the lactate column there was no stimulation of enumerable IRB populations over the control present in the column sediments as there was with the acetate column, though there were similar concentrations of reduced Fe in the pore water. Both the acetate and lactate amended columns had a similar production of aqueous MeHg in terms of percentage, though a higher mass of MeHg was observed in the acetate column effluent. Speciation of the solid phases of Fe and Mn present in the sediments before column packing compared to at the end of column life could be beneficial to understanding what was happening to the solid-phase Fe and Mn in the different organic amended environments. The speciation of Fe and Mn can be done through Fe and Mn extractions, or through synchrotron-based techniques.

A comparison of bacterial species identified through PCR in the column sediments to a living table of Hg methylators (ORNL, 2013) indicated that the lactate-sulfate column had the greatest counts of known methylating bacteria, specifically *Desulfovibrio putealis*. The species *Desulfobvibrio putealis* may be responsible for the majority of the MeHg production in the lactate-sulfate column. *Geobacter spp.* was identified in the control, acetate and lactate columns, and was the only known methylator identified in the control column. As *Geobacter* was only identified in the control column, it may suggest that under SO_4^{2-}-limited conditions *Geobacter* contributed partially to MeHg production, a similar conclusion to Yu et al. (2012). To confirm the role of *Geobacter* in the South River sediments another column could be constructed with an influent containing acetate and $NaMoO_4$, resulting in a combination of a *Geobacter* stimulant (Lovely et al., 1991) with a known inhibitor of SO_4^{2-} reduction (Taylor & Oremland, 1979). The presence of methylating bacterial species did appear to correspond to the mass of MeHg produced in the pore water of the columns.

There was no significant accumulation of solid-phase MeHg observed within the column sediments, with MeHg concentrations accounting for <0.02% of the THg present in the sediments of the control, acetate and lactate columns. The lactate-sulfate column, with the greatest pore water MeHg concentrations reached a maximum of <0.33% of the THg present. There was no significant decrease in the THg concentrations in the sediment, confirming the persistent nature of Hg as a contaminant in the South River sediments.

The column experiments in Chapter 3 focused on determining the ability of the biochar treatment material to retain the Hg that was loaded onto it over a period of time. The biochar was subjected to influents from a high-Hg containing water to SRW and simulated ARW after the period of Hg loading. Though there was 35.3-40.2 μg of total Hg calculated to have accumulated on the biochar, no significant release of Hg was observed in the effluent when the biochar was exposed to an influent of SRW. When the influent was switched to ARW, there was a very brief increase of Hg before concentrations declined to influent levels, and a slight increase in Hg in the pore water along the column length. Once the column was dissected, analysis of the biochar revealed the majority of the Hg remained on the biochar closest to the influent. The Hg concentration that remained on the biochar suggested that biochar was a resilient material for retaining Hg under saturated flow conditions as well as under acidic conditions for an extended period of time. The MeHg on the solid material closest to the influent was low, accounting for <0.08% of the THg concentration, and suggested that biochar was not a significant promoter of methylation. The low MeHg concentrations corresponded to previous research (Desrochers, 2013) where the aqueous MeHg of this column remained at concentrations of <0.1 ng L^{-1}.

References

Achtnich, C., Bak, F., & Conrad, R. (1995). Competition for electron donors among nitrate reducers, ferric iron reducers, sulfate reducers, and methanogens in anoxic paddy soil. *Biology and Fertility of Soils, 19*, 65-72

Aiken, G. R., Hsu-Kim, H., & Ryan, J. N. (2011). Influence of dissolved organic matter on the environmental fate of metals, nanoparticles, and colloids. *Environmental Science and Technology, 45*(8), 3196-3201

Allison, J. D., Brown, D., S., & Novo-Gradac, K. J. (1990). MINTEQA2/PRODEFA2, a geochemical assessment model for environmental systems: Version 3.0 User's Manual; U.S. Environmental Protection Agency; Athens, GA: 106 pp.

Anderson, R. T., Vrionis, H. A., Ortiz-Bernad, I., Resch, C. T., Long, P.E., Dayvault, R., Karp, K., Marutzky, S., Metzler, D. R., Peacock, A., White, D. C., Lowe, M., & Lovley, D.R. (2003). Stimulating the in situ activity of Geobacter species to remove uranium from the groundwater of a uranium-contaminated aquifer. *Applied and Environmental Microbiology, 69* (10): 5884-5891

Atlas, R.M. (1984). *Microbiology: Fundamentals and Applications*. Macmillan, New York.

Bakir, F., Damluji, S.F., Amin-Zaki, L., Murtadha, M., Khalidi, A., Al-Rawi, N. Y., Tikriti, S., Dhahir, H. I., Clarkson, T. W., Smith, J. C., & Doherty, R. A. (1973). Methylmercury poisoning in Iraq. *Science , New Series, 181* (4096), 230-241

Bartlett, M., Zhuang, K., Mahadevan, R., & Lovley, D. (2012). Integrative analysis of Geobacter spp. and sulfate-reducing bacteria during uranium bioremediation. *Biogeosciences, 9*, 1033-1040

Benner, S.G., Blowes, D.W., Gould, W.D., Herbert Jr., R.B. & Ptacek, C.J. (1999). Geochemistry of a permeable reactive barrier for metals and acid mine drainage. *Environmental Science and Technology, 33*(16), 2793-2799

Benoit, G., Schwantes, J.M., Jacinto, G.S., & Goud-Collins, M.R. (1994). Preliminary study of the redistribution and transformation of HgS from cinnabar mine tailings deposited in Honda Bay, Palawan, Philippines. *Marine Pollution Bulletin, 28* (12), 754-759

Bloom, N.S., Preus, E., Katon, J. & Hiltner, M. (2003). Selective extractions to assess the biogeochemically relevant fractionation of inorganic mercury in sediments and soils. *Analytica Chimica Acta, 479* (2), 233-248

Blowes, D.W., Al, T.A., Lortie, L., Gould, W.D. & Jambor, J.L. (1996). Microbiological, chemical, and mineralogical characterization of the Kidd Creek mine tailings impoundment, Timmins area, Ontario. *Geomicrobiology Journal, 13*: 13–31

Blowes, D. W., Ptacek, C.J., Benner, S.G., McRae, C.W.T., Bennett, T.A., & Puls, R. W. (2000). Treatment of inorganic contaminants using permeable reactive barriers. *Journal of Contaminant Hydrology, 45*, 123-137

Boening, D.W. (2000). Ecological effects, transport, and fate of mercury: a general review. *Chemosphere, 40*, 1335-1351

Burgin, A.J., & Hamilton, S.K. (2007). Have we overemphasized the role of denitrification in aquatic ecosystems? A review of nitrate removal pathways. *Frontiers in Ecology and the Environment, 5*(2): 89-96

Carter, L. J. (1977). Chemical plants leave unexpected legacy for two Virginia rivers. *Science, New Series, 198* (4321), 1015-1020

Chapelle, F. H., Bradley, P. M., Thomas, M. A., & McMahon, P. B. (2009). Distinguishing iron-reducing from sulfate-reducing conditions. *Ground Water, 47*(2), 300-305

Cochran, W. G. (1950). Estimation of bacterial densities by means of the "most probable number". *Biometrics, 6*(2), 105-116

Dar, S.A, Kleerebezem, R., Stams, A.J. M., Kuenen, J.G. and & Muyzer, G. (2008). Competition and coexistence of sulfate-reducing bacteria, acetogens and methanogens in a lab-scale anaerobic bioreactor as affected by changing substrate to sulfate ratio. *Applied Microbiology Biotechnology 78*,1045-1055

D'Itri, P.A., & D'Itri, F.M. (1978). Mercury contamination: a human tragedy. *Environmental Management, 2* (1), 3-16

DeSantis, T. Z., Hugenholtz, P., Larsen, N., Rojas, M., Brodie, E. L., Keller, K., Huber, T., Dalevi, D., Hu, P., &. Andersen, G. L. (2006). Greengenes, a chimera-checked 16S rRNA gene database and workbench compatible with ARB. *Applied and Environmental Microbiology, 72*(7), 5069-5072.

Desrochers, K. (2013). *Geochemical characterization and assessment of stabilization mechanisms for mercury-contaminated riverbank sediments from the South River, Virginia (USA).* Master of Science Thesis, University of Waterloo, Waterloo, Ontario, Canada

Dietz, R., Sonne, C., Basu, N., Braune, B., O`Hara, T., Letcher, R.J., Scheuhammer, T., Andersen, M., Andreasen, C., Andriashek, D., Asmund, G., Aubail, A., Baagøe, H., Born, E.W., Cham, H.M., Derocher, A.E., Grandjean, P., Knott, K., Kirkegaard, M., Krey, A., Lunn, N., Messier, F., Obbard, M., Olsen, M.T., Ostertag, S., Peacock, E., Renzoni, A., Rigét, F.F., Skaare, J.U., Stern, G., Stirling, I., Taylor, M., Wiig, Ø., Wilson, S., & Aars, J. (2013). What are the toxicological effects of mercury in Arctic biota? *Science of the Total Environment, 443*, 775-790

Dowd, S. E., Callaway, T. R., Wolcott, R. D., Sun, Y., McKeehan, T., Hagevoort, R. G., & Edrington, T. S. (2008). Evaluation of the bacterial diversity in the feces of cattle using 16S rDNA bacterial tag-encoded FLX amplicon pyrosequencing (bTEFAP). *BMC Microbiology*, 8:125

Dowd, S.E., Sun, Y., Wolcott, R.D., Domingo, A., & Carroll, J.A. (2008). Bacterial tag–encoded FLX amplicon pyrosequencing (bTEFAP) for microbiome studies: bacterial diversity in the ileum of newly weaned salmonella-infected pigs. *Foodborne Pathogens and Disease, 5*(4): 459-472

Druhan, J.L., Steefel, C.I., Molins, S., Williams, K.H., Conrad, M.E., & DePaolo, D.J. (2012). Timing the onset of sulfate reduction over multiple subsurface acetate amendments by measurement and modeling of sulfur isotope fractionation. *Environmental Science and Technology, 46,* 8895-8902

Edgar, R. C. (2010). Search and clustering orders of magnitude faster than BLAST. Bioinformatics 26(19): 2460-2461

Eggleston, Jack (USGS). (2009). *Mercury Loads in the South River and Simulation of Mercury Total Maximum Daily Loads (TMDLs) for the South River, South Fork Shenandoah River, and Shenandoah River: Shenandoah Valley, Virginia.* Scientific Investigations Report 2009–5076

Ehrlich, H. L., & Newman, D. K. (2009). *Geomicrobiology*. (5th ed.). Boca Raton: CRC Press.

FDA (U. S. Food and Drug Administration). (2013). Mercury Levels in Commercial Fish and Shellfish (1990–2010). Retrieved September 20, 2013 from: http://www.fda.gov/food/foodborneillnesscontaminants/metals/ucm115644.htm

Flanders, J. R., Turner, R. R., Morrison, T., Jensen, R., Pizzuto, J., Skalak, K., & Stahl, R. (2010). Distribution, behavior, and transport of inorganic and methylmercury in a high gradient stream. *Applied Geochemistry, 25*(11), 1756-1769

Fleming, E. J., Mack, E. E., Green, P. G., & Nelson, D. C. (2006). Mercury methylation from unexpected sources: Molybdate-inhibited freshwater sediments and an iron-reducing bacterium. *Applied and Environmental Microbiology, 72*(1), 457-464

Gilmour, C.C., & Henry, E.A. (1991). Mercury methylation in aquatic systems affected by acid deposition. *Environmental Pollution, 71,* 131-169

Gilmour, C.C., Henry, E.A., & Mitchell, R. (1992). Sulfate stimulation of mercury methylation in freshwater sediments. *Environmental Science and Technology, 26,* 2281-2287

Gilmour, C.C., Riedel, G.S., Ederington, M.C., Bell, J.T., Benoit, J.M., Gill, G.A., & Stordal, M.C. (1998). Methylmercury concentrations and production rates across a trophic gradient in the northern Everglades. *Biogeochemistry, 40,* 327-345

Gilmour,C.C., Elias, D.A., Kucken, A. M., Brown, S. D., Palumbo, A. V., Schadt, C.W., & Wall, J.D. (2011). Sulfate-reducing bacterium *Desulfovibrio desulfuricans* ND132 as a model for understanding bacterial mercury methylation. *Applied and Environmental Microbiology, 77*(12), 3938-3951

Gould, W.D., Stichbury, M., Francis, M., Lortie, L. & Blowes, D.W. (2003). An MPN method for the enumeration of iron-reducing bacteria. In: Spiers G, Beckett P, Conroy H, editors. *Proceedings of Mining and the Environment III*. Sudbury, ON, Canada: Laurentian University. P 153–157

Hansen, T.A. (1993). Carbon metabolism of sulfate-reducing bacteria. In: Odom, J.M. & Singleton Jr., R. editors. *The Sulfate-Reducing Bacteria: Contemporary Perspectives*. Springer-Verlag, New York: pp. 21–40

Harmon, S.M., King, J.K., Gladden, J.B., & Newman, L.A. (2007). Using sulfate-amended sediment slurry batch reactors to evaluate mercury methylation. *Archives of Environmental Contamination and Toxicology, 52,* 326-331

Hines, M. E., Horvat, M., Faganeli, J., Bonzongo, J.-C. J., Barkay, T., Major, E. B. Scott, K.J., Bailey, E.A., Warwick, J.J. & Lyons, W. B. (2000). Mercury biogeochemistry in the Idrija River, Slovenia, from above the mine into the Gulf of Trieste. *Environmental Research, 83*(2), 129-139

Horvat, M., Kontić, B., Kotnik, J., Ogrinc, N., Jereb, V., Fajon, V., Logar, M., Faganeli, J., Rajar, R., Sirca, A., Petkovšek , Zagar, D., & Dizdavevič, T. (2003). Remediation of mercury polluted sites due to mining activities. *Critical Reviews in Analytical Chemistry, 33*(4), 291-296

Hsu-Kim, H., Kucharzyk, K.H., Zhang, T., & Deshusses, M.A. (2013). Mechanisms regulating mercury bioavailability for methylating microorganisms in the aquatic environment: A critical review. *Environmental Science and Technology, 47* (6), 2441-2456

Hu, H., Lin, ,H., Zheng, W., Tomanicek, S.J., Johs, A., Feng, X., Elias, D.A., Liang, L., & Gu, B. (2013). Oxidation and methylation of dissolved elemental mercury by anaerobic bacteria. *Nature Geoscience.* doi:10.1038/ngeo1894

Isa, Z., Grusenmeyer, S., & Verstraete, W. (1986). Sulfate reduction relative to methane production in high-rate anaerobic digestion: Technical aspects. *Applied and Environmental Microbiology, 51*(3), 572-579

Jiang, T-Y., Jiang, J., Xu, R-K., & Li, Z. (2012). Adsorption of Pb(II) on variable charge soils amended with rice-straw derived biochar. *Chemosphere, 89*, 249-256

Kerin, E. J., Gilmour, C. C., Roden, E., Suzuki, M. T., Coates, J. D., & Mason, R. P. (2006). Mercury methylation by dissimilatory iron-reducing bacteria. *Applied and Environmental Microbiology, 72*(12), 7919-7921

King, J.K., Kostka, J.E., Frischer, M.E., & Saunders, F.M. (2000). Sulfate-reducing bacteria methylate mercury at variable rates in pure culture and in marine sediments. *Applied and Environmental Microbiology, 66*(6), 2430-2437

Langford, N. J., & Ferner, R. E. (1999). Toxicity of mercury. *Journal of Human Hypertension, 13*(10), 651-656

Lechler, P. J., Miller, J. R., Lacerda, L. D., Vinson, D., Bonzongo, J. -., Lyons, W. B., & Warwick, J. J. (2000). Elevated mercury concentrations in soils, sediments, water, and fish of the Madeira River Basin, Brazilian Amazon: A function of natural enrichments?. *Science of the Total Environment, 260*(1-3), 87-96

Lehmann, J. (2007). A handful of carbon. *Nature, 447*, 143-144

Lindsay, M. B. J., Wakeman, K. D., Rowe, O. F., Grail, B. M., Ptacek, C. J., Blowes, D. W., & Johnson, D. B. (2011). Microbiology and geochemistry of mine tailings amended with organic carbon for passive treatment of pore water. *Geomicrobiology Journal, 28*(3), 229-241

Liu, Z., Demisie, W., & Zhang, M. (2013). Simulated degradation of biochar and its potential environmental implications. *Environmental Pollution, 179,* 146-152

Lovley, D.R. (1991). Dissimilatory Fe (III) and Mn (IV) reduction. *Microbiological Reviews, 55* (2), 259-287

Lovley, D.R., Phillips, E.J.P., Gorby, Y.A., & Landa, E.R. (1991). Microbial reduction of uranium. *Nature, 350,* 413-416

Lowry, G. V., Shaw, S., Kim, C. S., Rytuba, J. J., & Brown Jr., G. E. (2004). Macroscopic and microscopic observations of particle-facilitated mercury transport from new Idrija and sulphur bank mercury mine tailings. *Environmental Science and Technology, 38*(19), 5101-5111

Marvin-Dipasquale, M., Lutz, M. A., Brigham, M. E., Krabbenhoft, D. P., Aiken, G. R., Orem, W. H., & Hall, B. D. (2009). Mercury cycling in stream ecosystems. 2. Benthic methylmercury production and bed sediment - pore water partitioning. *Environmental Science and Technology, 43*(8), 2726-2732

Miller, J., Barr, R., Grow, D., Lechler, P., Richardson, D., Waltman, K., & Warwick, J. (1999). Effects of the 1997 flood on the transport and storage of sediment and mercury within the Carson River Valley, West-Central Nevada. *The Journal of Geology, 107*(3), 313-327

Mosher, J.J., Vishnivetskaya, T.A., Elias, D.A., Podar, M., Brooks, S.C., Brown, S.D., Brandt, C.C. & Palumbo, A.V. (2012). Characterization of the Deltaproteobacteria in contaminated and uncontaminated stream sediments and identification of potential mercury methylators. *Aquatic Microbial Ecology, 66,* 271-282

Oak Ridge National Laboratory. (2013). Predicted methylators. Retrieved from http://www.esd.ornl.gov/programs/rsfa/data/PredictedMethylators/PredictedMethylators_20130627.pdf

Oremland, R.S., Culbertson, C.W., & Winfrey, M.R. (1991). Methylmercury decomposition in sediments and bacterial cultures: Involvement of methanogens and sulfate reducers in oxidative demethylation. *Applied and Environmental Microbiology, 57*(1), 130-137

Oremland, R. S., Miller, L. G., Dowdle, P., Connell, T., & Barkay, T. (1995). Methylmercury oxidative degradation potentials in contaminated and pristine sediments of the Carson River, Nevada. *Applied and Environmental Microbiology, 61*(7), 2745-2753

Oyekola, O. O., van Hille, R. P., & Harrison, S. T. L. (2009). Study of anaerobic lactate metabolism under biosulfidogenic conditions. *Water Research, 43*(14), 3345-3354

Oyekola, O. O., van Hille, R. P., & Harrison, S. T. L. (2010). Kinetic analysis of biological sulphate reduction using lactate as carbon source and electron donor: Effect of sulphate concentration. *Chemical Engineering Science, 65*(16), 4771-4781

Oyekola, O.O., Harrison, S.T.L., & van Hille, R.P. (2012). Effect of culture conditions on the competitive interaction between lactate oxidizers and fermenters in a biological sulfate reduction system. Bioresource Technology, 104, 616-621

Park, J.H., Choppala, G.K., Bolan, N.S., Chung, J.W., & Chuasavathi, T. (2011). Biochar reduces the bioavailability and phytotoxicity of heavy metals. *Plant Soil, 348*, 439-451

Parks, J. M., Johs, A., Podar, M., Bridou, R., Hurt Jr., R. A., Smith, S. D., Tomanicek, S. J., Qian, Y., Brown, S.D., Brandt, C.C., Palumbo, A.V., Smith, J.C., Wall, J.D., Elias, D.A., &. Liang, L. (2013). The genetic basis for bacterial mercury methylation. *Science, 339*(6125), 1332-1335

Pizzuto, J., & O'Neal, M. (2009). Increased mid-twentieth century riverbank erosion rates related to the demise of mill dams, South River, Virginia. *Geology, 37*(1), 19

Postgate, J. R. (1984). *Sulphate-reducing Bacteria*. (2nd ed.). Cambridge Cambridgeshire: Cambridge University Press

Ravichandran, M., Aiken, G. R., Ryan, J. N., & Reddy, M. M. (1999). Inhibition of precipitation and aggregation of metacinnabar (mercuric sulfide) by dissolved organic matter isolated from the florida everglades. *Environmental Science and Technology, 33*(9), 1418-1423

Ravichandran, M. (2004). Interactions between mercury and dissolved organic matter—a review. *Chemosphere, 55*, 319-331

Santos-Francés, F., García-Sánchez, A., Alonso-Rojo, P., Contreras, F., & Adams, M. (2011). Distribution and mobility of mercury in soils of a gold mining region, Cuyuni river basin, Venezuela. *Journal of Environmental Management, 92*, 1268-1276

Schuster, E. (1991). The behavior of mercury in the soil with special emphasis on complexation and adsorption processes –A review of the literature. *Water, Air and Soil Pollution, 56* (1), 667-680

Slowey, A. J. (2010). Rate of formation and dissolution of mercury sulfide nanoparticles: The dual role of natural organic matter. *Geochimica et Cosmochimica Acta, 74*(16), 4693-4708

Stamenkovic, J., Gustin, M. S., Marvin-DiPasquale, M. C., Thomas, B. A., & Agee, J. L. (2004). Distribution of total and methyl mercury in sediments along Steamboat Creek (Nevada, USA). *Science of the Total Environment, 322*(1-3), 167-177

Stumm, W., & Morgan, J.J. (1996). *Aquatic Chemistry: Chemical Equilibria and Rates in Natural Waters*, 3rd ed. John Wiley & Sons, Inc., New York, 1022p

Taylor, B.F., & Oremland, R.S. (1979). Depletion of adenosine triphosphate in Desulfovibrio by oxyanions of Group VI elements. *Current Microbiology, 3*, 101-103

Uchimiya, M., Chang, S., & Klasson, K.T. (2011). Screening biochars for heavy metal retention in soil: role of oxygen functional groups. *Journal of Hazardous Materials, 190*, 432-441

U.S. EPA (1996). Method 3050b: Acid digestion of sediments, sludges and soils.

U.S. EPA (2001). Method 1630: Methyl mercury in water by distillation, aqueous ethylation, purge and trap, and CVAFS. EPA-821-R-01-020

U.S. EPA (2002). Method 1631, Revision E: Mercury in water by oxidation, purge and trap, and cold vapor atomic fluorescence spectrometry. EPA-821-R-02-019

USGS. (2007). Acid rain in Shenandoah National Park, Virginia. Retrieved from: http://pubs.usgs.gov/fs/2007/3057/pdf/FS2007-3057.pdf

Utgikar, V.P., Harmon, S.M., Chaudhary, N., Tabak, H.H., Govind, R., & Haines, J.R. (2002). Inhibition of sulfate-reducing bacteria by metal sulfide formation in bioremediation of acid mine drainage. *Environmental Toxicology, 17*(1), 40-48

Van der Heide, T., Smolders, A.J.P., Lamers, L.P.M., van Katwijk, M.M., & Roelofs, J.G.M. (2010). Nutrient availability correlates with bicarbonate accumulation in marine and freshwater sediments- empirical evidence from pore water analyses. *Applied Geochemistry, 25*, 1825-1829

Wang, Q., Kim, D., Dionysiou, D.D., Sorial, G.A., & Timberlake, D. (2004). Sources and remediation for mercury contamination in aquatic systems – a literature review. *Environmental Pollution, 131*, 232-336

Waybrant, K. R., Ptacek, C. J., & Blowes, D. W. (2002). Treatment of mine drainage using permeable reactive barriers: Column experiments. *Environmental Science and Technology, 36*(6), 1349-1356

Widdel, F., & Pfennig, N. (1982). Studies on dissimilatory sulfate-reducing bacteria that decompose fatty acids. II. Incomplete oxidation of propionate by *Desulfobulbus propionicu*s gen. nov., spp. nov. *Archives of Microbiology, 131*(4), 360-365

Williams, K.H., Long, P.E., Davis, J.A., Wilkins, A., N'Guessan, L., Steefel, C.I., Yang, L., Newcomer, D., Spane, F.A., Kerkhof, L.J., McGuinness, L., Dayvault, R. & Lovley, D.R. (2011). Acetate availability and its influence on sustainable bioremediation of uranium-contaminated groundwater. *Geomicrobiology Journal, 28*: 5-6, 519-539

Yu, R.-Q., Flanders, J.R., Mack, E.E., Turner, R., Mirza, B.M., & Barkay, T. (2012). Contribution of coexisting sulfate and iron reducing bacteria to methylmercury production in freshwater river sediments. *Environmental Science and Technology, 46,* 2684-2691

Zhang, L., Wang, S., Meng, Y., Hao, Jiming. (2012). Influence of mercury and chlorine content of coal on mercury emissions from coal-fired power plants in China. *Environmental Science and Technology, 46*(11), 6385-6392

Zhang, T., Kim, B., Levard, C., Reinsch, B. C., Lowry, G. V., Deshusses, M. A., & Hsu-Kim, H. (2012). Methylation of mercury by bacteria exposed to dissolved, nanoparticulate, and microparticulate mercuric sulfides. *Environmental Science and Technology, 46*(13), 6950-6958

Zimmerman, A. R. (2010). Abiotic and microbial oxidation of laboratory-produced black carbon (biochar). *Environmental Science and Technology, 44,* 1295-1301

Appendix A: *Supplementary Plots for Chapter 2*

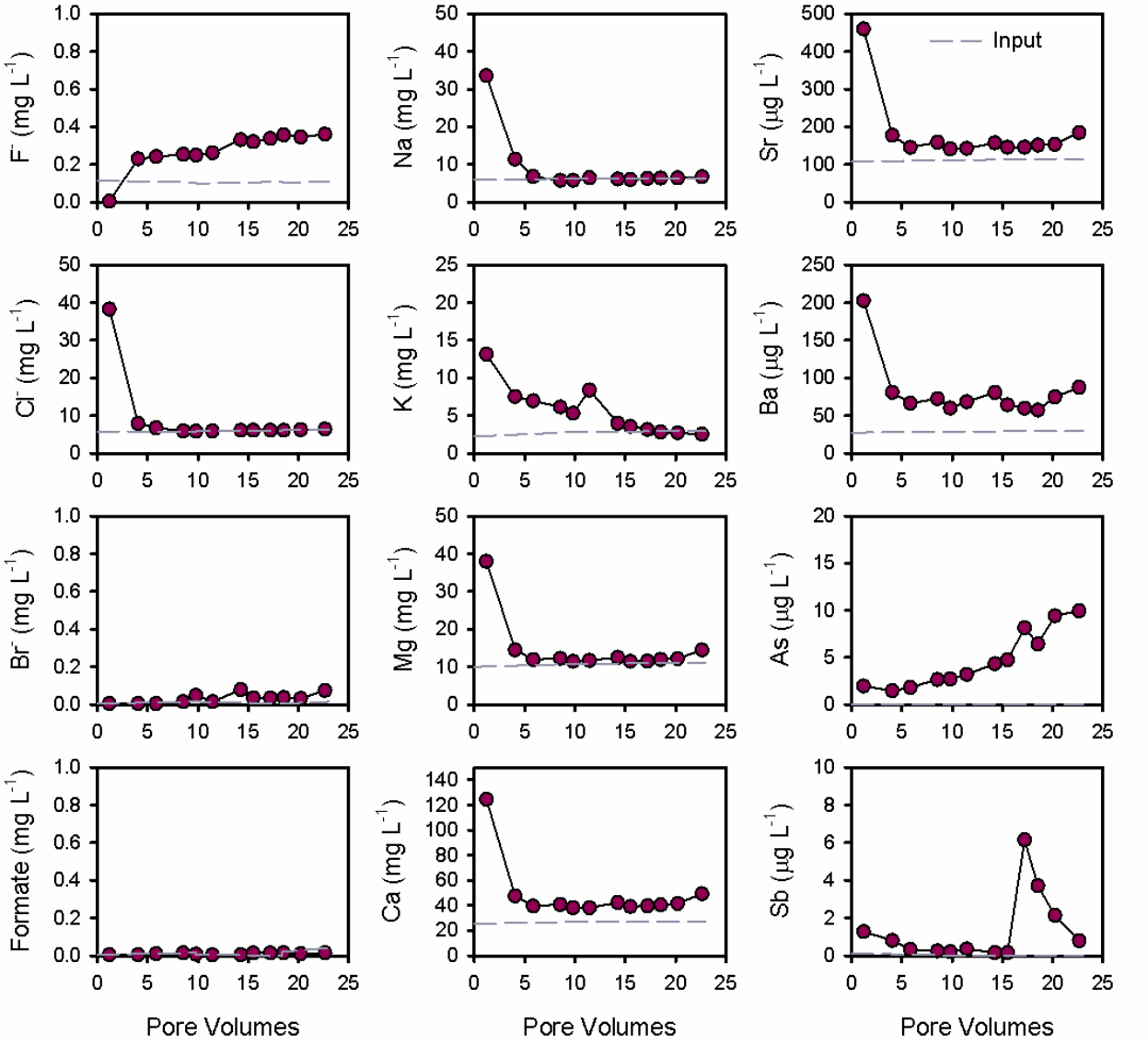

Fig. A.1: Additional measured effluent parameters of the control column.

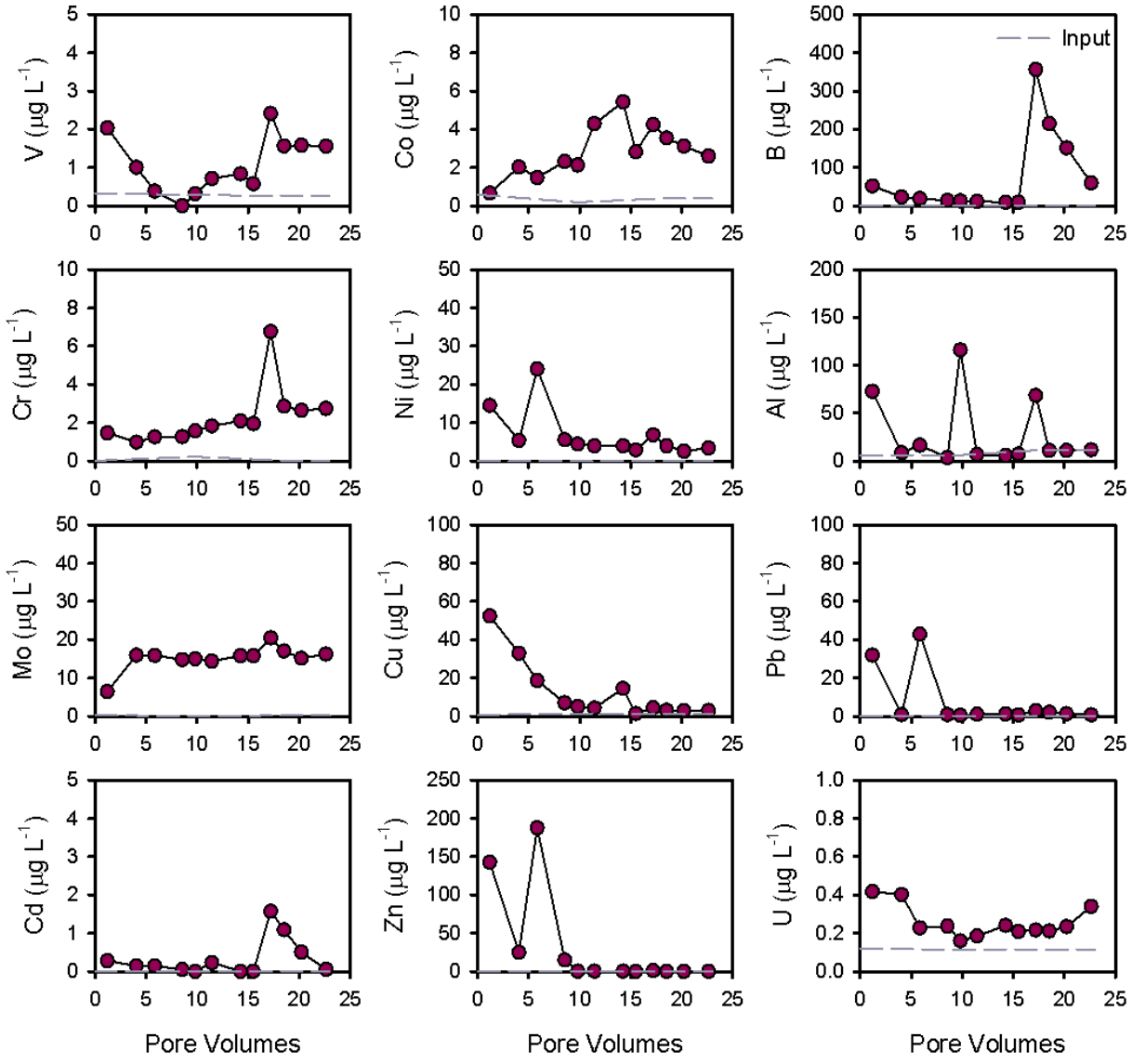

Fig. A.2: Additional trace metals for the control column.

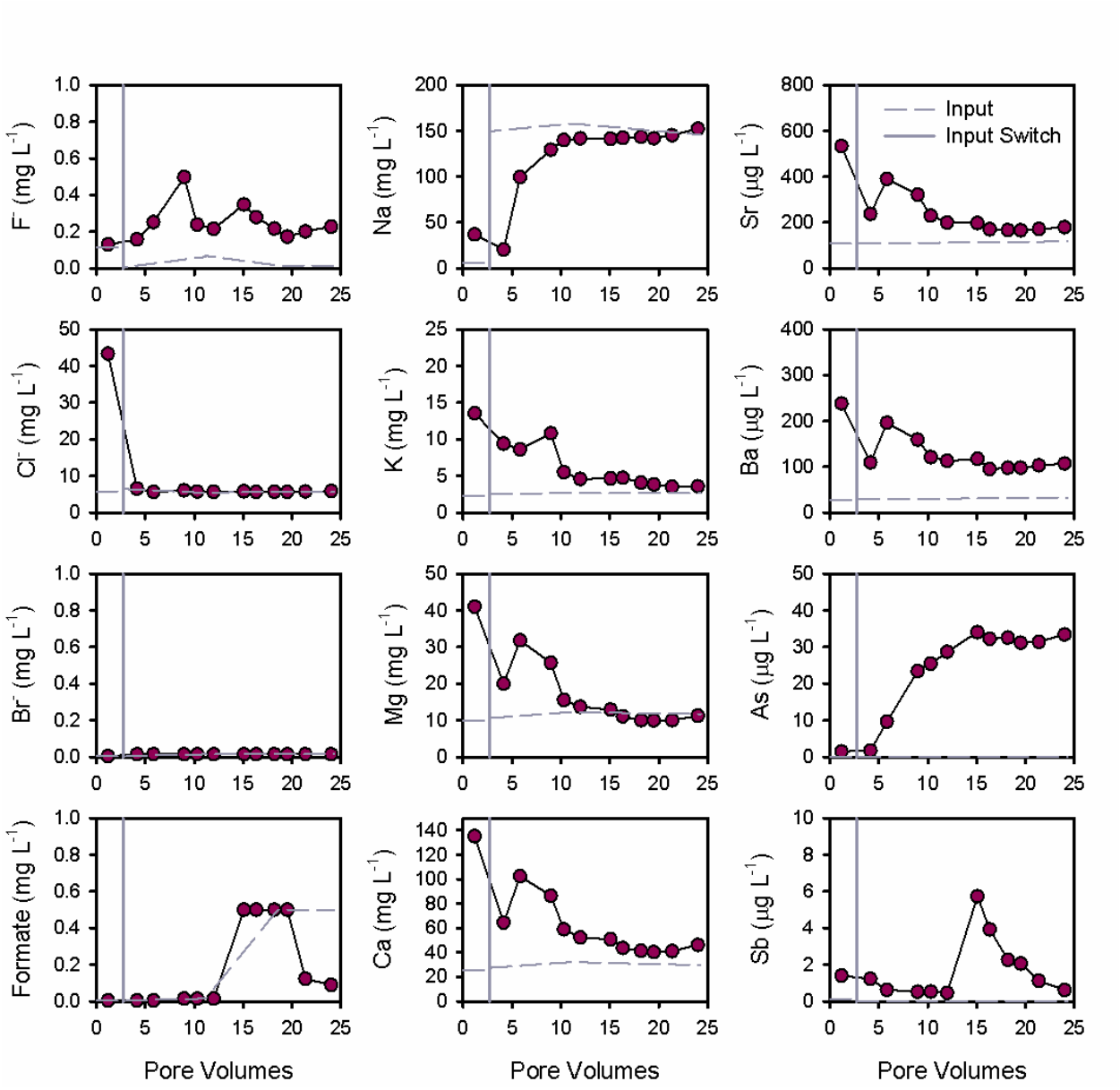

Fig. A.3: Additional measured effluent parameters for the acetate column. Vertical gray line indicates switch from SRW to acetate influent.

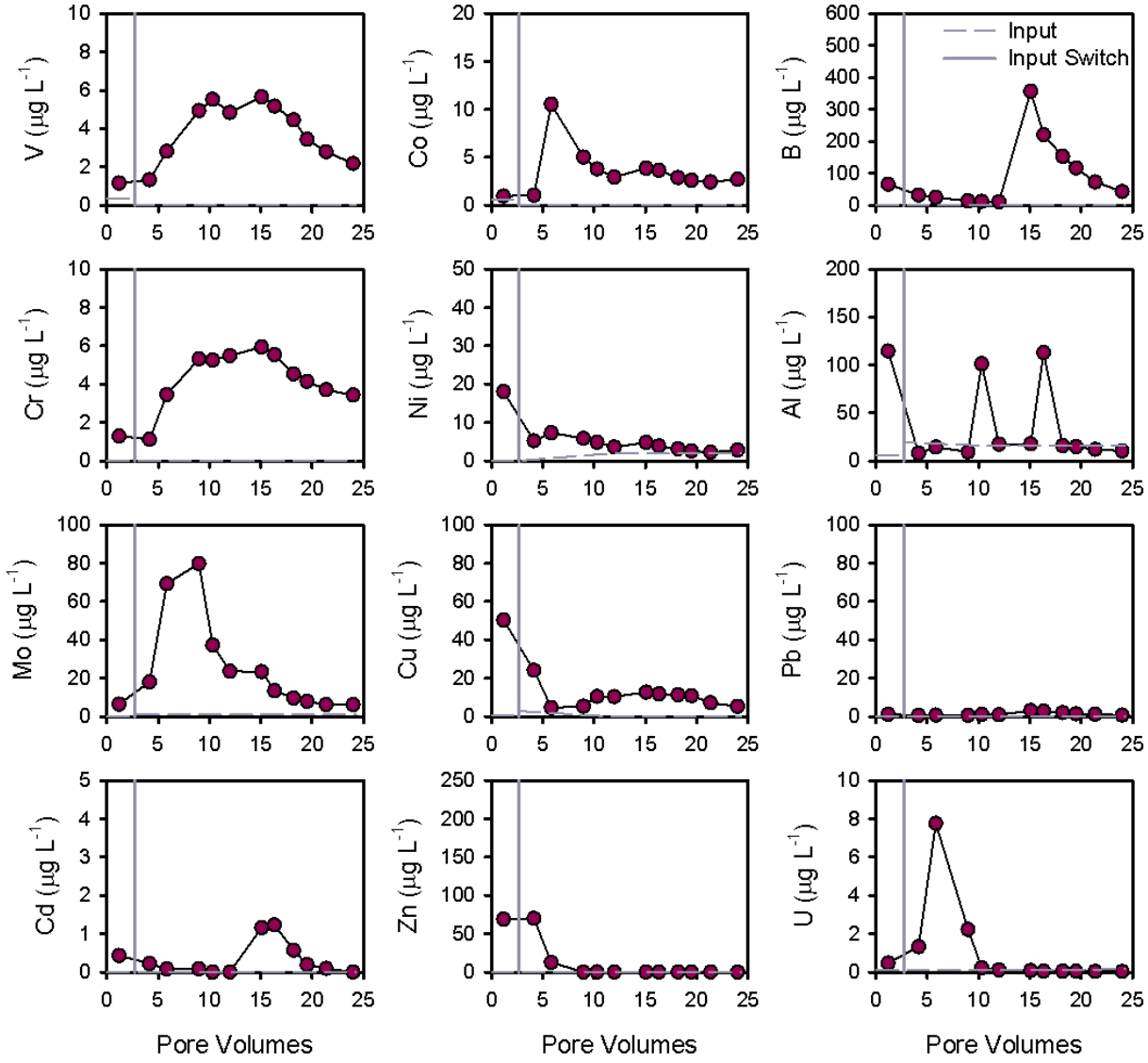

Fig. A.4: Additional trace metals for the acetate column. Vertical gray line indicates switch from SRW to acetate influent.

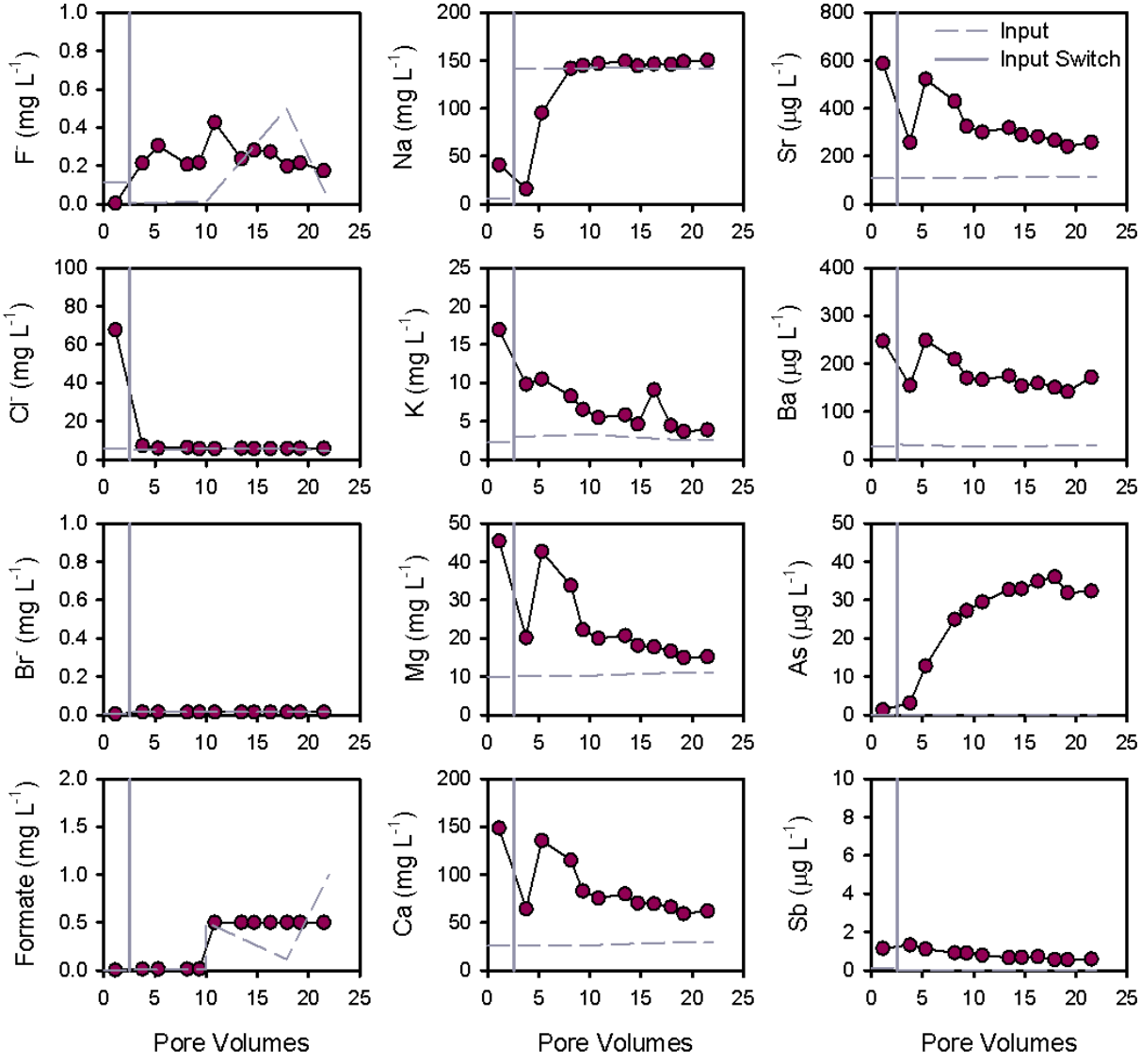

Fig. A.5: Additional measured effluent parameters for the lactate column. Vertical gray line indicates switch from SRW to lactate influent.

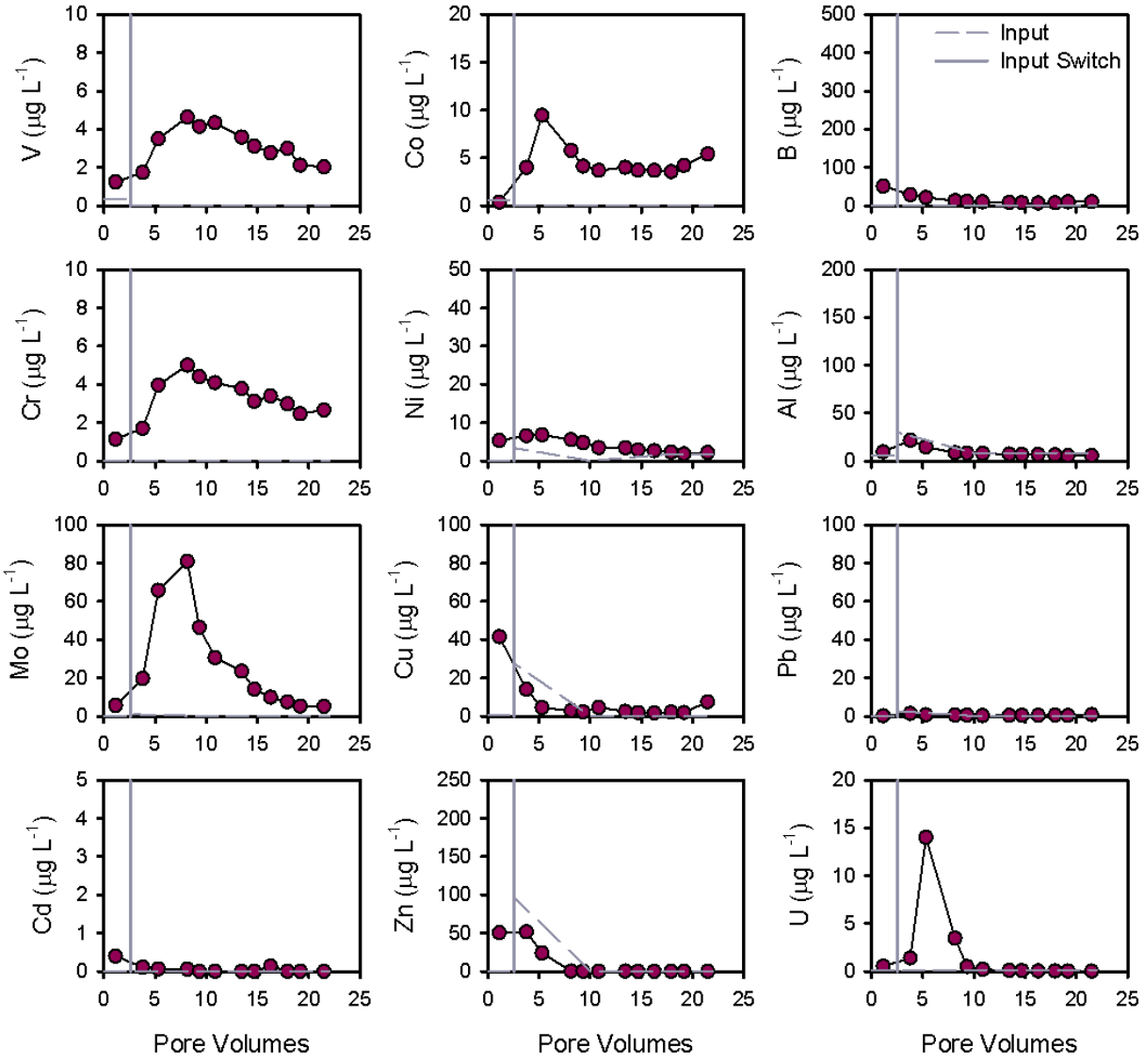

Fig. A.6: Additional trace metals for the lactate column. Vertical gray line indicates switch from SRW to lactate influent.

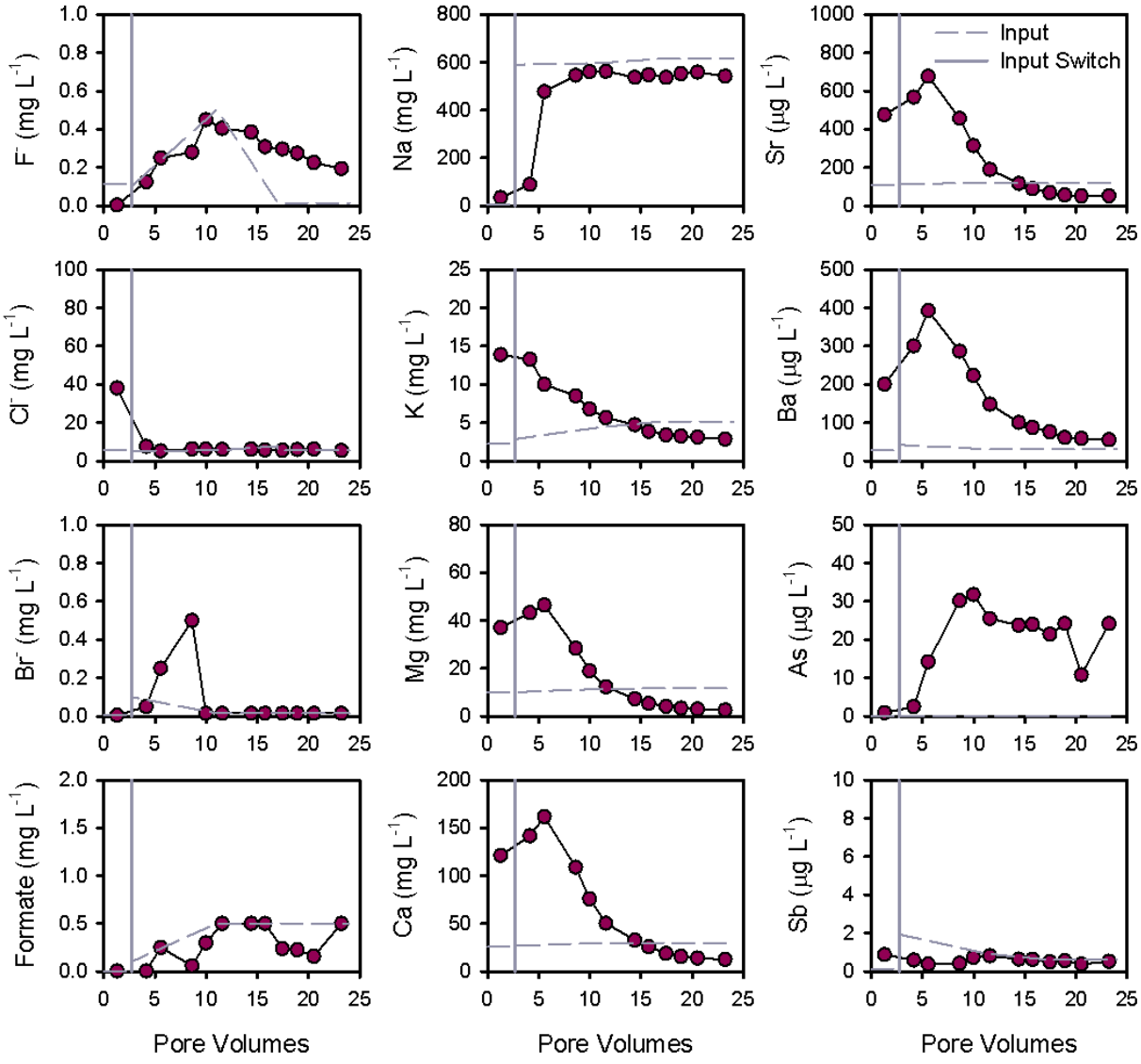

Fig. A.7: Additional measured effluent parameters for the lactate-sulfate column. Vertical gray line indicates switch from SRW to lactate-sulfate influent.

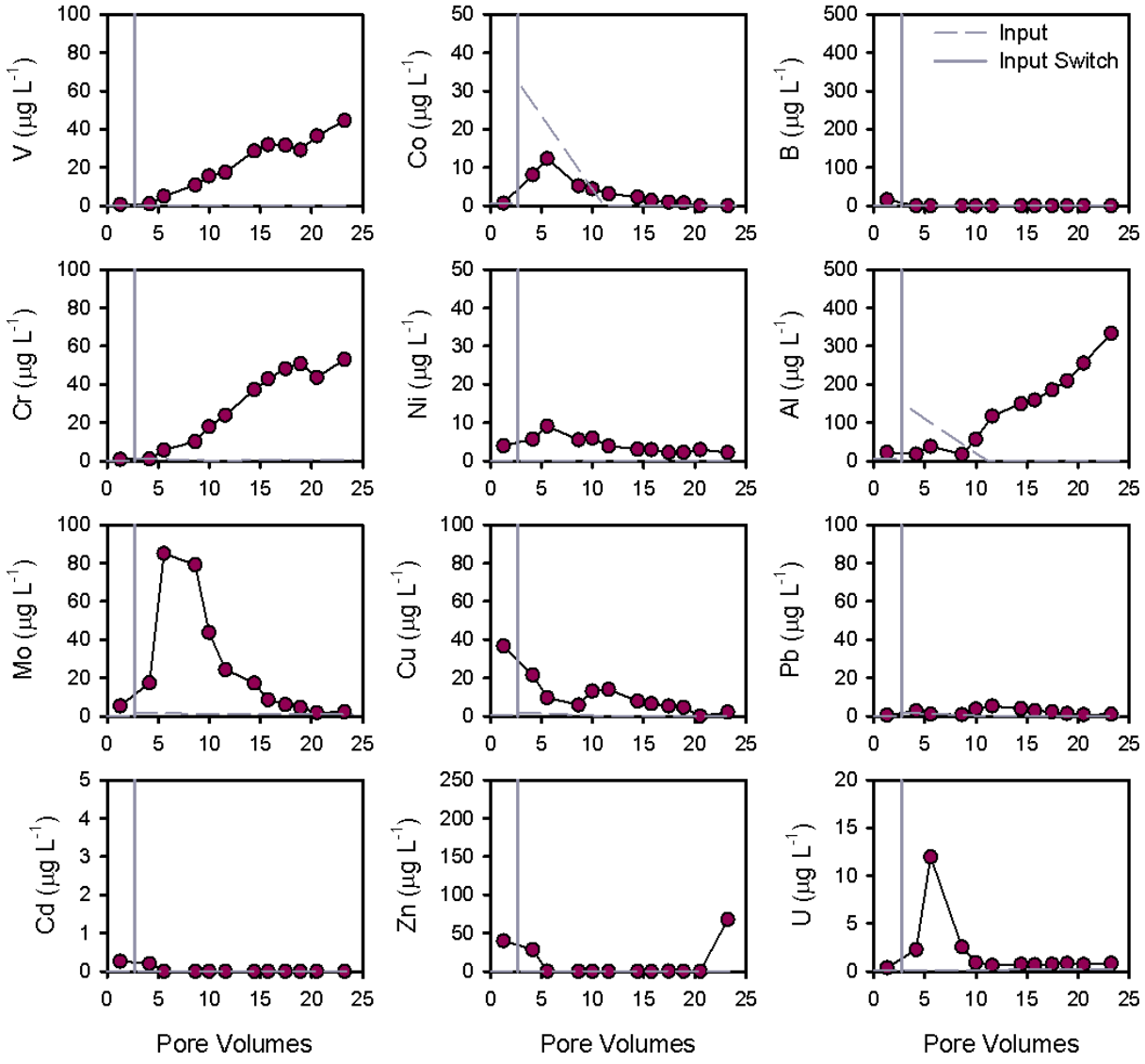

Fig. A.8: Additional trace metals for the lactate-sulfate column. Vertical gray line indicates switch from SRW to lactate-sulfate influent.

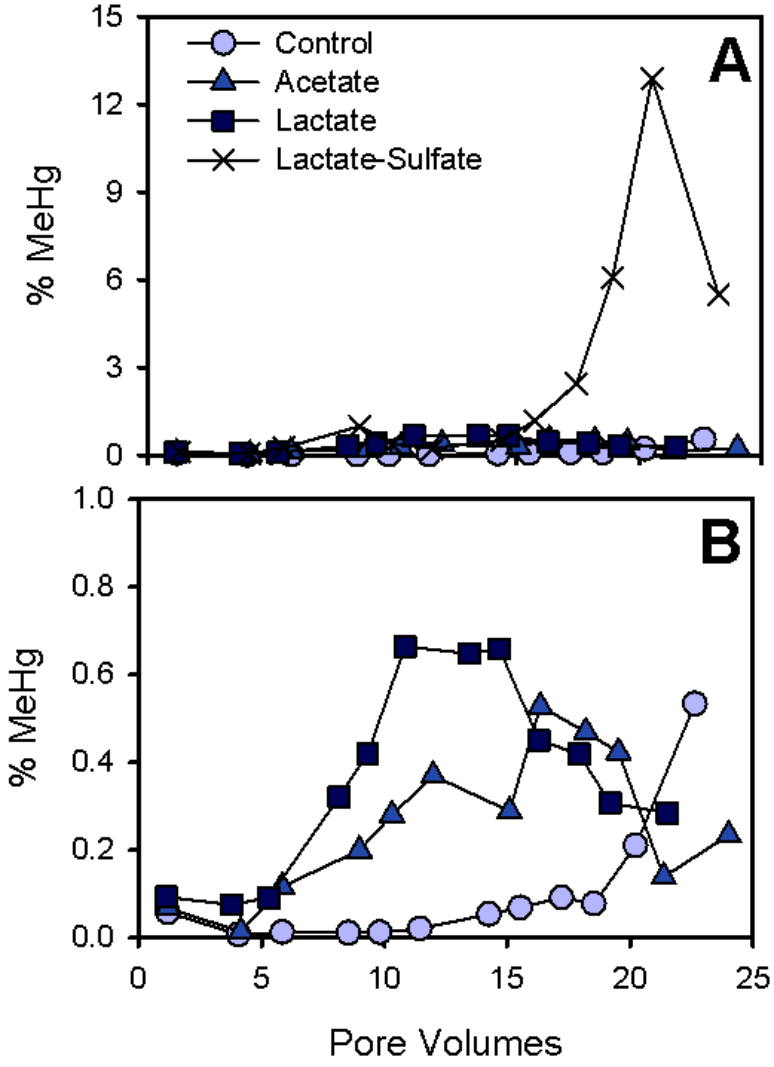

Fig. A.9: Percent MeHg in the column effluent. Top Fig. (A) represents all 4 columns, while bottom Fig. (B) focuses on the lactate, acetate and control column effluents.

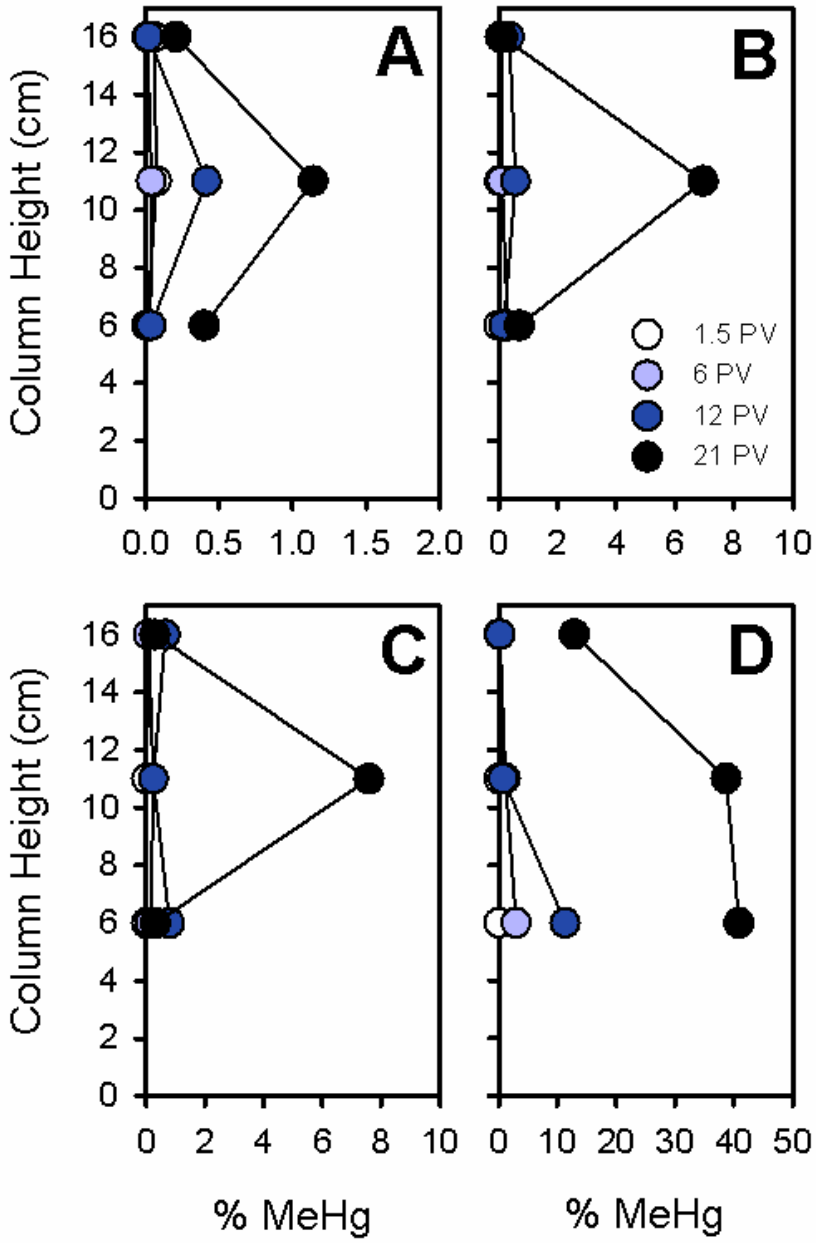

Fig. A.10: MeHg as a percentage along the length of the column at different pore volumes. The letters A, B, C, D refer to the control, acetate, lactate, and lactate-sulfate column respectively.

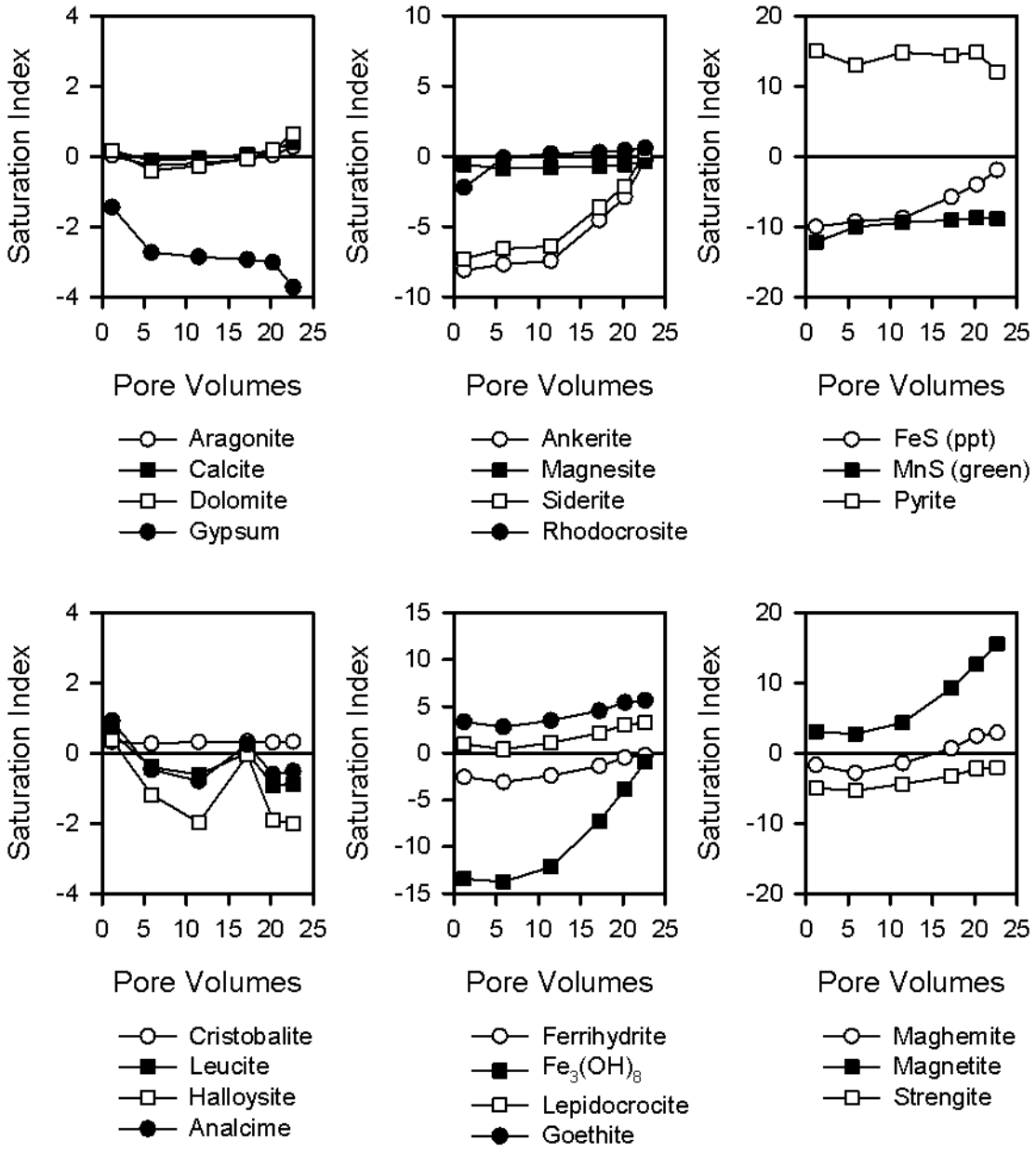

Fig. A.11: Saturation indices for select minerals for the control column effluent.

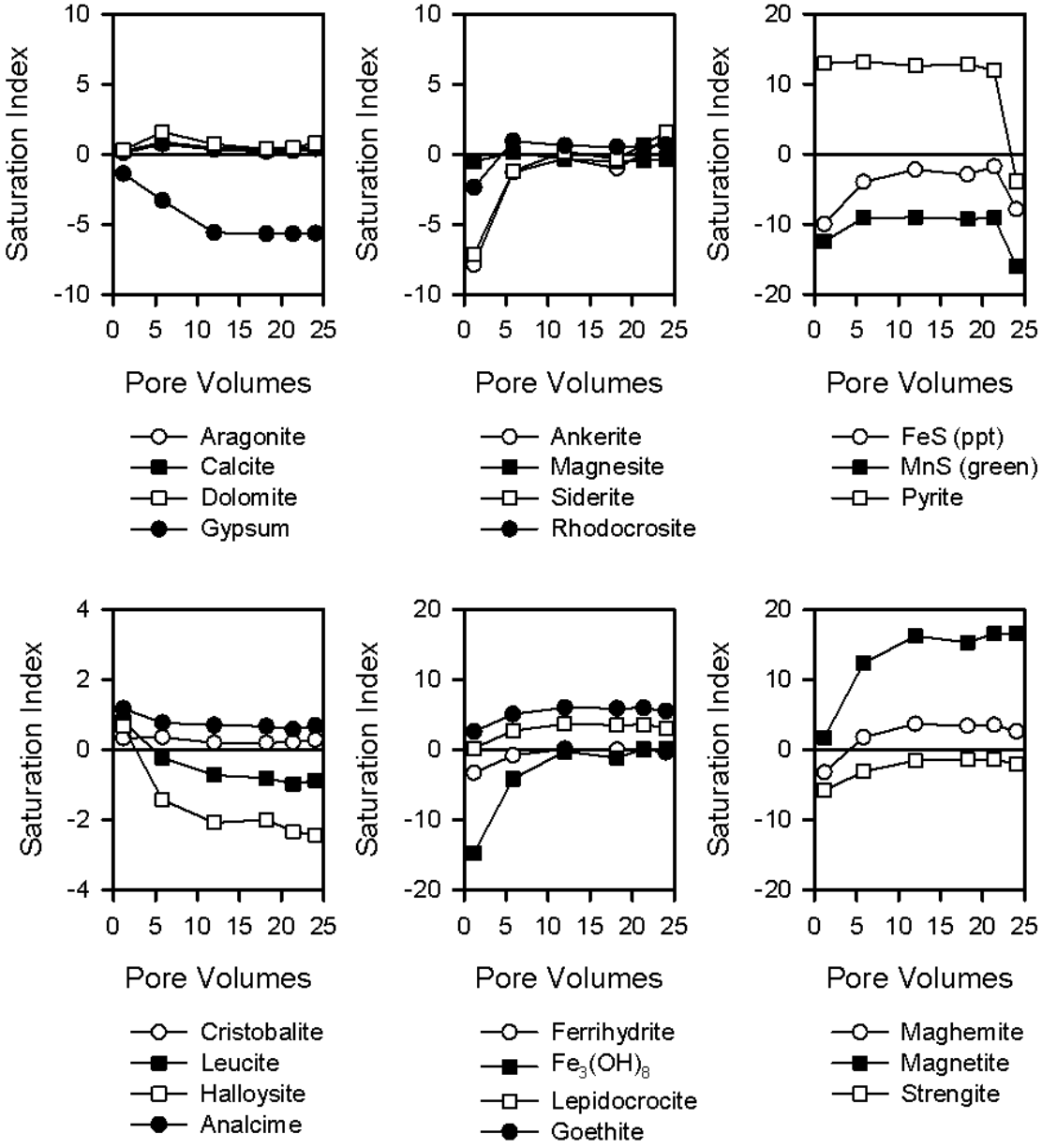

Fig. A.12: Saturation indices for select minerals for the acetate column effluent.

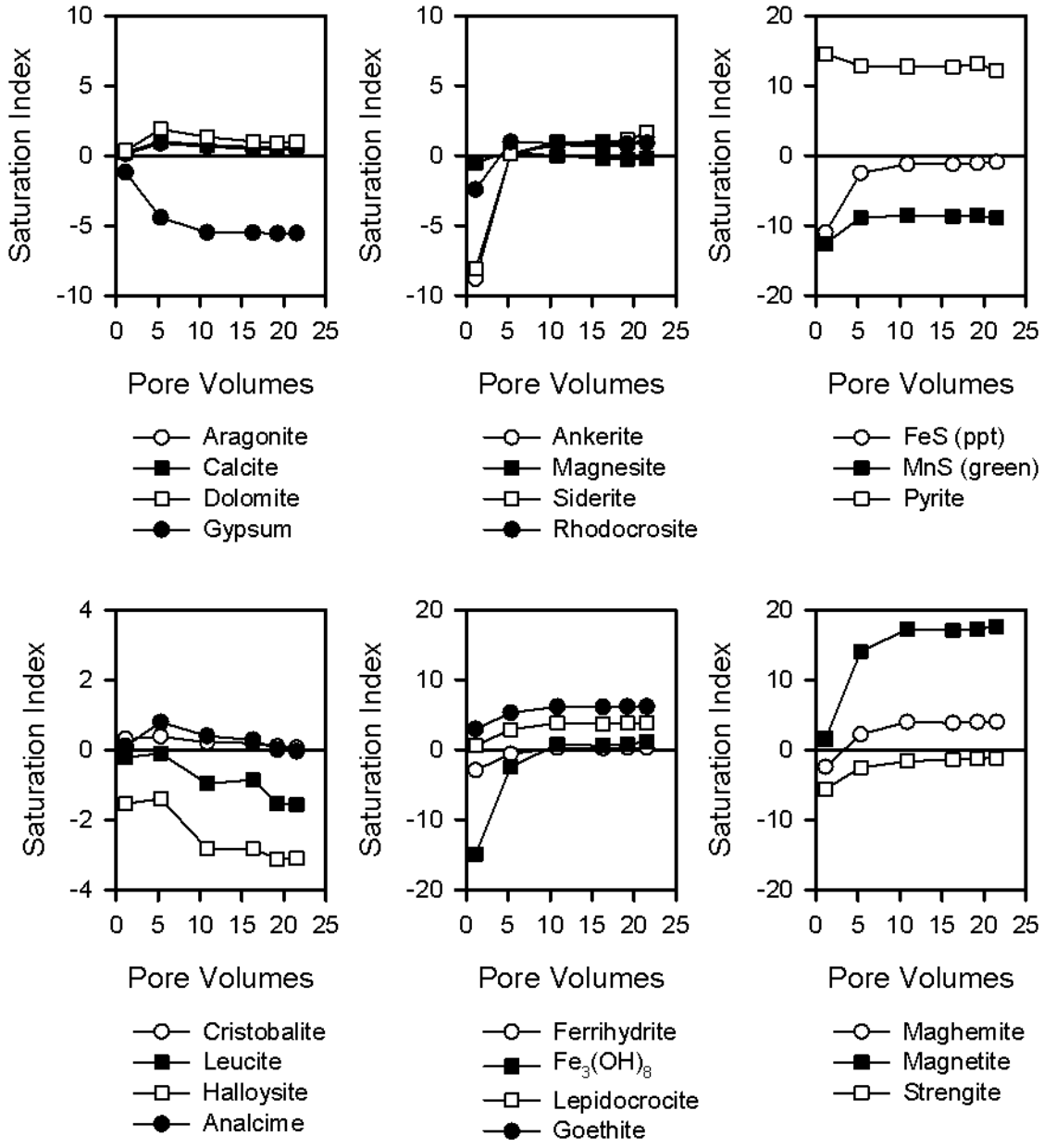

Fig. A.13: Saturation indices for select minerals in the lactate column effluent.

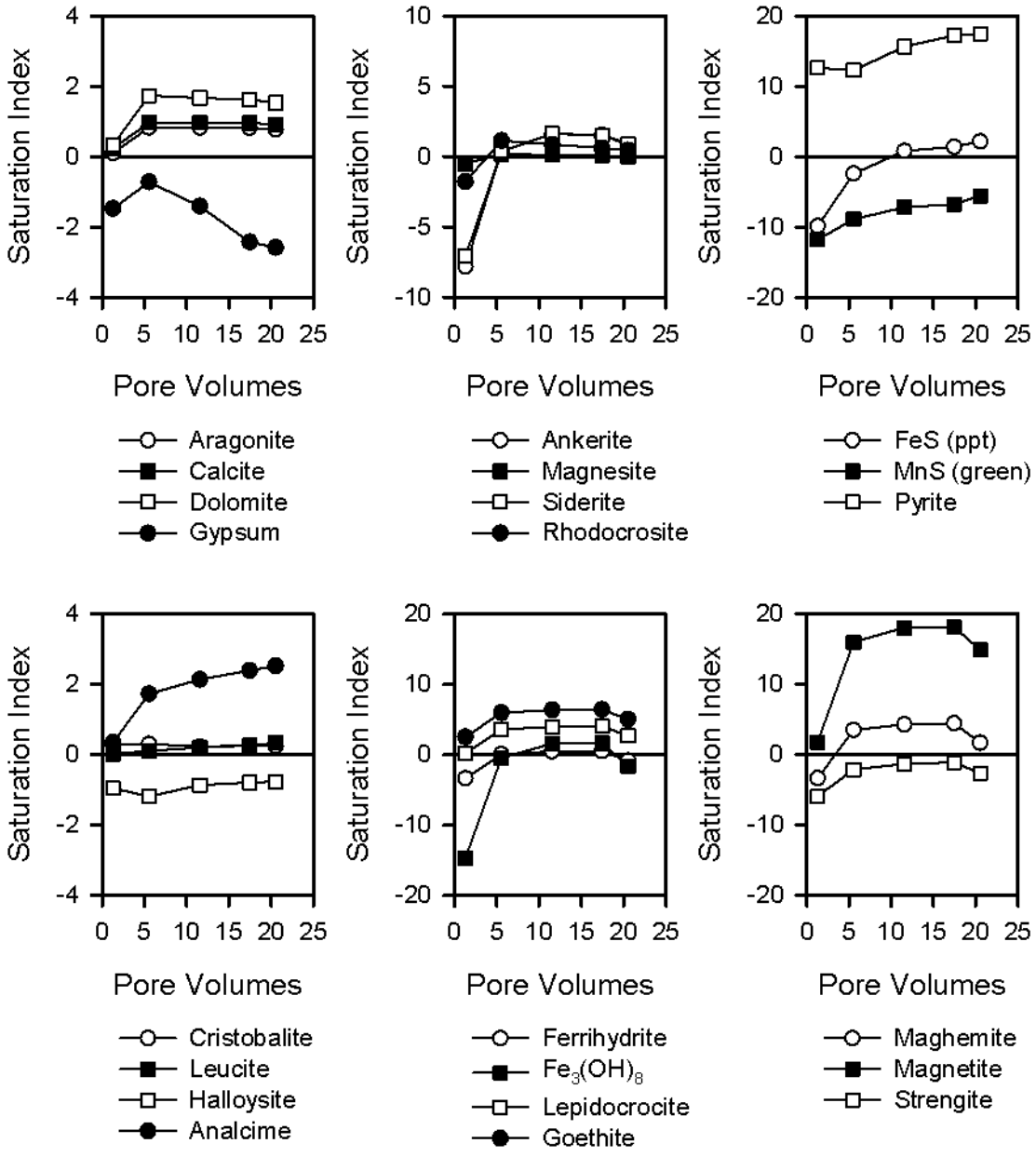

Fig. A.14: Saturation indices for select minerals in the lactate-sulfate column effluent.

Appendix B: *Quality Assurance and Quality Control for Chapters 2 and 3*

Table B.1: THg QA/QC for the control column aqueous samples.

Sample ID	Date Sampled	Date Analyzed	THg (ng L^{-1})	Duplicate	Repeat	Relative Percent Difference (%)	Matrix Spike Recovery (%)
SRWD-1	14-Feb-13	28-Feb-13	1140	1210		5.45	92.0
SRWD-3	25-Feb-13		7160	7060		1.39	
SRWD-Bottom Port	28-Feb-13	March 27, April 4 2013	8060		8050	0.07	
SRWD-4 (UNF)	04-Mar-13		6800		7050	3.70	
SRWD-5 (UNF)	07-Mar-13		6630		6720	1.45	
SRWD-6	11-Mar-13		5500	5510		0.20	107.4
SRWD-Top Port	13-Mar-13		590		680	13.21	
SRWD-Bottom Port	14-Mar-13		6390		6730	5.20	
SRWD-7	18-Mar-13		4430		4480	1.01	
SRWD-7 (UNF)			5820		5920	1.57	
SRWD-8	21-Mar-13		3880		4050	4.49	
SRWD-8 (UNF)			5560		5700	2.34	
SRWD-9	25-Mar-13		3470		3590	3.34	
SRWD-10	28-Mar-13	April 24, May 14 2013	2920				100.5
SRWD-11	01-Apr-13	24-Apr-13	2060	2010		2.65	
SRWD-12	07-Apr-13		1580	1700		7.18	
Method Detection Limit Average as of May, 2013			0.14				

Table B.2: THg QA/QC for the acetate column aqueous samples.

Sample ID	Date Sampled	Date Analyzed	THg (ng L^{-1})	Duplicate	Repeat	Repeat	Relative Percent Difference (%)	Matrix Spike Recovery (%)
ACED-1	16-Feb-13	28-Feb-13	1100	1070			3.31	88.81
ACED-2	23-Feb-13	February 28, May 7 2013	8880		9210		3.65	
ACED-2 (UNF)			6980		6960		0.33	
ACED-3	27-Feb-13	March 27, March 28 2013	6440	6460			0.19	
ACED-Bottom Port	01-Mar-13	March 27, April 4 2013	7090		7690		8.05	
ACED-6	13-Mar-13	March 27, March 28 2013	8670	9890			13.16	103.3
ACED-Top Port	14-Mar-13	March 27, April 4 2013	3310		3710		11.31	
ACED-Bottom Port	16-Mar-13		8800		9740		10.18	
ACED-9	27-Mar-13	24-Apr-13	9260	9380			1.24	
ACED-10	30-Mar-13	April 24, May 7 2013	9450		9460		0.13	
ACED-10 (UNF)		April 24, May 7, May 14 2013	8990		8090	9430	2.55	
ACED-11	03-Apr-13	Apr-13	9640	9410			2.41	104.31
ACED-12	09-Apr-13	25-Apr-13	10280	9410			8.81	
Method Detection Limit Average as of May, 2013			0.14					

Table B.3: THg QA/QC for the lactate column aqueous samples.

Sample ID	Date Sampled	Date Analyzed	THg (ng L^{-1})	Duplicate	Repeat	Repeat	Relative Percent Difference (%)	Matrix Spike Recovery (%)
LACD-1	18-Feb-13	28-Feb-13	1560	1570			1.15	90.92
LACD-2	25-Feb-13		4340		4320		0.46	
LACD-3	01-Mar-13	March 27, March 28 2013	6740	7950			16.45	
LACD-Bottom Port	04-Mar-13	March 27, April 4 2013	10540		10330		2.00	
LACD-6	15-Mar-13	March 27, March 28, April 4 2013	3570	4210	3900		12.00	110.59
LACD-Bottom Port	19-Mar-13	March 28, April 4 2013	2070		2290		10.09	
LACD-9	29-Mar-13	25-Apr-13	4550	4540			0.22	
LACD-10	02-Apr-13	April 25, May 7 2013	4110		3920	3920	4.73	
LACD-10 (UNF)			4030		4130		2.50	
LACD-11	05-Apr-13	25-Apr-13	4110	4070			1.00	
LACD-Top Port	07-Apr-13	April 25, May 7 2013	710		640		10.39	
LACD-Bottom Port	08-Apr-13		6980		6900		1.04	
LACD-12	11-Apr-13	25-Apr-13	4360	4440			1.93	98
Method Detection Limit Average as of May, 2013			0.14					

Table B.4: THg QA/QC for the lactate-sulfate column aqueous samples.

Sample ID	Date Sampled	Date Analyzed	THg (ng L^{-1})	Repeat	Duplicate	Repeat	Repeat	Relative Percent Difference (%)	Matrix Spike Recovery (%)
CLSD-1	22-Feb-13	February 28, March 1 2013	810		940			14.56	97.56
CLSD-3	05-Mar-13	28-Mar-13	5420		5620			3.65	
CLSD-Top Port	06-Mar-13	March 28, April 4 2013	3830	4220				9.58	
CLSD-Bottom Port	08-Mar-13		4760	5130				7.52	
CLSD-6	19-Mar-13	28-Mar-13	19700		23400			17.56	106.51
CLSD-8	29-Mar-13	April 25, May 7 2013	15300	14200				7.27	
CLSD-8 UNF	29-Mar-13		13000	13200				1.96	
CLSD-9	02-Apr-13	25-Apr-13	15900		16600			4.33	
CLSD-10	05-Apr-13	April 25, May 7 2013	14500	15700				8.07	
CLSD-10 UNF			11900	13700				14.36	
CLSD-11	09-Apr-13	April 25, May 14 2013	14100		14600			3.84	122.22
CLSD-12	15-Apr-13	April 25, May 7, May 14 2013	15500	17800	15500	15200	16900	4.84	
Method Detection Limit Average as of May, 2013			0.14						

Table B.5: THg QA/QC on aqueous samples from biochar treatment column

Sample ID	Date Sampled	Date of Analysis	THg (ng L^{-1})	Duplicate	Relative Percent Difference (%)	Matrix Spike Recovery (%)
ACCL2-63	22-Feb-12	18-Oct-12	4.4	5.2	16.91	
ACCL2-81	20-Aug-12	20-Sep-12	7.3			56.88
ACCL2-86	24-Sep-12	04-Oct-12	5.7			124.92
ACCL2-88	10-Oct-12	18-Oct-12	5.3			96.26
ACCL2-89 (UNF)	12-Oct-12	18-Oct-12	4.7	4.5	3.27	
ACCL2-90 (0.45)	19-Oct-12	01-Nov-12	6.4			85.98
ACCL2-90 (UNF)	19-Oct-12	01-Nov-12	5.9	5.5	7.74	
ACCL2-91 (0.45)	26-Oct-12	01-Nov-12	5	5.3	5.69	
ACCL2-91 (UNF)	26-Oct-12	01-Nov-12	5.7	5.9	4.49	
ACCL2-92 (0.45)	02-Nov-12	15-Nov-12	5.3			87.77
ACCL2-92 (UNF)	02-Nov-12	15-Nov-12	4.9	4.5	9.28	
ACCL2-96 (0.45)	30-Nov-12	05-Dec-12	6.5			96.91
ACCL2-96 (UNF)	30-Nov-12	05-Dec-12	6.7	7	4.85	
ACCL2-101 (0.45)	04-Jan-13	09-Jan-13	4.3			110.59
ACCL2-101 (UNF)	04-Jan-13	09-Jan-13	4.7	4.7	0.63	
ACCL2-104 (0.45)	25-Jan-13	31-Jan-13	4.3	3.6	19.04	
Method Detection Limit (average as of Jan. 31, 2013)			0.12			

Table B.6: External and internal laboratory comparison of aqueous MeHg analyses

Sample ID	MeHg (ng L^{-1})		Relative Percent Difference (%)
	Internal	External	
SRWD-3 (2)	0.86	1.53	56.07
ACED-6 (2)	34.3	22.00	43.61
LACD-9 (2)	20.5	14.10	36.90
CLSD-11 (2)	1850	993.00	60.18
SRWD-Influent (new)	0.18	0.13	34.71
ACED-Influent (new)	0.03	0.13	120.39
LACD-Influent (new)	0.11	0.27	82.43
CLSD-Influent (new)	1.13	0.06	181.46

Table B.7: THg QA/QC for the Hg sequential extractions of the column sediments.

		THg (μg g^{-1} dry weight)				
Sample ID	**Date of Analysis**	**F1**	**F2**	**F3**	**F4**	**F5**
SRD-UW	November, 2012	0.3	0.5	6.0	29.0	132.0
SRD-UW-2	September, 2013	0.3	0.2	10.1	53.1	94.7
SRD-UW-3		0.2	0.4	8.4	48.3	119.5
Relative Standard Deviation (%)		21.7	41.7	25.2	29.3	16.5
ACED-M	July, 2013	1.4	4	13	33	112
ACED-M-Dup	August, 2013	0.9	0.7	8	44	137
Relative Percent Difference (%)		43.5	140.4	47.6	28.6	20.1
LACD-B	July, 2013	1.4	2.5	8.0	37.0	122.0
LACD-B-DUP	August, 2013	1.1	0.9	7.0	39.0	117.0
LACD-B-TRIP		1.4	1.4	7.0	36.0	125.0
Relative Standard Deviation (%)		13.3	51.2	7.9	4.1	3.3
CLSD-M	July, 2013	2.8	0.2	8.0	49.0	123.0
CLSD-M-DUP		1.4	0.1	7.0	33.0	114.0
CLSD-M-TRIP		1.2	0.1	7.0	29.0	112.0
Relative Standard Deviation (%)		48.4	43.3	7.9	28.6	5.0

Table B.8: Solid phase MeHg QA/QC

	MeHg					
Sample ID	(ng L^{-1})	(ng g^{-1} dry weight)	Duplicate (ng g^{-1} dry weight)	Relative Percent Difference (%)	Matrix Spike Recovery (%)	Recovery (%)
SRWD-M	100	18			71.64	
ACED-B	110	29			76.86	
LACD-T	130	25			84.81	
CLSD-M	940	182			123.88	
CLSD-B	2200	456	602	28		
Distillation Blank	0.03					
ERM-CC580	356	73				98
ERM-CC580	347	80				107
Method Detection Limit	0.02					

Table B.9: Charge balance errors of the column effluent calculated with MINTEQA2.

	Sample ID					
	1	3	6	9	11	12
Control	1.03	4.86	2.80	1.86	1.02	1.29
Acetate	0.85	3.02	0.78	0.18	0.93	4.15
Lactate	14.48	2.00	0.00	2.65	2.65	0.13
Lactate-Sulfate	0.64	7.91	3.92	2.63	3.65	

Table B.10: Cation analysis QA/QC from May, 2013. The lab blank is from the anaerobic column experiments in Chapter 2.

	Instrument Detection Limits		Lab Blank Concentrations	
Element	X Series 2 ICP-MS (μg L^{-1})	iCAP 6000 ICP-OES (mg L^{-1})	X-Series2 (μg L^{-1})	iCap-OES (mg L^{-1})
Li	0.0344	0.1	< 0.03	<0.1
Be	0.0074		< 0.007	
B	0.1507		< 0.2	
Na	0.1709	0.2	40.6	<0.2
Mg	0.0426	0.2	9.09	<0.2
Al	0.0414	0.2	12.56	<0.2
Si	9.2539	0.07	< 31	<0.07
P	3.0164		< 3	
K	4.3986	0.1	< 15	<0.1
Ca	1.3525	0.2	39.59	<0.2
Ti	0.0455		< 0.05	
V	0.0067		< 0.007	
Cr	0.0066	0.2	0.116	<0.2
Mn	0.0110	0.1	< 0.01	<0.1
Fe	0.0603	0.2	2.393	<0.2
Co	0.0050	0.1	< 0.02	<0.1
Ni	0.0123	0.1	< 0.01	<0.1
Cu	0.0150	0.2	0.81	<0.2
Zn	0.2427	0.2	< 0.2	<0.2
As	0.0090	0.1	< 0.009	<0.1
Sr	0.0032	0.03	0.087	<0.03
Mo	0.0048		0.093	
Ag	0.0044		0.351	
Cd	0.0014	0.2	< 0.001	<0.2
Sn	0.0336		< 0.03	
Sb	0.0026	0.09	0.08	<0.09
Ba	0.0029		< 0.003	
Tl	0.0007	0.2	< 0.0007	<0.2
Pb	0.0009	0.2	0.259	<0.2
U	0.0006		< 0.0006	
S		0.2		<0.2
Se		0.1		<0.2

Appendix C: *Column Properties from Chapters 2 and 3*

Table C.1: Properties of columns from Chapter 2.

	Column ID			
Parameter	Control	Acetate	Lactate	Lactate-Sulfate
Pore Volume (mL)	89.6	86.4	94.4	86.6
Average PV/week	2.97	3.15	2.78	2.91
Length of column (cm)	14.6			
Inner diameter of column (cm)	3.81			
Cross-sectional area of column: A (cm^2)	11.4			
Volume of column (mL)	177.5	175.4	186.4	177.2
n (porosity)	0.505	0.493	0.506	0.489
Average linear velocity (cm hr^{-1})	0.275	0.288	0.271	0.269
Average linear velocity (m day^{-1})	0.066	0.069	0.065	0.065

Table C.2: Properties of columns from Chapter 3.

	Column ID	
Parameter	Column 1	Column 2
Pore Volume (mL)	86.0	100.6
Average PV/week	3.2	3.0
Length of column (cm)	14.60	
Inner diameter of column (cm)	3.81	
Cross-sectional area of column: A (cm^2)	11.40	
Volume of column (mL)	176.7	176.7
n (porosity)	0.487	0.569
Average linear velocity (cm hr^{-1})	0.295	0.277
Average linear velocity (m day^{-1})	0.071	0.066